

AFRL-IF-RS-TR-2006-228
Final Technical Report
July 2006



A VIDEO TRANSMISSION SYSTEM FOR SEVERELY DEGRADED CHANNELS

Rensselaer Polytechnic Institute

APPROVED FOR PUBLIC RELEASE; DISTRIBUTION UNLIMITED.

**AIR FORCE RESEARCH LABORATORY
INFORMATION DIRECTORATE
ROME RESEARCH SITE
ROME, NEW YORK**

STINFO FINAL REPORT

This report has been reviewed by the Air Force Research Laboratory, Information Directorate, Public Affairs Office (IFOIPA) and is releasable to the National Technical Information Service (NTIS). At NTIS it will be releasable to the general public, including foreign nations.

AFRL-IF-RS-TR-2006-228 has been reviewed and is approved for publication.

APPROVED: /s/

DAVID HENCH
Project Engineer

FOR THE DIRECTOR: /s/

WARREN H. DEBANY, Jr.
Technical Advisor, Information Grid Division
Information Directorate

REPORT DOCUMENTATION PAGE				<i>Form Approved</i> OMB No. 0704-0188	
<small>Public reporting burden for this collection of information is estimated to average 1 hour per response, including the time for reviewing instructions, searching data sources, gathering and maintaining the data needed, and completing and reviewing the collection of information. Send comments regarding this burden estimate or any other aspect of this collection of information, including suggestions for reducing this burden to Washington Headquarters Service, Directorate for Information Operations and Reports, 1215 Jefferson Davis Highway, Suite 1204, Arlington, VA 22202-4302, and to the Office of Management and Budget, Paperwork Reduction Project (0704-0188) Washington, DC 20503.</small>					
PLEASE DO NOT RETURN YOUR FORM TO THE ABOVE ADDRESS.					
1. REPORT DATE (DD-MM-YYYY) JULY 2006		2. REPORT TYPE Final		3. DATES COVERED (From - To) Sep 01 – Jun 06	
4. TITLE AND SUBTITLE A VIDEO TRANSMISSION SYSTEM FOR SEVERELY DEGRADED CHANNELS				5a. CONTRACT NUMBER	
				5b. GRANT NUMBER F30602-01-1-0591	
				5c. PROGRAM ELEMENT NUMBER 62702F	
6. AUTHOR(S) William A. Pearlman and Gary J. Saulnier				5d. PROJECT NUMBER 558B	
				5e. TASK NUMBER II	
				5f. WORK UNIT NUMBER 06	
7. PERFORMING ORGANIZATION NAME(S) AND ADDRESS(ES) Center for Image Processing Research Rensselaer Polytechnic Institute Troy NY 12180-3590				8. PERFORMING ORGANIZATION REPORT NUMBER	
9. SPONSORING/MONITORING AGENCY NAME(S) AND ADDRESS(ES) AFRL/IFGC 525 Brooks Rd Rome NY 13441-4505				10. SPONSOR/MONITOR'S ACRONYM(S)	
				11. SPONSORING/MONITORING AGENCY REPORT NUMBER AFRL-IF-RS-TR-2006-228	
12. DISTRIBUTION AVAILABILITY STATEMENT APPROVED FOR PUBLIC RELEASE; DISTRIBUTION UNLIMITED. PA# 06-485					
13. SUPPLEMENTARY NOTES					
14. ABSTRACT The goal of this program was to integrate the error-resilient set partitioning in hierarchical trees (ER-SPIHT) video codec into a system for transmission over an orthogonal frequency-division multiplexing (OFDM) channel with rate adaptation. The bit stream from video codec should be distributed among the subcarriers for optimum throughput with minimum probability of decoding error.					
15. SUBJECT TERMS Orthogonal frequency-division multiplexing (OFDM), Inter-Carrier Interference (ICI), Channel State Information (CSI), Code Division Multiplexing (CDM)					
16. SECURITY CLASSIFICATION OF:			17. LIMITATION OF ABSTRACT UL	18. NUMBER OF PAGES 165	19a. NAME OF RESPONSIBLE PERSON David Hench
a. REPORT U	b. ABSTRACT U	c. THIS PAGE U			19b. TELEPHONE NUMBER (Include area code)

Contents

Introduction	1
Summary	1
Personnel	2
Publications	2
 I ROBUST OFDM FOR FADING CHANNELS	 4
 1 Introduction, Background and Literature Survey	 5
1.1 Introduction	5
1.2 Background	6
1.2.1 Wireless Communication Channels	6
1.2.2 OFDM	9
1.2.3 Water-Filling Solution and Bit-Loading	14
1.3 Literature Survey	15
1.3.1 Inter-Carrier Interference Mitigation	15
1.3.2 Water-Filling Solution and Bit-Loading	18
 2 General Self-Cancellation Scheme	 24
2.1 Motivation	24
2.2 Zhao-Haggman's Self-Cancellation Scheme	26
2.3 System Description	26
2.3.1 Special Case 1: Conventional System	29
2.3.2 Special Case 2: Zhao-Haggman's System	29
2.4 SIR Analysis	30
2.5 BER Analysis	31
2.5.1 Effect of Windowing on Signal and Noise Power	31
2.5.2 BER Calculation	32
2.6 Window Design	35
2.6.1 SIR based Design	35
2.6.2 BER based Design	38
2.7 Results	39

2.7.1	Mitigation of ICI due to Frequency Offset	41
2.7.2	Mitigation of ICI due to Channel Fading	45
2.8	Summary	48
3	Sub-Channel Selective MC-SS and MC-CDMA	51
3.1	Motivation	51
3.2	System Description	52
3.3	Drop and Add Algorithm	53
3.3.1	Algorithm Description	53
3.3.2	Convergence	54
3.4	BER Analysis	57
3.5	Results	60
3.5.1	Single-user System	60
3.5.2	Multi-user System	62
3.6	Summary	64
4	Robust Bit-Loaded OFDM	66
4.1	Motivation	66
4.2	Sensitivity of Bit-Loaded OFDM to Unreliable CSI	66
4.2.1	Causes of Unreliable CSI	67
4.2.2	Effect of Unreliable CSI	67
4.3	CDM based Robust Bit-Loaded OFDM	70
4.3.1	System Description	70
4.3.2	Computational Complexity	75
4.4	Robust Bit-Loaded MIMO OFDM	76
4.4.1	Space-Frequency Sub-Channels	76
4.4.2	Robust Bit-loading in Space and Frequency	77
4.5	Results	78
4.5.1	Robust Bit-Loaded OFDM	78
4.5.2	Robust Bit-Loaded MIMO OFDM	80
4.6	Summary	82
5	Conclusion and Future Direction	84
5.1	Future Direction	85
II	JOINT SOURCE-CHANNEL CODING	87
6	SPIHT Source Coding	88
6.1	Introduction	88
6.2	SPIHT Image Compression	89
6.2.1	Performance measures	89

7	The SPIHT Algorithm	90
7.1	SPIHT simulator for MATLAB	93
7.2	Distortion-Rate Profile of SPIHT	94
7.2.1	SPIHT Error Response	96
8	Joint Source and Channel Coding for Binary Symmetric and Fading	
	Channels	99
8.1	Approximating the Performance of Reed Solomon Codes	99
8.2	Distortion-Rate Function and JSCC	100
8.3	JSCC over BSC using EEP and UEP	102
8.4	Energy and Rate Constrained Transmission over Rayleigh Fading Channels	111
8.4.1	Conclusion	112
8.5	Summary	112
9	Robust OFDM Transmission over Fading Channels	117
9.1	Introduction	117
9.2	The Joint Source-Channel Coding System	118
9.3	SPIHT Demultiplexing and D-R estimator	120
9.4	OFDM and Frequency Selective Channels	121
9.4.1	Dual Loading Algorithms	121
9.5	Dual Stream Joint Source Channel Coding	122
9.6	Simulation Results	124
9.7	Discussion and Conclusion	125
10	Real-Time Video Transmission over MIMO OFDM Channels using	
	Space-Time Block Codes	128
10.1	Introduction	128
10.2	Analytic formulation	129
10.2.1	MIMO OFDM using OSTBC	130
10.3	Analytical Simulation for MIMO OFDM OSTBC	132
10.4	Monte Carlo Simulation for MIMO OFDM	132
10.5	Conclusion	134
	BIBLIOGRAPHY	136
	APPENDICES	151
A	Fischer's Bit-Loading Algorithm	151
B	Matrix Forms for ZF and MRC Receivers	153
B.1	ZF Receiver	153
B.2	MRC Receiver	154

List of Figures

1.1	Multi-path channel.	6
1.2	MIMO channel.	9
1.3	Frequency spectrum of OFDM sub-carriers.	11
1.4	Use of cyclic prefix for OFDM symbols.	12
1.5	Basic OFDM system.	12
1.6	Embedded pilots for PSA channel estimation.	22
1.7	Water-filling solution for parallel channels.	22
1.8	Water-filling solution for a channel with colored noise.	22
1.9	Multi-user channels: (a) Multi-access channel, (b) Broadcast channel and (c) Interference channel.	23
2.1	Creation of ICI in presence of a fixed frequency shift.	25
2.2	Block diagram of an OFDM system employing the general self-cancellation scheme.	27
2.3	SIR of the conventional, Zhao-Haggman and proposed (Designs A and B) systems, for $L = 2$	36
2.4	$I'_{\delta, \mathbf{c}}(\nu)$ for the conventional, Zhao-Haggman and the proposed system (Design A).	37
2.5	SIR of the conventional, Zhao-Haggman and proposed (Designs C and D) systems, for $L = 4$	38
2.6	Required E_b/N_0 of the conventional, Zhao-Haggman and proposed (Designs E and F) systems for $L = 2$ and $p = 10^{-4}$	40
2.7	BER comparison of designs A, B, E and F, over a flat AWGN channel with perfect equalization.	41
2.8	Calculated and simulated BER for the conventional, Zhao-Haggman and proposed system (Design A), over a flat AWGN channel with perfect equalization.	42
2.9	BER of the conventional, Zhao-Haggman and proposed system (Design A) with pilot based channel estimation, over a flat AWGN channel.	43
2.10	BER of the conventional, Zhao-Haggman and proposed system (Design A) with DQPSK modulation, over a flat AWGN channel.	44

2.11	BER performance of the proposed system (Design A) and a 1/2 rate coded OFDM system, over a frequency selective Rayleigh fading channel with perfect equalization.	46
2.12	BER of the conventional, Zhao-Haggman and proposed system (Design A), over a frequency selective Rayleigh fading channel with perfect equalization.	47
2.13	BER of the conventional, Zhao-Haggman and proposed system (Design A) with pilot based channel estimation, over a frequency selective Rayleigh fading channel.	48
2.14	BER of the conventional, Zhao-Haggman and proposed system (Design A) with DQPSK modulation, over a frequency selective Rayleigh fading channel.	49
2.15	BER of the conventional and proposed system (Design A), over a frequency selective Rayleigh fading channel with DQPSK modulation and 1/2 rate convolutional code.	50
3.1	Conventional MC-SS system	52
3.2	Sub-Channel Selective MC-SS system	53
3.3	Convergence of the DA algorithm for a four user system over a flat multi-access AWGN channel.	55
3.4	Convergence of the DA algorithm for a two user system over a frequency selective multi-access AWGN channel.	56
3.5	BER performance of single user conventional and SCS MC-SS systems over a frequency selective AWGN channel.	61
3.6	Calculation and simulation results for conventional and SCS MC-SS systems with independent sub-channel fading.	62
3.7	BER performance of single user conventional and SCS systems over a frequency selective fading channel.	63
3.8	BER performance of $K = 4$ user conventional and SCS systems over a flat multi-access AWGN channel.	64
3.9	BER performance of $K = 2$ user conventional and SCS systems over a frequency selective multi-access AWGN channel.	65
4.1	BER of bit-loaded OFDM in presence of outdated CSI.	70
4.2	Multi-stage detector with decorrelating first stage for CDM.	73
4.3	OFDM system with CDM based robust bit-loading.	74
4.4	BER performance of the proposed system with $L = 4$ and $R = 1$ compared to that of a conventional system.	79
4.5	BER performance of the proposed system with different numbers of iterations of the MUD scheme.	80
4.6	BER performance of the proposed algorithm with different group sizes.	81
4.7	BER of bit-loaded MIMO-OFDM in presence of outdated CSI.	82

4.8	BER performance of the proposed MIMO OFDM system with different numbers of iterations of the MUD technique.	83
7.1	Tree structure in the two-dimensional wavelet transform	91
7.2	Variation of PSNR as a function of different bit errors	98
8.1	EEP vs. UEP for Lenna at transmission rate of .1089 bpp	105
8.2	Optimum UEP vs Optimum EEP for the Susie sequence over a BSC of 0.01	109
8.3	Probability of decoding failure for the Susie sequence using the optimum UEP and optimum EEP schemes over a BSC of .01	110
8.4	Optimum UE-UEP and EEP for Lena.	113
8.5	Information and Energy Allocation per block for Susie at 0.0453 bpp	114
8.6	Analytic simulation results for optimum UE-UEP for Lena at 1.00 bpp	115
9.1	Diagram of the transmission and receiver systems	119
10.1	A generic model of the MIMO OFDM system	131
10.2	Analytic simulation results for optimum EEP for Lena at 0.5 bpp in MIMO	133
10.3	Analytic simulation results for optimum EEP for Susie at 0.1 bpp in MIMO	133

List of Tables

2.1	Design parameters obtained from the SIR based design method, $N = 64, L = 2, M = 1$	36
2.2	Design parameters obtained from the SIR based design method, $N = 64, L = 4, M = 1$	38
2.3	Design parameters obtained from the BER based design method, $N = 64, L = 2, M = 1, p = 10^{-4}$	39
2.4	Delay profile of the frequency selective Rayleigh fading channel. . . .	45
4.1	Delay profile of the GSM 12 tap Hilly Terrain (HTx) channel model. .	69
7.1	Performance of MATLAB and original SPIHT	94
7.2	Actual and estimated D-R points of SPIHT images and video at the end of each threshold	97
8.1	Coefficients for approximation of RS block failure	101
8.2	PSNR for average MSE for Lena image over a memoryless BSC with BER 0.01	107
8.3	PSNR for average MSE for Goldhill image over a memoryless BSC with BER 0.01	107
8.4	PSNR for average MSE for Susie sequence over a memoryless BSC with BER 0.01 using 3-D SPIHT	107
8.5	PSNR for average MSE for Susie sequence over a memoryless BSC with BER 0.01 and .001 using 3-D SPIHT	107
8.6	PSNR for average MSE for Table tennis sequence over a memoryless BSC with BER 0.01 and .001 using 3-D SPIHT	108
8.7	PSNR for average MSE for Football sequence over a memoryless BSC with BER 0.01 and .001 using 3-D SPIHT	108
8.8	PSNR for average MSE for Flower garden sequence over a memoryless BSC with BER 0.01 and .001 using 3-D SPIHT	108
8.9	optimal UE-UEP PSNR obtained for y-component of SUSIE	116
8.10	optimal EEP PSNR obtained for y-component of SUSIE	116
9.1	SPIHT-Transmission OFDM Simulation Parameters	126
9.2	PSNR results for SPIHT OFDM system	126

9.3	Single vs Dual stream OFDM transmission of SPIHT-encoded Lena image	126
-----	---	-----

Introduction

Summary

The goal of this program was to integrate the error-resilient set partitioning in hierarchical trees (ER-SPIHT) video codec into a system for transmission over an orthogonal frequency-division multiplexing (OFDM) channel with rate adaptation. The bit stream from video codec should be distributed among the subcarriers for optimum throughput with minimum probability of decoding error. To reach this goal, the investigations are divided into two main tasks:

- Improving OFDM performance over adverse channels
- Partitioning of SPIHT compressed bitstream among the subcarriers (called "loading")

Part I of this report discusses the application of OFDM to degraded channels. OFDM and Multi-Carrier (MC) systems have proved to be some of the most promising techniques for high data rate communication over wireless channels. These systems have excellent performance when they operate over frequency selective slow fading channels. However, various issues arise when they operate over channels with faster time variations. In the first part of this report we consider some of the issues regarding the operation of the OFDM and MC systems over frequency selective fading channels, and propose solutions that can resolve these issues. We first consider the creation of Inter-Carrier Interference (ICI) as a result of frequency shifts. We generalize existing ICI self-cancellation schemes and show that using windowing operations at the transmitter and the receiver we can considerably reduce the amount of ICI created as a consequence of a frequency mismatch between the local oscillators at the transmitter and receiver, or created as a result of fast time variations in the channel. We then consider Multi-Carrier Spread Spectrum (MC-SS) and Multi-Carrier Code Division Multiple Access (MC-CDMA) systems operating over frequency selective channels and propose sub-channel selective MC-SS and MC-CDMA systems, where only a fraction of sub-channels are selected for chip transmission based on their quality. We also provide a distributed algorithm that converges to near optimal sub-channel assignment in an MC-CDMA system. Finally, after demonstrating

the sensitivity of bit-loaded OFDM systems to unreliable Channel State Information (CSI), we propose a robust bit-loaded OFDM system where frequency domain Code Division Multiplexing (CDM) is used to achieve frequency diversity without any loss in transmission rate. We show that this system is considerably less sensitive to unreliability in CSI. Thus, it can provide desired performance when operating over frequency selective channels with faster time variations. Overall, we provide solutions for mitigation of some of the most important problems of wireless MC and OFDM systems. These solutions help make the use of MC and OFDM modulations schemes for high data rate wireless applications more practical and feasible.

Part II of this report discusses joint source and channel coding (JSCC). Extensive results for 2-D and 3-D SPIHT encoded images and video at various transmission rates and various multipath spread and Doppler frequency for various multi-antenna systems are presented. Also, an operational real-time distortion-rate (D-R) based algorithm is developed. If the transmitter does not have any knowledge of the channel, then a JSCC algorithm must naturally be designed for a worst case scenario. We also give results of the PSNR degradation using the worst case scenario. The results establish that by using Multiple-Input, Multiple-Output (MIMO) OFDM and a real time JSCC algorithm under a transmission rate constraint, a higher PSNR can be achieved relative to the Single-Input, Single-Output (SISO) system for image and image sequence transmission at low signal-to-noise (SNR) ratio. We will also use time and frequency interleaving if more protection is needed against fading.

Personnel

The personnel who worked on this effort are listed below.

- Prof. William A. Pearlman and Prof. Gary J. Saulnier, Co-principal investigators
- Alireza Seyed, Ph.D. received Aug. 2004,
Dissertation: *Robust Multi-Carrier Communication Systems for Fading Channels*, ECSE Dept., Rensselaer Polytechnic Institute, May 2004.
- Masoud Farshchian, Ph.D. Candidacy Exam passed in May, 2005, expected graduation August 2006.

Publications

The work described in the publications below were supported in part by this effort.

1. Alireza Seyed and Gary J. Saulnier, Symbol error rate analysis of Fischers bit-loading algorithm, *IEEE Transactions on Communication*, Vol. 52, pp. 180-1483, Sept 2004.

2. Alireza Seyed and Gary J. Saulnier General self-cancellation scheme for mitigation of ICI in OFDM systems, *Proceedings of IEEE ICC'04*, pp. 2653-2657, June 2004.
3. Alireza Seyed and Gary J. Saulnier, A novel reception method to mitigate frequency offset in OFDM receivers, in *Proceedings of IEEE ICC'03*, vol. 4, pp. 2355-2359, 2003.
4. Alireza Seyed and Gary J. Saulnier, General ICI self-cancellation scheme for OFDM systems, *IEEE Transactions on Vehicular Technology*, Vol. 54, pp. 198-210, Jan. 2005.
5. M. Farshchian, S. Cho, W. A. Pearlman, Robust Image and Video Transmission Using a new Joint Source Channel Coding Algorithm and Dual Adaptive OFDM, *Visual Communications and Image Processing 2004*, Proc. SPIE 5308, pp. 636-646, Jan. 2004.
6. M. Farshchian, S. Cho, and W. A. Pearlman, Optimal error protection for real time image and video transmission, *IEEE Signal Processing Letters*, Vol. 11, No. 10, pp. 780-783, Oct. 2004.
7. M. Farshchian, S. Cho, and W. A. Pearlman, Optimal error protection for real time image and video transmission, *IEEE Int. Conf. on Acoustics, Speech, and Signal Processing (ICASSP 2004)*, Vol. 4, pp. 625-628, May 2004.
8. M. Farshchian, S. Cho, and W. A. Pearlman, Robust SPIHT transmission over frequency selective channels using a new joint source-channel coding algorithm and OFDM, accepted and withdrawn from *IEEE Vehicular Technology Conference-Spring 04* and re-submitted and rejected by *IEEE Globecom Wireless Communications Workshop*, Nov. 2004.
9. A. Seyed and G. J. Saulnier, "CDM based Robust Bit-loading for Wireless OFDM and MIMO-OFDM Systems, submitted to *IEEE Trans on Wireless Communications*, Aug. 2005.
10. M. Farshchian and W. A. Pearlman, "Real-Time Video Transmission over MIMO OFDM Channels using Space-Time Block Codes," *Conference on Information Sciences and Systems 2006*, Princeton, NJ, Mar. 2006.
11. M. Farshchian and W. A. Pearlman, "Enhancement of video quality for energy constrained cellular applications," *IEEE Int. Conf. on Image Processing 2006 (ICIP 2006)*, Atlanta, GA, Oct. 2006.

Part I

**ROBUST OFDM FOR FADING
CHANNELS**

Chapter 1

Introduction, Background and Literature Survey

1.1 Introduction

With increasing demand for high data rate wireless communications, interest in designing transmission schemes that can deliver high rate data over mobile wireless channels has greatly increased. Orthogonal Frequency Division Multiplexing (OFDM) has been found to be one of the most promising candidates. OFDM, has been used in the Wireless Local Area Network (WLAN) standards such as IEEE 802.11, IEEE 802.16 and HIPERLAN II, as well as the European digital video and audio broadcast standards DVB-T and DAB.

In this dissertation, we consider some of the problems of a high data rate OFDM system transmitting over wireless channels, and propose solutions for these problems. We first consider the problem of the sensitivity of OFDM systems to frequency shifts which can be caused by a frequency mismatch between the transmitter and the receiver or by a time varying channel, and propose a method to decrease this sensitivity. We then consider a sub-optimal water-filling and bit-loading (chip-loading) method proposed for MC-SS and MC-CDMA systems and show that this method can increase the power efficiency of these systems. Also, we consider the problem of unreliability of Channel State Information (CSI) in bit-loaded OFDM systems and propose a robust bit-loaded OFDM system.

The outline of this proposal is as follows. In the remainder of this chapter, in Section 1.2, we define and explain the basic concepts and models for wireless communication channels, OFDM systems and water-filling and bit-loading algorithms. Then in Section 1.3, we present a survey of the literature on the two specific problems regarding OFDM systems, namely the sensitivity to frequency shifts and the water-filling and bit-loading methods. In Chapter 2 we consider the sensitivity of OFDM systems to frequency shifts. We generalize the Inter-Carrier Interference (ICI) self-cancellation schemes using windowing operations. We then show that better windows

can be designed in this generalized framework, thus improving the performance of the system in presence of frequency shifts. Chapter 3 discusses the proposed sub-channel selective MC-SS and MC-CDMA systems. The analysis and simulation results for this simple sub-optimal loading algorithm are presented and compared to the conventional system. In Chapter 4 we consider the unreliability in CSI, and the resulting performance loss in bit-loaded systems. We also propose a robust bit-loaded system that employs frequency diversity to battle unreliable CSI. Chapter 5 concludes part of the report and discusses possible directions for future research regarding the considered problems and proposed solutions.

1.2 Background

1.2.1 Wireless Communication Channels

In this section we describe the properties and characteristics of radio communication channels. Furthermore, we discuss the more popular mathematical models that can be used to represent these channels.

Multi-path and Doppler Effects

The multi-path effect [75][77] is caused by the fact that the received signal is a superposition of the multiple copies of the transmitted signal that arrive at the receiver from different paths (Figure 1.1). A multi-path channel can be modelled by the linear, but potentially time-variant, channel impulse response

$$h_t(\tau) = \sum_i \alpha_i(t) \delta(\tau - \tau_i(t)), \quad (1.1)$$

where $\alpha_i(t)$ and $\tau_i(t)$ are the received amplitude and the delay of path i at time t , respectively. Due to the difference in the length and environment of the paths, the

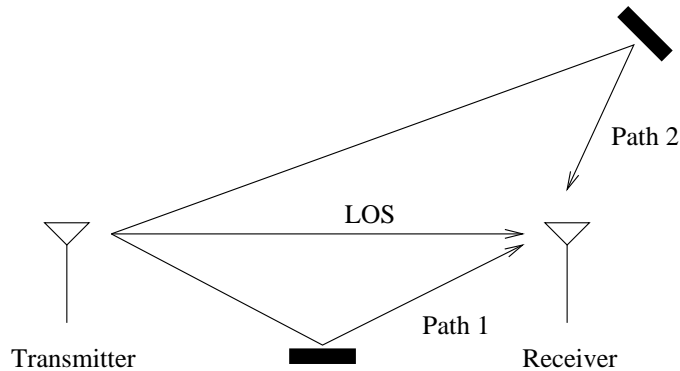


Figure 1.1: Multi-path channel.

arrived signals have different power levels and phase shifts. If the paths are constant in time, the resulting power and phase at the receiver will also remain constant in time. However since the paths are a function of the location of the transmitter, the receiver and the other objects in the environment, any motion of the transmitter, the receiver or other objects will result in the time-variability of the received signal power and phase.

The multi-path effect causes frequency selectivity in the channel. In other words, the channel acts as a linear filter which has different gains at different frequencies, which are determined by the Fourier transform of the impulse response $h_t(\tau)$.

The Doppler effect [75][77] occurs when the receiver is moving with respect to the transmitter. Due to the Doppler effect the received frequency of the signal is different from the transmitted frequency. The difference is given by

$$f_D = f_{Received} - f_{Transmitted} = \frac{v \cos \theta}{\lambda}, \quad (1.2)$$

where λ is the wavelength, v is the velocity of the receiver with respect to the transmitter and θ is the angle between the direction of the motion of the receiver and its orientation with respect to the transmitter ($v \cos \theta$ is the relative velocity of the receiver towards the transmitter). Note that since the Doppler shift is a function of the transmission frequency (wavelength), different frequency components of the signal are shifted differently and, thus, the signal is distorted.

Mathematical Models

In an equivalent baseband system, the combination of the multi-path and the Doppler effect is often modelled as a random discrete linear time-variant filter.

$$h_k[m] = \sum_n \alpha_k[n] \delta[m - n], \quad (1.3)$$

where $\alpha_k[n]$ are complex random variables, n represents the path delay and k is the time index. Generally $\alpha_k[n_1]$ and $\alpha_k[n_2]$ are assumed to be independent when $n_1 \neq n_2$, but $\alpha_{k_1}[n_1]$ and $\alpha_{k_2}[n_1]$ are assumed to be correlated.

When a large number of paths exist, a large number of random variables with random amplitudes and phases are summed to result in the channel gain. Therefore, due to the Central Limit Theorem, each random variable $\alpha_k[n]$ has a Gaussian distributed real and imaginary parts. If a Line Of Sight (LOS) path does not exist, the Gaussian distributions have zero mean, thus the magnitude of each α has a Rayleigh probability distribution function (pdf):

$$f_\alpha(x) = \begin{cases} \frac{x}{\sigma^2} \exp(-\frac{x^2}{2\sigma^2}) & x \geq 0 \\ 0 & x < 0 \end{cases}, \quad (1.4)$$

where σ^2 is the variance of each Gaussian component. In presence of a LOS, the Gaussian components have non-zero mean (equal to the magnitude of the LOS path) and the magnitude has a Rician pdf

$$f_\alpha(x) = \begin{cases} \frac{x}{\sigma^2} \exp(-\frac{x^2+A^2}{2\sigma^2}) I_0(\frac{Ax}{\sigma^2}) & x \geq 0 \\ 0 & x < 0 \end{cases}, \quad (1.5)$$

where A is the magnitude of the LOS component and $I_0(\cdot)$ is the modified Bessel function of the first kind.

The average power of the channel gains $\alpha_k[n]$ as a function of the path delay n is known as the delay profile. Often, either a uniform delay profile,

$$\sigma_{\alpha[n]}^2 = \begin{cases} \frac{1}{D} & 0 \leq n \leq D-1 \\ 0 & \text{otherwise} \end{cases}, \quad (1.6)$$

or an exponential one,

$$\sigma_{\alpha[n]}^2 = \begin{cases} \exp(-\frac{n}{D}) & 0 \leq n \\ 0 & \text{otherwise} \end{cases}, \quad (1.7)$$

is assumed.

The dependence of the channel gains $\alpha_{k_1}[n]$ and $\alpha_{k_2}[n]$ is often described by the Power Spectral Density (PSD) of $\alpha[n]$, under the assumption that $\alpha[n]$ is a Wide Sense Stationary (WSS) random variable. The power spectral density normally used is

$$S_{\alpha\alpha}(f) = \begin{cases} \frac{K}{[1-(f/f_D)]^{1/2}} & |f| < f_D \\ 0 & \text{otherwise} \end{cases}, \quad (1.8)$$

which is known as the Jakes' model [44].

The parameter f_D is known as the Doppler spread and the inverse of the Doppler spread, $T_C = 1/f_D$, is known as the coherence time. These parameters represent the extent of the time variability of the channel. In other words, the channel can be assumed to be correlated for a time period equal to or smaller than the coherence time.

Similarly, delay spread, D_S , is defined as the difference between the maximum and the minimum delays, and the coherence bandwidth, $B_C = 1/D_S$, is its reciprocal. These parameters represent the extent of the frequency selectivity of the channel. In other words, the channel can be assumed to be correlated in a bandwidth equal to or smaller than the coherence bandwidth.

In general, based on the symbol duration (relative to the coherence time) and the bandwidth used (relative to the coherence bandwidth), the channels can be classified into four groups:

- Additive White Gaussian Noise (AWGN) channel: No time or frequency variations.

- Frequency selective channel: No time variation, some frequency variations.
- Flat fading channel: No frequency variations, some time variations.
- Frequency selective fading channel: Both time and frequency variations.

Multi-Input Multi-Output Channels

The use of multiple antennas at the transmitter and the receiver results in a Multi-Input Multi-Output (MIMO) channel (Figure 1.2). It has been shown that if the channel has rich scattering characteristics, the capacity of a MIMO channel is significantly larger compared to that of a Single-Input Single-Output (SISO) channel. This additional capacity can be used to employ diversity schemes such as space-time coding and improve the power efficiency of the system for fixed data rate, or it can be used in a multiplexing scheme to increase the data rate over the given channel [30][130].

The channel between a specific pair of antennas at the transmitter and the receiver, can be considered a simple SISO channel, and can be analyzed and modelled as explained in Sections 1.2.1 and 1.2.1. Therefore, the MIMO channel, consisting of all the channels between the antenna pairs, must be modelled using vector and matrix notations. For example, if M_T and M_R antennas are used at the transmitter and the receiver respectively, an AWGN MIMO channel can be modelled by

$$\mathbf{y}_{M_R \times 1} = \mathbf{H}_{M_R \times M_T} \mathbf{s}_{M_T \times 1} + \mathbf{n}_{M_R \times 1}, \quad (1.9)$$

where \mathbf{s} is the vector of transmitted symbols, \mathbf{y} is the vector of received values, \mathbf{n} is a white Gaussian noise vector and \mathbf{H} is the channel matrix. In this model, each component of \mathbf{H} represents the gain between a pair of transmit and receive antennas. It has been shown [2][28][31][57] that with proper pre-coding and post-processing, the MIMO channel is equivalent to r parallel independent channels, where $r = \text{rank}(\mathbf{H})$.

1.2.2 OFDM

Orthogonal Frequency Division Multiplexing (OFDM) [6][104] is a special form of Multi-Carrier (MC) modulation, where the data stream is transmitted using multiple

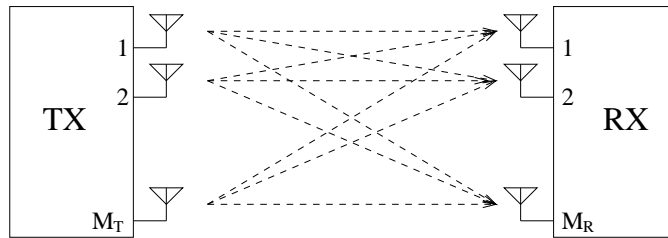


Figure 1.2: MIMO channel.

carriers. OFDM can be historically traced back to mid 1960's, where the original idea of parallel data transmission over frequency divided sub-channels was proposed [14][84]. However, the proposed scheme only became popular after the advances in Digital Signal Processing (DSP) overcame the practical implementation problems by use of the Discrete Fourier Transform (DFT) in implementation of the OFDM systems [108]. This implementation is known as Digital Multi-Tone (DMT). Later the Fast Fourier Transform (FFT) algorithms allowed the computational complexity to reduce from order of N^2 to $N \log_2 N$, and made the OFDM system more affordable. Although technically different in definition, the terms MC modulation, OFDM and DMT are sometimes used interchangeably in the literature.

In 1980's OFDM was employed to build high data rate modems [38][39]. These efforts later led to the employment of OFDM in Digital Subscriber Line (DSL) modems [18][19]. More recently, OFDM has been used in wireless data transmission standards such as IEEE 802.11, IEEE 802.16 and HIPERLAN II, as well as the European broadcast standards Digital Audio Broadcast (DAB) and Digital Video Broadcast-Terrestrial (DVB-T).

Basic OFDM

In a basic OFDM system, the input data stream is split into N parallel lower rate sub-streams. These sub-streams, are then modulated over N orthogonal sub-carriers (also known as sub-channels). Although the frequency spectrum of these sub-carriers overlap, because of their orthogonality, the receiver is able to separate the sub-streams. The overlapping frequency spectrums enable the OFDM systems to have considerably higher spectral efficiency than Frequency Division Multiplexing (FDM) systems. Figure 1.3 displays the frequency spectrum of four such sub-carriers. The sub-carrier spacing is designed to be smaller than the coherence bandwidth such that each sub-channel only experiences a flat channel. Hence, the OFDM receivers have lower complexity compared to receivers designed for single carrier systems operating over frequency selective channels.

In general, the baseband form of the transmitted signal can be written as

$$s_T(t) = \sum_k \sum_{n=0}^{N-1} S_{n,k} \frac{1}{\sqrt{N}} \exp(j2\pi nt/T) \Pi(t - kT), \quad (1.10)$$

where T is the OFDM symbol duration, N is the number of sub-carriers, $S_{n,k}$ is the complex symbol modulated on sub-carrier n at time slot k and $\Pi(t)$ is the pulse (window) shape. Normally the data symbol $S_{n,k}$ is a M-QAM or M-PSK symbol carrying $\log_2 M$ bits. Although often a rectangular pulse shape is used,

$$\Pi(t) = \begin{cases} 1 & 0 < t < T \\ 0 & \text{otherwise} \end{cases}, \quad (1.11)$$

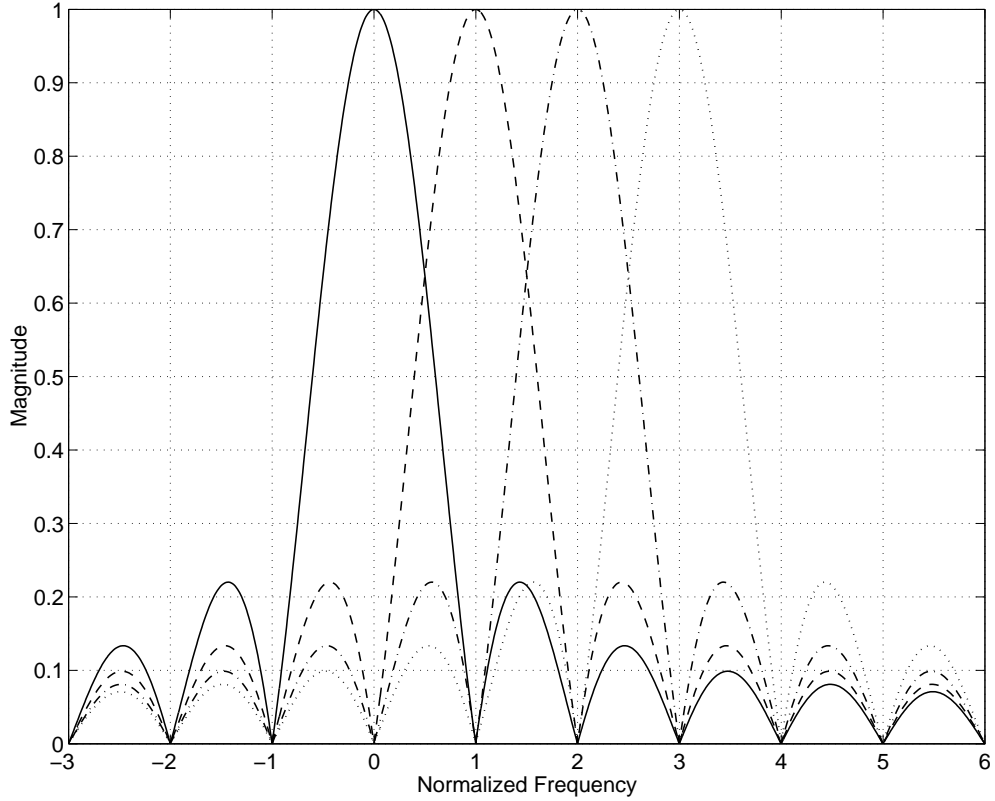


Figure 1.3: Frequency spectrum of OFDM sub-carriers.

non-rectangular pulse shapes (windowing) can be employed to reduce the effects of interference and/or synchronization errors [66][102].

Contrary to what (1.10) suggests, in practice the OFDM signal is not generated by separate modulations of each sub-carrier. Instead, IFFT/FFT blocks are generally used to modulate and demodulate all sub-carriers at the same time.

A guard interval can be added to the beginning of each OFDM symbol to avoid Inter Symbol Interference (ISI) caused by the multi-path delays in the channel. The guard interval can solve the problem of ISI. However, even when the channel is constant for the duration of one OFDM symbol, the channel delay still causes ICI since the delayed versions of the sub-carriers are no longer orthogonal. To battle the ICI problem, instead of a simple guard interval, a cyclic extension of each OFDM symbol is added to the beginning of the symbol (Figure 1.4). In other words, a copy of the last part of each symbol is appended to its beginning. This is commonly known as the Cyclic Prefix (CP). The cyclic prefix is removed at the receiver. When CP is used, any channel delay that is smaller than the CP length, will only cause a circular shift in the OFDM symbol. Therefore, both ISI and ICI are avoided.

The basic OFDM system with FFT/IFFT implementation is depicted in Figure 1.5.

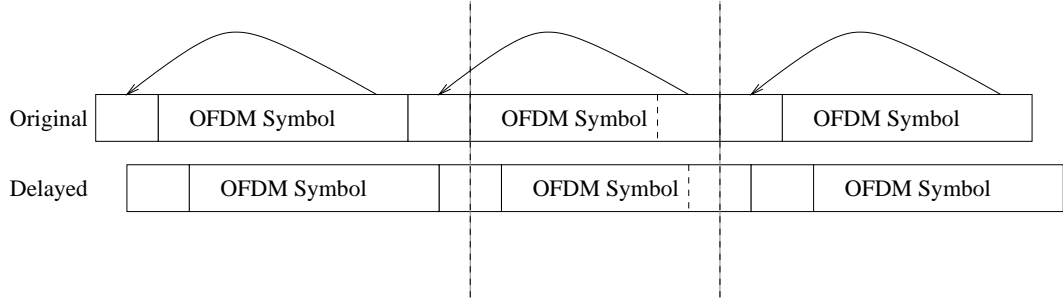


Figure 1.4: Use of cyclic prefix for OFDM symbols.

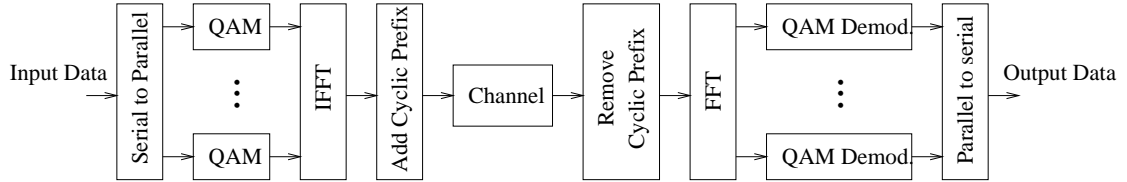


Figure 1.5: Basic OFDM system.

The key advantages of the OFDM scheme are

- Compared to single carrier modulation systems, an OFDM receiver requires lower complexity when used over frequency selective channels.
- OFDM is bandwidth efficient.
- OFDM is robust against narrow-band interference.

On the other hand, OFDM has two important weaknesses:

- OFDM is very sensitive to frequency shifts and phase noise.
- OFDM has large peak-to-average power ratio, which reduces the efficiency of RF amplifiers.

MC-SS, MC-CDMA and MC-CDM

The basic OFDM framework can be utilized to create a Spread Spectrum (SS) communication system known as OFDM Spread Spectrum (OFDM-SS) or Multi-Carrier Spread Spectrum (MC-SS) [131]. In this scheme the same data symbol, with different phases, is transmitted on many sub-channels. The phase of the symbol on each sub-channel is chosen according to the chips of a pseudo-random sequence or code. At the receiver the copies of the symbol obtained from different sub-channels are combined to create the decision variable. MC-SS transmission allows us to gain

frequency diversity as well as processing gain. The MC-SS system is effectively the dual of Direct Sequence SS (DS-SS).

Using MC-SS, multiple users can utilize the same bandwidth at the same time if they use orthogonal (or almost orthogonal) codes. Such a Code Division Multiple Access system is known as MC-CDMA [36][116].

If all the orthogonal codes are assigned to the same user, a Code Division Multiplexing scheme known as MC-CDM is generated [47]. Similar to the MC-SS system, an MC-CDM system provides frequency diversity gain, but operates at higher data rates. However, since a frequency selective channel destroys the orthogonality of the codes, more complex receivers are needed.

OFDMA

Orthogonal Frequency Division Multiple Access (OFDMA) [104] is another multiple access scheme based on the OFDM idea. In an OFDMA system, a number of sub-channels are assigned to each user. Therefore, OFDMA is similar to a simple Frequency Division Multiple Access (FDMA) scheme, but does not require guard-bands needed in an FDMA system and, thus, is more bandwidth efficient.

Channel Estimation for OFDM

Several blind channel estimation techniques for the OFDM systems have been proposed. However, a non-blind, Pilot Symbol Assisted (PSA) channel estimation results in better performance [40][62].

In a PSA channel estimation technique, known pilot symbols are transmitted on a pre-specified time-frequency grid (Figure 1.6). At the receiver, using the known pilot values, samples of the channel at these locations are found. These samples are then interpolated in time and frequency to obtain the estimate of the channel at all time and frequency locations.

MIMO OFDM

When multiple antennas are used at the transmitter and the receiver and the system is operating over a frequency selective channel, it is desirable to use a MIMO OFDM system. In such a system an IFFT is used for each transmit antenna and an FFT for each receive antenna.

If the sub-channel spacing is narrower than the coherence bandwidth of the channel, each sub-channel has a flat frequency response. In this case each sub-channel can be modelled by (1.9). Under this design constraint, equalization of each sub-channel does not require a high degree of computational complexity. As a result, MIMO OFDM receivers can be implemented with lower complexity, compared to receivers needed for a single carrier modulation scheme operating over frequency selective channels.

1.2.3 Water-Filling Solution and Bit-Loading

The concept of water-filling was first discussed in [41]. In this section an overview of the water-filling solution is given. More detailed discussion can be found in [20].

Water-filling, in its most basic form, is a solution to the following problem: *Assuming that N parallel channels exist and channel n has gain H_n and additive white Gaussian noise with power $P_{N,n}$. For a given total transmission power P_S , how the power should be distributed over N parallel channels, such that the total channel capacity is maximized.*

If the received signal of each channel n is scaled with the factor $1/H_n$, we find an equivalent problem with N parallel channels with equal gains and equivalent noise power

$$P'_{N,n} = \frac{P_{N,n}}{|H_n|^2}. \quad (1.12)$$

Since the capacity of the channel is a function of the signal to noise ratio, the equivalent channels have the same capacity.

Mathematically, given the channel capacity as

$$C = \frac{1}{2} \log_2 \left(1 + \frac{P_S}{P_N} \right), \quad (1.13)$$

where P_S is the transmission power and P_N is the AWGN power, the problem can be formulated as the following optimization problem: *Given P_S , find $P_{S,n}$, $n = 0, \dots, N-1$, such that the total capacity*

$$C = \sum_{n=0}^{N-1} \frac{1}{2} \log_2 \left(1 + \frac{P_{S,n}}{P'_{N,n}} \right), \quad (1.14)$$

is maximized, under the constraint

$$\sum_{n=0}^{N-1} P_{S,n} = P_S. \quad (1.15)$$

The solution to this problem, known as the water-filling solution, is

$$P_{S,n} = (\theta - P'_{N,n})^+ \quad (1.16)$$

$$P_S = \sum_{n=0}^{N-1} (\theta - P'_{N,n})^+, \quad (1.17)$$

where θ is the water level and

$$(x)^+ = \begin{cases} x & x \geq 0 \\ 0 & x < 0 \end{cases}. \quad (1.18)$$

The name water-filling can be justified by considering the values $P'_{N,n}$ as the bottom of the container and the total power as the amount of water filled in this container. Figure 1.7 shows the water-filling solution for four parallel channels. Note that more power is assigned to the channels with less noise (smaller $P'_{N,n}$) and less or potentially no power might be assigned to the channels with higher noise levels (larger $P'_{N,n}$).

The above discussion can be extended to a single frequency selective channel with frequency response $H(f)$ and colored Gaussian noise $P_N(f)$. Once again, a frequency selective channel can be considered a flat channel with frequency selective (colored) noise

$$P'_N(f) = \frac{P_N(f)}{|H(f)|^2}, \quad (1.19)$$

if the channel is properly equalized at the receiver.

To extend the water-filling solution to a channel with colored Gaussian noise, we can divide such a channel in frequency into N sub-channels, each having bandwidth B/N , where B is the bandwidth of the original channel, and apply the water-filling to the N sub-channels. Then, by considering the limit $N \rightarrow \infty$, we can conclude the water-filling solution for the channel with colored noise

$$P_S(f) = (\theta - P'_N(f))^+ \quad (1.20)$$

$$P_S = \int (\theta - P'_N(f))^+ df. \quad (1.21)$$

Figure 1.8 depicts the water-filling solution for such a channel.

When the channel is known at the transmitter, the concept of water-filling can be used to implement a form of adaptive modulation in frequency domain and thus improve the performance of an OFDM system over a frequency selective channel. In other words, the channels with large Signal to Noise Ratio (SNR) can use larger constellations and carry more bits. On the other hand, sub-channels with lower SNR, will carry fewer or no bits. To do this, an algorithm is needed to calculate the number of bits and the power assigned to each sub-channel, based on the channel information. These algorithms are known as bit-loading algorithms. Once the bit and power allocation is found, it must be adapted to the variation of the channel. Another set of algorithms called the bit-swapping algorithms try to find the new bit and power allocation given the previous one, and thus reduce computational complexity. A survey of existing bit-loading algorithms can be found in Section 1.3.2.

1.3 Literature Survey

1.3.1 Inter-Carrier Interference Mitigation

One of the main drawbacks of the OFDM scheme is that it is extremely sensitive to any frequency shift in the signal. A fixed frequency shift can be caused by an

offset between the local oscillators at the transmitter and the receiver. A spread of frequency shifts (Doppler spread) can be caused by time variations of the channel. Frequency shifts destroy the orthogonality of the sub-carriers and generate ICI.

Pollet [74] shows the sensitivity of the OFDM scheme to frequency offset by presenting an approximate analysis of the performance of an OFDM system and comparing it to that of the single carrier modulation. Also, to evaluate the sensitivity of the OFDM system to frequency offset, Sathananthan [85] calculates an approximate expression for the BER of an OFDM system by assuming Gaussian distribution for the ICI. A loose upper bound, based on the worst case ICI assumption is calculated by Zhao and Haggman [128]. In the same paper, in order to calculate accurate BER for the OFDM system with a frequency offset, a numerical method based on the use of expansion series for the error function has been proposed. Similarly, Sathananthan and Tellambura [87] calculate the accurate Symbol Error Rate (SER) if BPSK, QPSK or 16-QAM modulation is used on each sub-carrier. Also Narasimhan [72] studies the performance of the OFDM system with a frequency offset when space-time or space-frequency diversity is used. Russell and Stuber [82] provide an analysis of the amount of ICI generated as a result of channel time variations, by assuming that the ICI has a Gaussian distributed. Using the same model, Robertson and Kaiser [79][80] analyze the effects of ICI on the performance of an OFDM system, then extend their work to an OFDMA case. Ye and Cimini [63] provide tight bounds for the ICI resulting from Doppler spread.

To deal with the ICI problem, two general approaches have been proposed in the literature. One approach is to estimate and then correct the frequency shift. These methods can often successfully remove ICI. However, they often require high degree of computational complexity. The alternative, which usually requires much lower computational complexity, is to decrease the amount of ICI created by frequency shifts by shaping the spectrum of the signal.

Taking the first approach, many authors have proposed data-aided frequency offset estimation methods. Moose [67] proposes an algorithm that estimates the frequency offset, when an OFDM symbol is repeatedly transmitted. Other authors have proposed the use of transmitted training data, either as pilot symbols or as preambles, to estimate the frequency offset. In [23] a method has been proposed that estimates the frequency offset using two training OFDM symbols, while [53] provides another method that only requires the dedication of one OFDM symbol for training. Training preambles have also been used in IEEE 802.11 standard to estimate the frequency offset. A method to utilize this preamble structure to estimate frequency offset has been proposed in [45]. In [26], an estimation algorithm has been proposed that utilizes the embedded pilot symbols intended for channel estimation, to estimate the frequency offset and, therefore, eliminates the need to dedicate special training data for frequency offset estimation. Many blind frequency offset estimation techniques have also been proposed. One blind estimation method has been introduced by Tureli *et al.* [101]. Biao and Hao [10] take a Maximum Likelihood (ML) approach to blind es-

timation and show that the obtained estimator is equivalent to the method proposed in [101]. In other publications, such as [103] and [114], the redundancy existing in the cyclic prefix of the OFDM symbol has been exploited for frequency offset estimation.

Many methods have also been proposed for reduction of ICI generated as a result of a time varying channel, using the estimation and correction approach. Leung and Ho [60] propose a method that uses a successive interference cancellation scheme, where a decision feedback and the knowledge of the channel is used to calculate and successively cancel ICI resulting from a Rayleigh fading channel. Linnartz and Gorokhov [64] use an adaptive Minimum Mean Square Error (MMSE) filter to cancel the ICI created as a result of a Doppler spread, when the channel is frequency selective. Similarly, an MMSE Weiner filter has been used by Sgraja and Lindner [92] for channel estimation and ICI cancellation. Xiaodong and Giannakis [113] propose low complexity MMSE and Decision Feedback Equalization (DFE) methods that remove the ICI created in a frequency selective Rayleigh fading channel. Mostofi *et. al.* [68] present two methods of interpolating the channel variations, by modelling the channel to have piecewise linear variations. By modelling the Doppler spread of the channel as a number of Doppler shifted propagation paths and estimating the parameters of each path, Nakamura *et. al.* [71] propose a method to estimate a fading channel. Kapoor *et. al.* [48] propose an adaptive scheme for reduction of ICI for a multi user system with multiple receive antennas at the base station. In this method, combining of the received signals from different antennas is adapted to minimize the created ICI. For a MIMO OFDM system, Stamoulis *et. al.* [97] provide a method for estimation of the channel variations within an OFDM transmission block, thus enabling the system to remove ICI.

While the estimation methods can usually estimate the frequency shift accurately, the computational complexity associated with these methods are high. Many methods have been proposed that with much lower computational complexity, reduce the sensitivity of the OFDM system to frequency shifts [5]. Another advantage of these methods is that since they do not specifically estimate the frequency shift, they can mitigate ICI, regardless of its source.

The use of windowing to reduce the sensitivity of the OFDM system to frequency offset has been proposed [35][70][99]. Zhao and Haggman [126] propose a simple but effective method, known as the Self-Cancellation Scheme, where the ICI created by the frequency offset is greatly reduced by modulation of the same data symbol on two adjacent sub-carriers, with opposite signs. This method reduces the sensitivity of the system to frequency offsets at the price of halving the transmission rate. The BER and the frequency spectrum of the signal performance of the Zhao-Haggman system have been studied in [128] and [125], respectively. Also a channel estimation method using the pilot symbol pairs (resulting from the use of this scheme) has been offered in [42].

Another similar method to the Zhao-Haggman method is proposed in [86], where the same data symbol is modulated on the sub-carriers l and $N - l$.

The Zhao-Haggman method has subsequently been extended to the case where the same symbol is modulated over L adjacent sub-carriers, with different gains [91][129]. While this extension reduces ICI to an even greater extent, it reduces the transmission rate by a factor of L . Other frequency domain coding schemes have also been proposed that require smaller or no loss of transmission rate, but only provide a small amount of reduction in ICI [88][127].

1.3.2 Water-Filling Solution and Bit-Loading

As mentioned in Section 1.2.3, to implement the concept of the water-filling solution for an OFDM system, bit-loading algorithms are needed that assign the number of bits and the transmission power to each sub-channel. Many algorithms have been proposed in the literature. Hughes-Hartogs [43] proposes an optimal bit-loading algorithm based on an approximation of the water-filling solution. Krongold *et. al.* [55][56] give another optimal algorithm using the Lagrangean techniques. Both these algorithms are optimal and have computational complexity of order $N \log_2 N$. Chow *et. al.* [17] propose a less complex sub-optimal loading algorithm where equal power but different number of bits are assigned to each used sub-channel. Later, it has been shown that degradation due to the equal power assignment is not significant [118]. Kim, Chen and Cioffi [52] modify Chow's algorithm to obtain lower computational complexity. By defining the concepts of *E-tightness* and *B-tightness*, Campello [11][12] and Levin [61], provide optimum bit-loading algorithms that have computational complexity of order N .

Other authors have proposed other methods to reduce the complexity of the algorithms, while preserving near optimal performance. Grunheid and Rohling [34] reduce the required computation, by using the same power and bit allocation for a block of adjacent sub-channels (sub-band). Keller and Hanzo combine this block (sub-band) based approach with spectral pre-distortion (pre-equalization) of the OFDM symbol in [49] and [50].

In most of the algorithms mentioned so far, the optimal or near optimal bit and power loading is achieved by iteratively adding bits to the system. Fischer and Huber [27] present another low complexity sub-optimal algorithm, where the power and the number of bits are assigned such that the SNR on each sub-channel is maximized. Other authors have also proposed non-iterative methods based on mathematically optimizing the SNR for all sub-channels [89][32].

While all above algorithms assign an integer number of bits to each sub-channel, if a fractional number of bits can be assigned, the final assignment can potentially be closer to the water-filling solution. Barreto and Furrer [7] use different coding rates as well as different constellation sizes to achieve this goal. Also, Sonalkar and Shively [93] use an additional MC-SS modulated signal where the channel quality is not good enough to support normal QAM constellations.

Other systems have been proposed that do not use the exact instantaneous CSI to

calculate the bit and power assignments. Song *et. al.* [94][95] propose the calculation of bit and power allocation based on the statistical average of channel gain. Dobre and Yao [22] present a system where separate data packets are transmitted on different sub-channels and the modulation of each sub-channel is adaptively adjusted based on the arrival of acknowledgment packets. Also, Maeda *et. al.* [65] use the fed-back delay profile information instead of using the CSI directly.

To the best of our knowledge, not many attempts have been made to analytically evaluate the performance of the bit loaded systems. However, Schurgers and Srivastava [90] obtain a single parameter model for the loaded OFDM system that can be useful for performing higher layer simulations.

The water-filling concept can also be extended to the multi-user channels. For multi-access channels (Figure 1.9 (a)), Cheng and Verdu [15][105] have obtained the capacity region and have showed that this capacity region can be achieved if multi-user water-filling is used. It is shown that if the users have equal priority, their optimal power spectra obtained from the water-filling solution do not overlap. In other words an FDMA type system can achieve capacity. Also, many algorithms have been proposed that calculate the water-filling power assignment for this channel [69][120][123]. Noting the duality of the broadcast channel (Figure 1.9 (b)) and the multi-access channel [46], Goldsmith and Effros obtain similar capacity region and water-filling solutions for the broadcast channel. While the exact capacity region for the interference channel (Figure 1.9 (c)) is an open problem, many bounds on the capacity region of this channel have been found [13][54]. However, from a more practical perspective, the general capacity region is not of much interest since it is generally assumed that the receivers can cooperate in decoding the received signals. For the more practical case where the receivers cannot cooperate, Yu, Ginnis and Cioffi [119][121] use a game theoretic approach to obtain the capacity region and the water-filling solution that can achieve this region.

Observing the water-filling for multi-user channels, many multi-user bit-loading algorithms have been proposed. For the down-link of a multi-user OFDM system, Rhee and Cioffi [78] propose a method where (similar to Chow's single-user algorithm) each user has a flat power spectral density. Also, Wong *et. al.* [111] propose another algorithm, where first through an iterative algorithm the sub-channels are assigned to different users, then the bit and power allocation are performed. Yin and Liu [117] propose a similar algorithm, where reduced complexity is achieved by breaking the problem into two smaller problems, namely resource allocation and sub-channel and bit assignment. Zhang and Letaief [124] combine the bit and sub-channel allocation with cell selection for the down-link of a cellular OFDM system.

For an interference channel, Lee, Sonalkar and Cioffi [58] provide a centralized multi-user bit loading algorithm based on the water-filling results, where it is assumed that a *spectrum management center* has the exact channel information for all channels. Later, Yu, Ginnis and Cioffi [121] propose a distributed bit-loading algorithm for the interference channel. In this algorithm, each user periodically performs

a single-user bit loading algorithm, while the interference generated by other users will automatically be considered as noise. Another decentralized bit-loading algorithm for multi-channel Wireless Local Area Networks (WLAN) has been proposed by Armada [3][4]. This algorithm assigns the sub-channels to different users using a Carrier Sense Multiple Access (CSMA) scheme.

The concept of water-filling can also be employed in the context of MIMO channels. Since with proper pre-coding and post-processing a memoryless MIMO channel with characteristic matrix \mathbf{H} is equivalent to $r = \text{rank}(\mathbf{H})$ disjoint parallel channels [28], a water-filling solution (in space) can be found to distribute the available power over these parallel channels [2][31][51][57]. This result has also been extended to multi-user cases [107][122]. When the channel has memory, OFDM can be used in conjunction with multiple transmitter and receiver antennas. Raleigh and Cioffi [76] show that in this case, each OFDM sub-channel will be equivalent to r disjoint parallel channels, and the water-filling can be performed in both space and frequency. In the same paper, a practical bit-loading algorithm is proposed for this case. Later, Gao and Faulkner [29] reduce the complexity of this bit-loading algorithm by using the block based bit-loading, where the same power and number of bits are assigned to a block of equivalent channels. Also, Wong *et. al.* [112] use the same concept with trellis coded M-QAM modulations.

In most of the literature concerning water-filling and bit-loading, it has been assumed that perfect CSI is available at the transmitter. While this assumption is not far from reality for non-fading channels, when channel has significant time variations, this assumption does not necessarily hold. Therefore, the water-filling and bit-loading algorithms do not perform as expected. Three factors contribute to the performance loss due to CSI error:

- The channel estimate obtained at the receiver is not exact. This is due to noise, and the limitations of the channel estimation method.
- The fed-back information (CSI or bit and power allocation) must be quantized. Therefore, if the feedback channel rate is limited, noticeable quantization error can occur.
- Due to the delay in the channel estimation, bit-loading algorithm and the feed-back link, the fed-back information is not up-to-date. Depending on the severity of fading and the length of the delay, the difference between the available and the actual CSI can be significant.

The effect of the channel estimation error at the receiver for M-QAM constellations is studied in [100]. Also, Leke and Cioffi [59] show that larger QAM constellations are more vulnerable to CSI error and conclude that in presence of CSI error, extra power should be assigned to the larger constellations. Cheong *et. al.* [16] consider the feed-back rate limitation for a bit-loaded OFDM system. They propose a reduced feedback scheme where only the number of assigned bits is fed-back and the assigned

power is estimated at the transmitter. The effect of outdated CSI has been considered in [89], where the CSI is updated periodically. Here, the power loading is performed assuming worst-case change in the channel condition. Salvekar and Cioffi [83] propose a robust bit-loading algorithm where *channel profile selection* (as opposed to channel estimation) is used. However, channel profile selection is not a suitable technique for general channels.

Souriyal and Pickholtz [96] consider a bit-loaded OFDM system where the reverse channel is implemented using Time Division Duplexing (TDD). In this case the channel can be estimated (or even predicted) at the transmitter. However, mismatch is still present between the estimated (or predicted) and exact CSI. The effect of outdated CSI for a Frequency Division Duplexing (FDD) based system has also been studied [98][115]. It has been suggested that slight increase in power together with some type of diversity can be used to create robust loading algorithms.

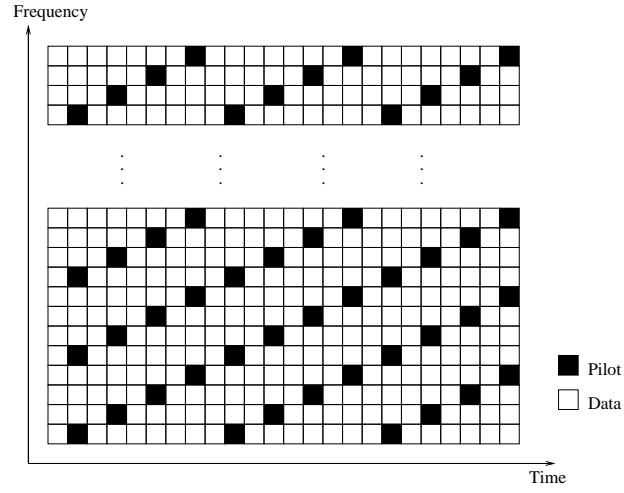


Figure 1.6: Embedded pilots for PSA channel estimation.

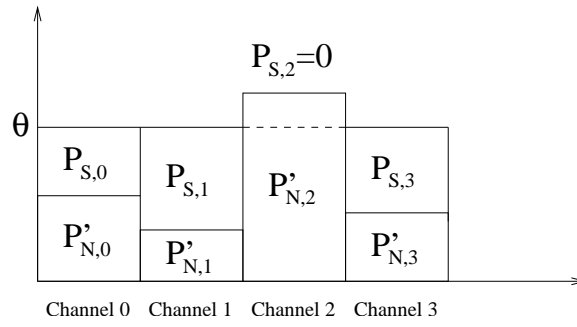


Figure 1.7: Water-filling solution for parallel channels.

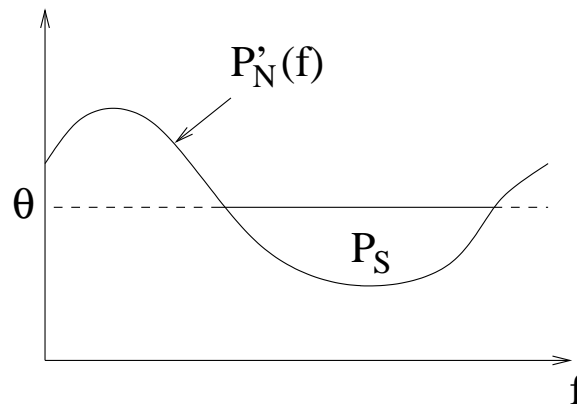


Figure 1.8: Water-filling solution for a channel with colored noise.

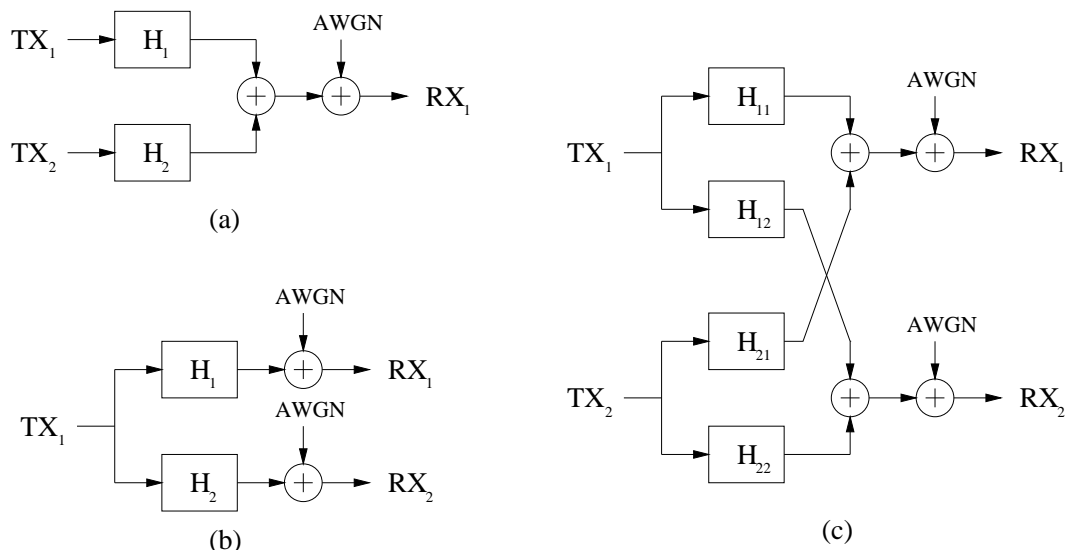


Figure 1.9: Multi-user channels: (a) Multi-access channel, (b) Broadcast channel and (c) Interference channel.

Chapter 2

General Self-Cancellation Scheme

In this chapter we introduce the general self-cancellation scheme. This method can significantly reduce the Inter-Carrier Interference (ICI) in an OFDM system by using windowing operations at the transmitter and the receiver. We first describe the proposed system and show that the self-cancellation scheme proposed by Zhao and Haggman is equivalent to a special case of this system. We then proceed to design the transmitter and receiver windows, based on different criteria. By comparing the performance results of the proposed, the Zhao-Haggman and the conventional OFDM systems, we show that the proposed system has superior performance in presence of an oscillator frequency offset, or when the system is operating over a time-varying channel.

2.1 Motivation

OFDM systems are particularly sensitive to any frequency shift in the signal. When the signal is shifted in frequency, the sub-carriers are no longer orthogonal and ICI is created. Due to particular spectral shape of the OFDM sub-carriers a small frequency shift can result in creation of significant ICI and degradation of the system performance.

Two sources can cause frequency shifts in the signal: oscillator frequency offset and time variations in channel. If the frequency of the local oscillators at the transmitter and the receiver are not matched, a fixed frequency shift is created. Figure 2.1 depicts the creation of ICI when a normalized frequency shift of $\varepsilon = (f_{TX} - f_{RX})T$, where T is the length of the OFDM symbol and f_{TX} and f_{RX} are the frequencies of the oscillators at the transmitter and the receiver, respectively. We can see that when the signal is shifted up by a normalized frequency shift of ε , sampling the signal on the 0th sub-carrier results in a smaller amplitude for the 0th symbol. More importantly, the sample also includes interference from the symbols modulated on other sub-carriers.

While a fixed frequency shift can be created as a result of oscillator frequency offset, a spread of frequency shifts (Doppler spread) is created when the system operates

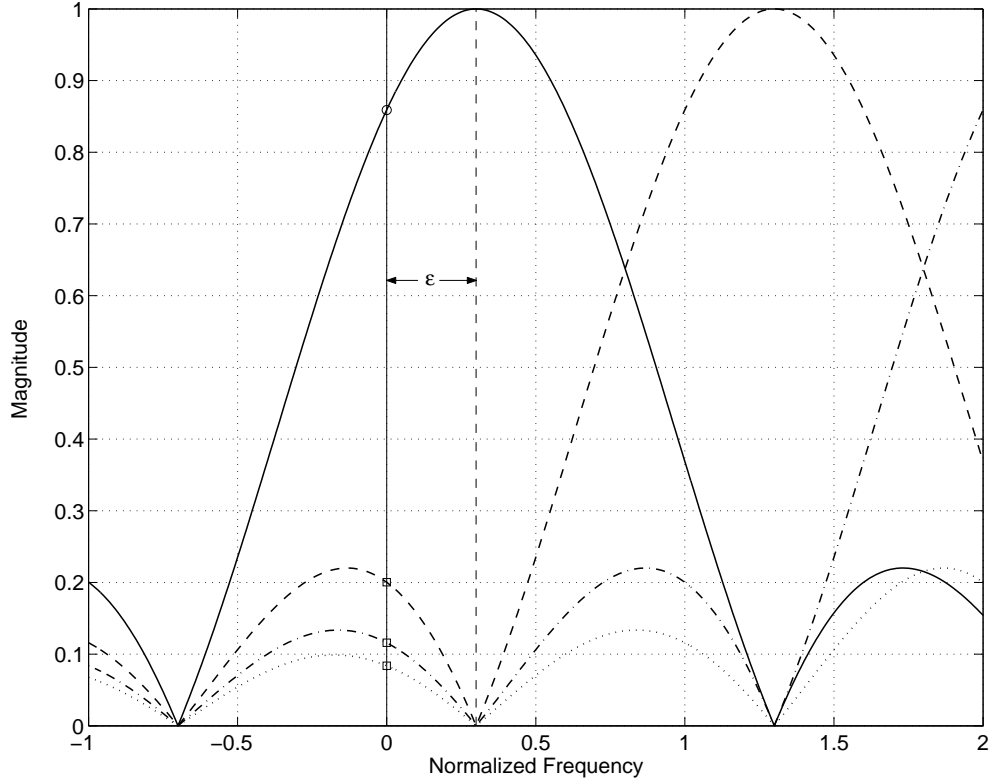


Figure 2.1: Creation of ICI in presence of a fixed frequency shift.

over a time varying (fading) channel. For analysis and design purposes this spread of frequency shifts can be considered a linear combination of many time varying frequency shifts.

Two general approaches to ICI mitigation can be considered. One approach is to estimate and correct the frequency shift. Many methods have been introduced in the literature that successfully estimate and correct a fixed frequency shift. The estimation and correction of a spread of frequency shifts have proved more difficult. The other approach is to use signal processing to shape the spectrum of OFDM sub-carriers such that less ICI is generated as a result of frequency shifts.

The second approach does not completely eliminate the ICI. However, the methods operating based on this approach have two important advantages compared to those using the estimate and correct approach. The first advantage is that these methods require considerably less computational complexity. More importantly, the other advantage of these methods is that since the frequency shift is not estimated, no specific knowledge of the model or the extent of the frequency shift is required. For example, the same method can mitigate ICI whether it is a product of oscillator frequency offset, or it is generated as a result of a time varying channel.

For the frequency offset problem, these methods can either be used with rather accurate oscillators, or it can be used as an alternative to the fine frequency offset

estimation (where the part of frequency offset which is smaller than half the sub-carrier spacing is estimated). For mitigation of the ICI caused by the channel fading, these methods can be used to lower the amount of ICI to tolerable levels.

In this chapter we improve the performance of an ICI mitigation method of the second kind, namely the Zhao-Haggman's self-cancellation scheme, by generalizing it. Particularly we show that the Zhao-Haggman's system is equivalent to using a special windowing operation at the transmitter and the receiver. Then, we proceed to design windows that can improve the performance of the system.

2.2 Zhao-Haggman's Self-Cancellation Scheme

A very simple but effective ICI cancellation scheme is Zhao-Haggman's self-cancellation scheme. In the simplest form of this scheme [126], each data symbol is modulated over two adjacent sub-carriers with opposite signs. In other words, $S_{n+1} = -S_n$, $n = 0, 2, \dots, N - 2$, where S_n is the symbol modulated on the n th sub-carrier. At the receiver these two copies are combined with opposite signs. As a result, the spectrum of the superposition of these two sub-carriers is shaped such that frequency shifts create less ICI. This method has been extended to use L adjacent sub-carriers for transmission of each symbol [129]. In this case the copy on the l th sub-carrier is weighted by the l th coefficient of the polynomial $(1 - D)^{L-1}$, where D denotes one sub-carrier shift in the frequency domain, or

$$a_l = (-1)^l \frac{(L-1)!}{l!(L-1-l)!}, \quad l = 0, \dots, L-1. \quad (2.1)$$

At the receiver these copies are combined with the same weights to produce the decision variable.

Zhao and Haggman have shown that this method can significantly reduce the ICI at the price of lowering the transmission rate by a factor of L . While lowering of the rate makes this method unattractive for larger values of L , Zhao and Haggman show that compared to a half rate convolutionally coded OFDM system, the system using self-cancellation scheme ($L = 2$) has better performance over fading channels or in presence of a frequency offset. In section 2.7, we will also show that our proposed system performs better than the half-rate convolutionally coded OFDM in the presence of frequency shifts.

2.3 System Description

In our general self-cancellation scheme (Figure 2.2), $L - 1$ zeros are inserted between each pair of symbols at the transmitter by the "sample-up" block. In other words,

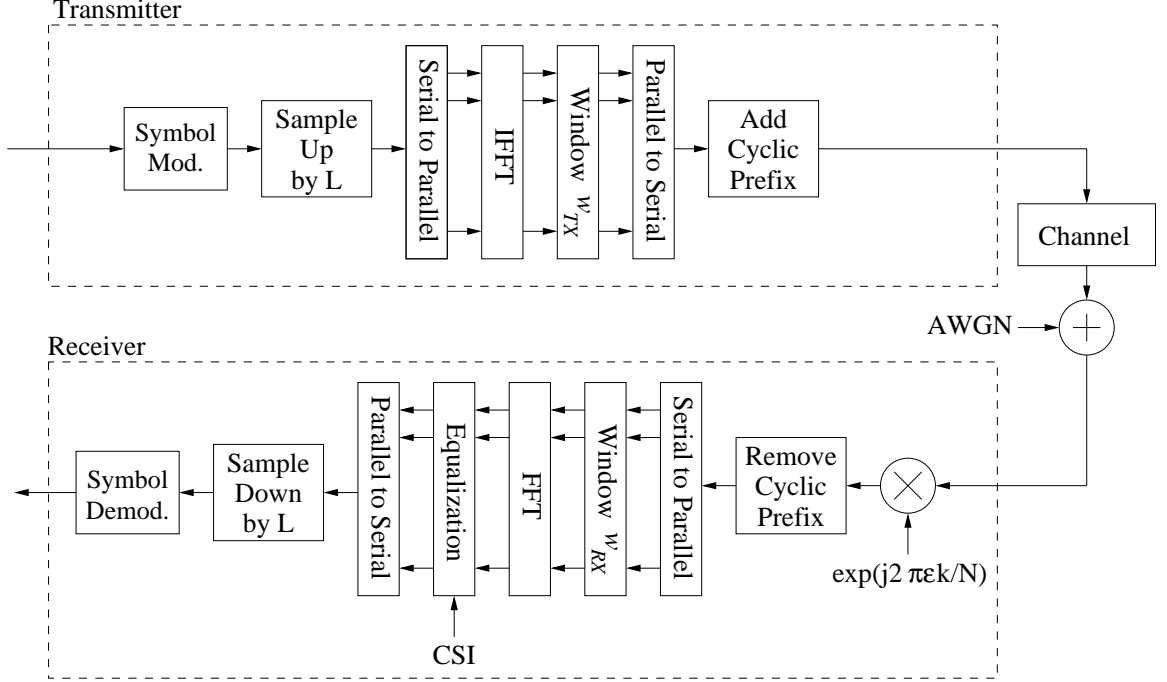


Figure 2.2: Block diagram of an OFDM system employing the general self-cancellation scheme.

in each OFDM symbol, one data symbol is placed on every L th sub-carrier, while the other $L - 1$ sub-carriers are set to zero. Then, after the IFFT operation the OFDM symbol is windowed by the transmit window $w_{TX,k}$, $k = 0, \dots, N - 1$. At the receiver, before the FFT operation the signal is windowed by the receive window $w_{RX,k}$, $k = 0, \dots, N - 1$. After the FFT operation an equalizer corrects the attenuation and phase rotation caused by the channel and/or by the frequency offset. Since two windowing operations with fixed windows are used, the additional complexity of the proposed system is exactly $2N$ multiplications per OFDM symbol, regardless of L .

To design the transmit and receive windows, first by neglecting the noise we design the over-all window $w_k = w_{TX,k}w_{RX,k}$ to reduce the ICI. Then, following the matched filter principle, to achieve the best noise performance, we split the overall window w_k between the transmitter and the receiver such that $|w_{TX,k}| = |w_{RX,k}|$. This is possible since a frequency shift of ε can be modelled with a window $w_{\varepsilon,k} = e^{j2\pi\varepsilon k/N}$, $k = 0, \dots, N - 1$ and the order of these windowing operations (by w_{TX}, w_{RX} and w_{ε}) has no effect on the ICI properties of the signal. Also, note that if circularly symmetric complex additive noise is assumed, the phase of w_k does not affect the noise performance and can be implemented at the transmitter, at the receiver or partially on both sides. For example, we can use

$$w_{TX,k} = \sqrt{|w_k|} e^{j\angle w_k}, \quad (2.2)$$

and

$$w_{RX,k} = \sqrt{|w_k|}. \quad (2.3)$$

Although the windowing operations are performed in the time domain, it is more convenient to explain the analysis and design of the system in the frequency domain. To do this, we represent the overall window as the sum of weighted complex exponentials, or

$$w_k = \sum_{m=-M}^M c_m e^{j2\pi\delta_m k/N}, \quad k = 0, \dots, N-1. \quad (2.4)$$

This means that the windowing operation is equivalent to the summation of $2M + 1$ frequency shifted copies of the signal, each having a normalized frequency shift $\delta_m, m = -M, \dots, M$ and complex weight $c_m, m = -M, \dots, M$. Note that the δ_m values are not constrained to be integers but, instead, frequency shifts that are not integer multiples of the sub-carrier spacing can be used. A frequency shift of δ_m can be performed by windowing the signal by $w_{\delta_m,k} = e^{j2\pi\delta_m k/N}, k = 0, \dots, N-1$.

When a rectangular window (no window) is used in an OFDM system, in the absence of a frequency shift, the frequency domain representation of the signal of sub-carrier n is

$$X_n(l) = S_n I(l - n), \quad (2.5)$$

where S_n is the data symbol modulated on sub-carrier n , l is the frequency index and

$$I(\nu) = \frac{\sin(\pi\nu)}{N \sin(\frac{\pi}{N}\nu)} e^{-j\pi(1-\frac{1}{N})\nu}. \quad (2.6)$$

If a frequency shift of Δf exists, the signal on the sub-carrier n is shifted in frequency by the normalized frequency shift $\varepsilon = \Delta f T$, and is equal to

$$X_{n,\varepsilon}(l) = S_n I(l - n - \varepsilon), \quad (2.7)$$

where T is the length of the OFDM symbol and $1/T$ is the sub-carrier spacing [129].

If instead of a rectangular window, w_k is used, we can write the signal of sub-carrier n in the frequency domain, as

$$\begin{aligned} X_{n,\varepsilon}(l) &= \sum_{m=-M}^M c_m S_n I(l - n - \varepsilon - \delta_m) \\ &= S_n \sum_{m=-M}^M c_m I(l - n - \varepsilon - \delta_m) \\ &= S_n I'_{\boldsymbol{\delta}, \mathbf{c}}(l - n - \varepsilon), \end{aligned} \quad (2.8)$$

where $\mathbf{c} = [c_{-M}, \dots, c_M]$, $\boldsymbol{\delta} = [\delta_{-M}, \dots, \delta_M]$ and $I'_{\boldsymbol{\delta}, \mathbf{c}}(\cdot)$ is defined by

$$I'_{\boldsymbol{\delta}, \mathbf{c}}(\nu) = \sum_{m=-M}^M c_m I(\nu - \delta_m). \quad (2.9)$$

Note that the desired spectrum shape, $I'_{\delta, \mathbf{c}}(\nu)$, is one that does not fall quickly around $\nu = 0$, and has small values (side-lobes) around the positions of other sub-carriers. Such a spectrum results in little ICI in presence of a frequency shift. This point can be better demonstrated by looking at the shape of $I'_{\delta, \mathbf{c}}(\nu)$ after we design the windows in Section 2.6.

2.3.1 Special Case 1: Conventional System

An OFDM system with a rectangular window where only every L th sub-carrier is used for data transmission is a special case of the proposed system with $\delta_0 = 0$, $c_0 = 1$ and $c_m = 0$ for $m \neq 0$. In this case, the windows are $w_{TX,k} = w_{RX,k} = 1$ and, therefore, do not need to be implemented. We refer to such a system as the conventional OFDM system. Note that both the proposed and the Zhao-Haggman systems operate at a lower rate (by a factor of L). Thus, for a fair comparison their performance should be compared to that of a conventional system with a similar L . Keep in mind that such system is less sensitive to frequency shifts than the conventional system with $L = 1$, since there are fewer sub-carriers producing ICI in each OFDM symbol.

2.3.2 Special Case 2: Zhao-Haggman's System

In the Zhao-Haggman method [129], at the transmitter, each symbol is modulated on L adjacent sub-carriers, with weights given by (2.1). This is equivalent to placing the symbol on the first sub-carrier ($l = 0$) and zero on the remaining $L - 1$ sub-carriers, then windowing the result by

$$w_{TX,k} = \sum_{l=0}^{L-1} a_l e^{j2\pi kl/N}, k = 0, \dots, N-1. \quad (2.10)$$

Note that the term with index l creates a copy of the symbol with a shift of l sub-carriers and weight a_l .

At the receiver these copies are combined with the same weights to produce the decision variable, which again is equivalent to windowing the received signal by

$$w_{RX,k} = \sum_{l=0}^{L-1} a_l e^{-j2\pi kl/N}, k = 0, \dots, N-1, \quad (2.11)$$

and taking the decision variable from the first position. Once again, note that the term with index l adds the copy of the symbol modulated on the l th sub-carrier to the result, with weight a_l . By combining the transmit and receive windows we can obtain the overall window

$$w_k = \left(\sum_{l=0}^{L-1} a_l e^{j2\pi kl/N} \right) \left(\sum_{r=0}^{L-1} a_r e^{-j2\pi kr/N} \right), k = 0, \dots, N-1. \quad (2.12)$$

Since a_l are the coefficients of $(1 - D)^{L-1}$, it can easily be shown that (2.12) is equivalent to a special case of the proposed scheme, with parameters

$$\begin{aligned} M &= L - 1 \\ \boldsymbol{\delta} &= [-M, \dots, -1, 0, 1, \dots, M] \\ \mathbf{c} &= [c_{-M}, \dots, c_{-1}, c_0, c_1, \dots, c_M], \end{aligned} \quad (2.13)$$

where c_m are the coefficients of $(1 - D)^{2(L-1)}$ (with a shift of $M = L - 1$ in the index), or

$$c_m = (-1)^m \frac{(2M)!}{(M+m)!(M-m)!}. \quad (2.14)$$

In the special case where $L = 2$ we have $M = 1$, $\boldsymbol{\delta} = [-1, 0, 1]$ and $\mathbf{c} = [-1, 2, -1]$, or

$$\begin{aligned} w_k &= 2 - e^{j2\pi k/N} - e^{-j2\pi k/N} \\ &= 2(1 - \cos(2\pi k/N)), \end{aligned} \quad (2.15)$$

which is a Hanning window [37].

2.4 SIR Analysis

The per-carrier Signal to (inter-carrier) Interference Ratio (SIR) is one measure of the signal degradation caused by frequency shifts. Here we obtain the SIR for the proposed system over a flat AWGN channel, assuming that a normalized frequency shift of ε exists. The result is also valid for the special cases of the conventional and Zhao-Haggman systems.

Given (2.8), the received signal at the sub-carrier l can be described as

$$\begin{aligned} y_l &= \sum_{n \in \mathcal{N}} X_{n,\varepsilon}(l) + n_l \\ &= \sum_{n \in \mathcal{N}} S_n I'_{\boldsymbol{\delta}, \mathbf{c}}(l - n - \varepsilon) + n_l, \end{aligned} \quad (2.16)$$

where \mathcal{N} is the set of all sub-carriers used for symbol transmission (multiples of L), and n_l is the complex AWGN. The term where $l = n$ is the desired term and all the other terms represent ICI. Therefore, neglecting the noise, we can write the SIR for the signal on the l th sub-carrier as

$$\begin{aligned} SIR_{\boldsymbol{\delta}, \mathbf{c}, l}(\varepsilon) &= \frac{|S_l|^2 |I'_{\boldsymbol{\delta}, \mathbf{c}}(-\varepsilon)|^2}{\sum_{n \in \mathcal{N}, n \neq l} |S_n|^2 |I'_{\boldsymbol{\delta}, \mathbf{c}}(n - l - \varepsilon)|^2} \\ &= \frac{|I'_{\boldsymbol{\delta}, \mathbf{c}}(-\varepsilon)|^2}{\sum_{n \in \mathcal{N}, n \neq l} |I'_{\boldsymbol{\delta}, \mathbf{c}}(n - l - \varepsilon)|^2}, \end{aligned} \quad (2.17)$$

where we have assumed that S_l are statistically independent and have zero mean and equal average power.

Since the position of the modulated symbols and the function $I'_{\delta, \mathbf{c}}(\cdot)$ are cyclically symmetric, without loss of generality we can remove the index l and have

$$SIR_{\delta, \mathbf{c}}(\varepsilon) = \frac{|I'_{\delta, \mathbf{c}}(-\varepsilon)|^2}{\sum_{n \in \mathcal{N}, n \neq 0} |I'_{\delta, \mathbf{c}}(n - \varepsilon)|^2}. \quad (2.18)$$

In Section 2.6.1 we use this result to numerically find the design parameters \mathbf{c} and δ , for a given minimum desired SIR.

2.5 BER Analysis

In this section we use a method similar to the one used in [87] to calculate the exact BER of the proposed system in the presence of a fixed frequency shift. We assume that the system operates over a flat AWGN channel and that the data symbols are QPSK modulated. Similar analysis is possible if a 16-QAM modulation is used [87]. We also assume that perfect equalization corrects the phase rotation caused by the frequency shift. This analysis is valid regardless of the design parameters L , M , δ and \mathbf{c} .

2.5.1 Effect of Windowing on Signal and Noise Power

Before we proceed to calculate the BER of the system with QPSK modulation, we look at the effect of the transmit and receive windows on the signal and noise power.

Signal Power

The OFDM symbol after the windowing operation can be written as

$$x_k = \sum_{n \in \mathcal{N}} w_{TX,k} f'_{k,n} S_n, \quad k = 0, \dots, N-1, \quad (2.19)$$

where $f'_{k,n} = \frac{1}{\sqrt{N}} e^{j2\pi kn/N}$ are the IFFT coefficients. Assuming that the S_n are statistically independent, the transmitted symbol energy for the symbol S_n is

$$\begin{aligned} E_s &= \sum_{k=0}^{N-1} |w_{TX,k} f'_{k,n} S_n|^2 \\ &= \frac{2}{N} \sum_{k=0}^{N-1} |w_{TX,k}|^2. \end{aligned} \quad (2.20)$$

We have assumed that the in-phase and quadrature components of S_n , $\text{Re}\{S_n\}$ and $\text{Im}\{S_n\}$, are chosen from $\{-1, 1\}$, therefore $|S_n|^2 = 2$. Thus,

$$E_b = \frac{1}{N} \sum_{k=0}^{N-1} |w_{TX,k}|^2, \quad (2.21)$$

where $E_b = E_s/2$ is the transmitted energy per bit.

Noise Power

At the receiver the value of noise on sub-carrier l is

$$n_l = \sum_{k=0}^{N-1} f_{l,k} w_{RX,k} e^{-j2\pi k\varepsilon/N} n'_k, \quad (2.22)$$

where $f_{n,k} = \frac{1}{\sqrt{N}} e^{-j2\pi kn/N}$ are the FFT coefficients and $e^{-j2\pi k\varepsilon/N}$ represents the frequency shift. Also, n'_k is the noise value added in the channel at time k and has zero mean and variance $\sigma_{n'}^2 = N_0$. The power of the noise on sub-carrier l can be given as

$$\begin{aligned} \sigma_n^2 &= \text{E}[n_l n_l^*] \\ &= \sum_{k=0}^{N-1} \sum_{r=0}^{N-1} w_{RX,k} w_{RX,r}^* \text{E}[n'_k n_r'^*] e^{-j2\pi k\varepsilon/N} e^{j2\pi r\varepsilon/N} f_{l,k} f_{l,r}^* \\ &= \frac{\sigma_{n'}^2}{N} \sum_{k=0}^{N-1} |w_{RX,k}|^2. \end{aligned} \quad (2.23)$$

Here we have used the fact that $\text{E}[n'_k n_r'^*] = 0$ for $k \neq r$ and $\text{E}[n'_k n_r'^*] = \sigma_{n'}^2$ for $k = r$.

2.5.2 BER Calculation

To calculate the BER of the proposed system with QPSK modulation, without any loss of generality, we consider the bit modulated on the in-phase component of the 0th sub-carrier. From (2.16), the received signal on the 0th sub-carrier is

$$y_0 = \sum_{l \in \mathcal{N}} I'_{\delta,c}(-l - \varepsilon) S_l + n_0, \quad (2.24)$$

where n_0 is Gaussian with zero mean and variance given by (2.23). If perfect equalization is assumed, the phase rotation of the symbol S_0 due to the frequency shift is exactly corrected and at the output of the equalizer we have

$$z_0 = \frac{I_{\delta,c}^*(-\varepsilon)}{|I'_{\delta,c}(-\varepsilon)|} y_0 = \sum_{l \in \mathcal{N}} I_l S_l + \frac{I_{\delta,c}^*(-\varepsilon)}{|I'_{\delta,c}(-\varepsilon)|} n_0, \quad (2.25)$$

where to simplify the notation we have defined

$$I_l = \frac{I'_{\delta, \mathbf{c}}(-l - \varepsilon) I'^*_{\delta, \mathbf{c}}(-\varepsilon)}{|I'_{\delta, \mathbf{c}}(-\varepsilon)|}. \quad (2.26)$$

Note that in general I_l are complex numbers. However, I_0 is a real number. Furthermore, without loss of generality we assume that the transmitted data bit is $\text{Re}\{S_0\} = 1$. Thus,

$$z_0 = I_0 + jI_0\text{Im}\{S_0\} + \sum_{l \in \mathcal{N}, l \neq 0} I_l S_l + \frac{I'^*_{\delta, \mathbf{c}}(-\varepsilon)}{|I'_{\delta, \mathbf{c}}(-\varepsilon)|} n_0. \quad (2.27)$$

To detect the considered bit, we must examine the real part of z_0 ,

$$\begin{aligned} \text{Re}\{z_0\} &= I_0 + \sum_{l \in \mathcal{N}, l \neq 0} \text{Re}\{I_l S_l\} + n''_0 \\ &= I_0 + \sum_{l \in \mathcal{N}, l \neq 0} (\text{Re}\{I_l\}\text{Re}\{S_l\} - \text{Im}\{I_l\}\text{Im}\{S_l\}) + n''_0, \end{aligned} \quad (2.28)$$

where $\text{Re}\{S_l\}$ and $\text{Im}\{S_l\}$ are the bits modulated on the in-phase and quadrature components of sub-carrier l and are independently chosen from the set $\{1, -1\}$ with equal probability, and

$$n''_0 = \text{Re} \left\{ \frac{I'^*_{\delta, \mathbf{c}}(-\varepsilon)}{|I'_{\delta, \mathbf{c}}(-\varepsilon)|} n_0 \right\}, \quad (2.29)$$

which has variance $\sigma_{n''}^2 = \sigma_n^2$. If we define $u_0 = \text{Re}\{z_0\} - n''_0$, the characteristic function of u_0 can be calculated as

$$\Phi_{u_0}(\omega) = e^{j\omega I_0} \prod_{l \in \mathcal{N}, l \neq 0} \cos(\omega \text{Re}\{I_l\}) \cos(\omega \text{Im}\{I_l\}). \quad (2.30)$$

Now, using Beaulieu series [8][9] we can calculate the BER of the system. An error in the considered bit will occur if $\text{Re}\{z_0\} < 0$ in other words

$$\begin{aligned} P_{b|u_0=u} &= \text{Prob}(\text{Re}\{z_0\} < 0) \\ &= Q\left(\frac{u}{\sigma_n}\right). \end{aligned} \quad (2.31)$$

If we use the $Q(\cdot)$ function representation given in [17, Eq. (10)],

$$Q(x) = \frac{1}{2} - \sum_{m \in \mathcal{M}} \frac{2}{\pi m} e^{-\frac{1}{2}m^2\omega_0^2} \sin(m\omega_0 x) + e(x, \omega_0), \quad (2.32)$$

where $\mathcal{M} = \{1, 3, 5, \dots\}$ and the error term $e(x, \omega_0)$ is negligible for small values of ω_0 , we have

$$P_{b|u_0=u} = \frac{1}{2} - \sum_{m \in \mathcal{M}} \frac{2}{\pi m} e^{-\frac{1}{2}m^2\omega_0^2} \sin\left(\frac{m\omega_0 u}{\sigma_n}\right) + e\left(\frac{m\omega_0 u}{\sigma_n}, \omega_0\right). \quad (2.33)$$

To calculate the average BER, we must average (2.33) with respect to u_0 , thus

$$P_b = \frac{1}{2} - \sum_{m \in \mathcal{M}} \frac{2}{\pi m} e^{-\frac{1}{2}m^2\omega_0^2} \mathbb{E}_{u_0} \left[\sin\left(\frac{m\omega_0 u}{\sigma_n}\right) \right], \quad (2.34)$$

where the error term has been neglected. The expected value term can easily be found from the characteristic function

$$\mathbb{E}_{u_0} \left[\sin\left(\frac{m\omega_0 u}{\sigma_n}\right) \right] = \text{Im} \left\{ \Phi_{u_0} \left(\frac{m\omega_0}{\sigma_n} \right) \right\}, \quad (2.35)$$

thus

$$P_b = \frac{1}{2} - \sum_{m \in \mathcal{M}} \frac{2}{\pi m} e^{-\frac{1}{2}m^2\omega_0^2} \text{Im} \left\{ \Phi_{u_0} \left(\frac{m\omega_0}{\sigma_n} \right) \right\}. \quad (2.36)$$

From (2.21) and (2.23) we have

$$\begin{aligned} \frac{E_b}{N_0} &= \frac{E_s}{2\sigma_{n'}^2} \\ &= \frac{1}{N^2\sigma_n^2} \left(\sum_{k=0}^{N-1} |w_{TX,k}|^2 \right) \left(\sum_{k=0}^{N-1} |w_{RX,k}|^2 \right), \end{aligned} \quad (2.37)$$

or

$$\sigma_n = \frac{1}{N\sqrt{E_b/N_0}} \sqrt{\left(\sum_{k=0}^{N-1} |w_{TX,k}|^2 \right) \left(\sum_{k=0}^{N-1} |w_{RX,k}|^2 \right)}. \quad (2.38)$$

By using (2.38) in (2.36) we find

$$\begin{aligned} P_b &= \frac{1}{2} - \sum_{m \in \mathcal{M}} \frac{2}{\pi m} e^{-\frac{1}{2}m^2\omega_0^2} \text{Im} \\ &\quad \left\{ \Phi_{u_0} \left(\frac{mN\omega_0}{\sqrt{\left(\sum_{k=0}^{N-1} |w_{TX,k}|^2 \right) \left(\sum_{k=0}^{N-1} |w_{RX,k}|^2 \right)}} \sqrt{\frac{E_b}{N_0}} \right) \right\}. \end{aligned} \quad (2.39)$$

Given the E_b/N_0 , the BER can be numerically calculated from (2.39).

2.6 Window Design

To design a system that will perform better than the conventional and the Zhao-Haggman systems given N , L and M , parameters $\boldsymbol{\delta}$ and \boldsymbol{c} must be found such that frequency shifts create less ICI. Note that $\boldsymbol{\delta}$ and \boldsymbol{c} can strongly depend on L and M . For example, with a larger L , the main lobe of $I'_{\boldsymbol{\delta}, \boldsymbol{c}}(.)$ can be wider. Therefore, the optimal design can be significantly different for different values of L . Also, a larger M allows for more flexibility in the window design process by increasing the number of degrees of freedom. In this section we provide two design methods to find such parameters. Note that since the system is implemented using fixed windows, the design parameters or the method in which they are found have no effect on the computational complexity of the system. To design the parameters independent of the channel response, we must give equal weights to all sub-carriers. This is equivalent to assuming an AWGN channel. Hence, we can use the SIR and BER equations obtained in Sections 2.4 and 2.5.

2.6.1 SIR based Design

One way to design the system parameters is to consider the SIR of the system. In this design method we search for the parameters that result in an SIR equal to or larger than a minimum desired SIR, SIR_{min} , for the largest range of ε . For a given M , let us define

$$\varepsilon_{max}(SIR_{min}, \boldsymbol{\delta}, \boldsymbol{c}) = \max \left\{ \varepsilon \mid \forall \beta, |\beta| < \varepsilon; SIR_{\boldsymbol{\delta}, \boldsymbol{c}}(\beta) \geq SIR_{min} \right\}. \quad (2.40)$$

In other words, $[-\varepsilon_{max}(SIR_{min}, \boldsymbol{\delta}, \boldsymbol{c}), \varepsilon_{max}(SIR_{min}, \boldsymbol{\delta}, \boldsymbol{c})]$ is the largest symmetric range of normalized frequency shifts where SIR is larger than or equal to SIR_{min} . Now, we find the design parameters $\boldsymbol{\delta}$ and \boldsymbol{c} that maximize $\varepsilon_{max}(SIR_{min}, \boldsymbol{\delta}, \boldsymbol{c})$, or

$$(\boldsymbol{\delta}_{opt}, \boldsymbol{c}_{opt}) = \arg \max_{(\boldsymbol{\delta}, \boldsymbol{c})} \varepsilon_{max}(SIR_{min}, \boldsymbol{\delta}, \boldsymbol{c}). \quad (2.41)$$

Since we want the system to have equal performance for positive and negative frequency shifts, the signal in frequency domain must be symmetric. Therefore, the search is simplified to a degree since symmetry dictates that $\delta_0 = 0$, $\delta_m = -\delta_{-m}$ and $c_m = c_{-m}^*$. Furthermore, all combining weights can be normalized such that $c_0 = 1$.

Given N , M and L , we find these parameters using a numerical exhaustive search. Note that while such a search might not find the optimum window, if the parameters are varied with small steps, the difference between the designed window and the optimal one will be small. Here we have used a step size equal to 0.01 for all c_m and δ_m parameters. Also, note that while the computational complexity of this search is large, since this search is only performed in the design process and not in the system itself, it does not increase the computational complexity of the system. For a simple case of $N = 64$, $L = 2$ and $M = 1$, the design parameters for $SIR_{min} = 25\text{dB}$ and

20dB have been found and are presented in Table 2.1. These SIR_{min} values have been chosen assuming that they represent tolerable amounts of ICI.

Table 2.1: Design parameters obtained from the SIR based design method, $N = 64, L = 2, M = 1$.

Design	SIR_{min}	δ_1	c_1	$\max \varepsilon_{max}$
A	25dB	0.77	$-0.39 - 0.33j$	0.54
B	20dB	0.19	$-0.51 + 0.34j$	0.69

The SIR of these designs as a function of normalized frequency shift has been compared to those of the conventional and the Zhao-Haggman systems (with $L = 2$) in Figure 2.3. Note that if the self-cancellation scheme is used to replace a fine frequency offset estimation method, we will only be interested in frequency shifts in the range $|\varepsilon| < 0.5$, but if it is used together with a rather accurate oscillator, or if it is used to mitigate ICI generated as a result of a fading channel, frequency shifts larger than 0.5 should also be considered. We can see that the proposed method can significantly increase the range of frequency shifts where the desired SIR (or better)

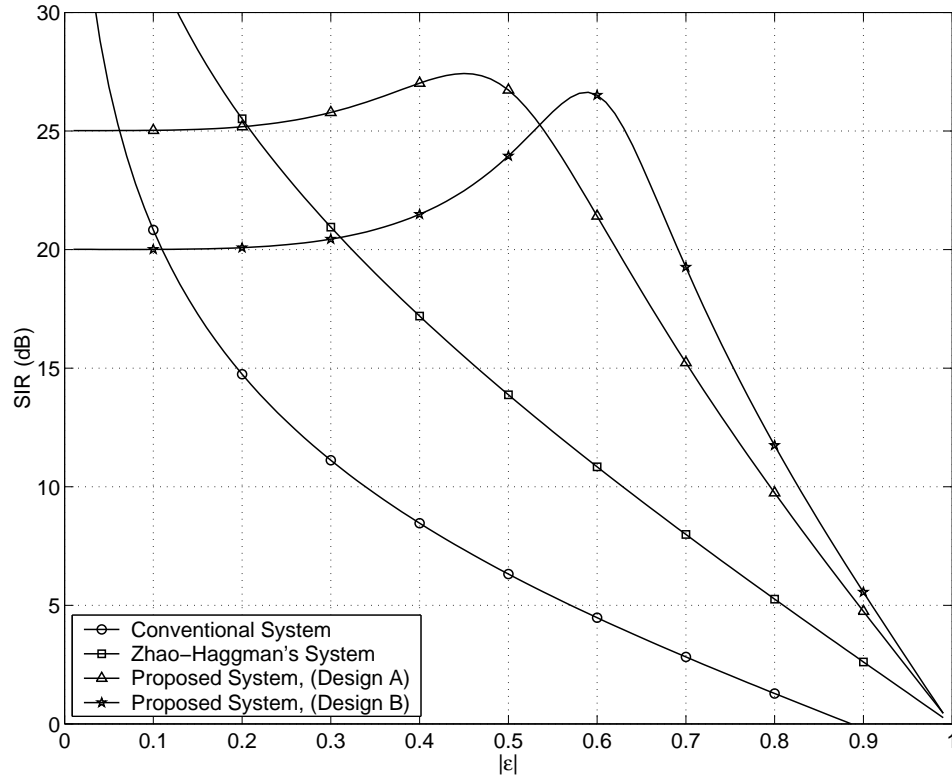


Figure 2.3: SIR of the conventional, Zhao-Haggman and proposed (Designs A and B) systems, for $L = 2$.

is obtained. Although at the low frequency shifts the proposed system has a lower SIR than the conventional and Zhao-Haggman systems, the SIR is still large enough to have little effect on the BER performance of the system. Later, in Section 2.7 we will show that the degradation in BER due to this small amount of ICI is negligible.

Figure 2.4 depicts $I'_{\delta,c}(\nu)$ for the conventional, Zhao-Haggman and the proposed system (Design A). By looking at the first side-lobe, we can see that the worst case interference that the symbol modulated on sub-carrier 0 generates on sub-carrier 2, for $|\varepsilon| < 0.54$, is significantly reduced. Here, this translates into a lower total ICI, since in this case the first side-lobe is dominant. In general, SIR is a more accurate measure, since it considers the total interference from all other used sub-carriers.

We have also found the designs with $N = 64$, $L = 4$, $M = 1$ and $SIR_{min} = 25\text{dB}$ and 20dB . These designs are given in Table 2.2.

Also the SIR performance of these designs is compared to those of the Zhao-Haggman system with $L = 4$ in Figure 2.5. Once again we observe that the designed windows can provide the desired SIR over a large range of frequency shifts compared to the existing systems. However, these designs may be of less interest since a large value of L means that the system must operate at a lower transmission rate.

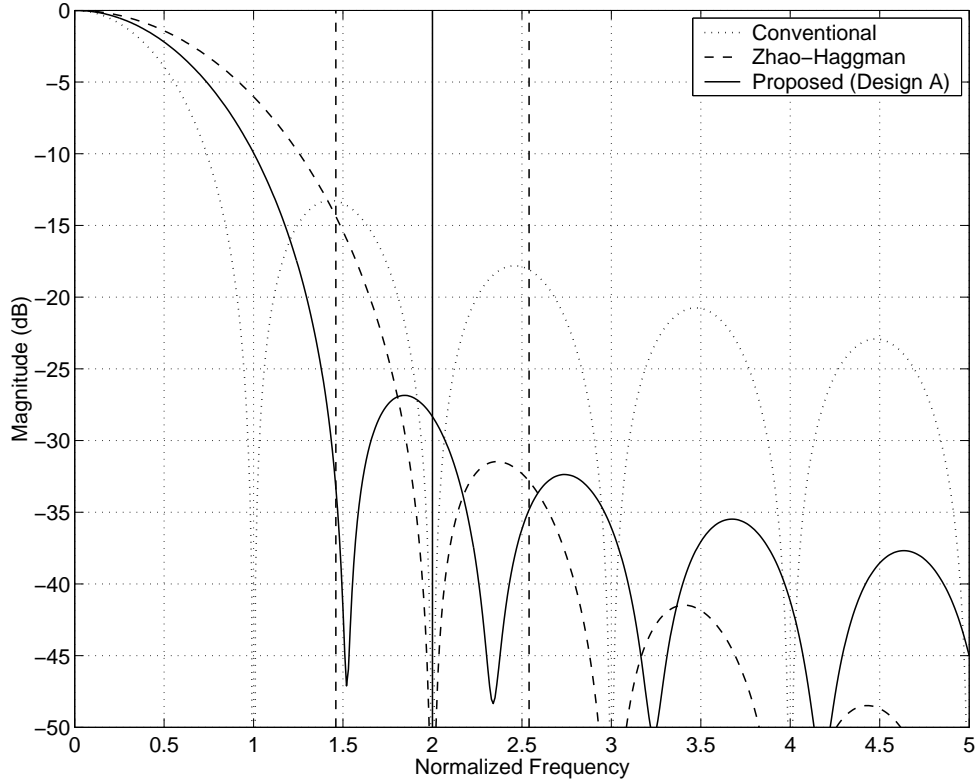


Figure 2.4: $I'_{\delta,c}(\nu)$ for the conventional, Zhao-Haggman and the proposed system (Design A).

Table 2.2: Design parameters obtained from the SIR based design method, $N = 64, L = 4, M = 1$.

Design	SIR_{min}	δ_1	c_1	ε_{max}
C	25dB	0.81	$-0.48 + 0.34i$	1.47
D	20dB	1.09	$-0.47 - 0.10i$	1.83

We have also considered the case where $N = 64, L = 2$ and $M = 2$. However, the larger value of M has only resulted in negligible increase in $\max \varepsilon_{max}$.

2.6.2 BER based Design

Since the SIR based parameter design does not consider the noise performance of the system, it is possible that the parameters obtained from the above design method cause noise enhancement and thus the BER performance of the designed system is not necessarily better than the existing systems. To address the potential noise problem, a design method based on the exact BER value (Section 2.5) is possible. In

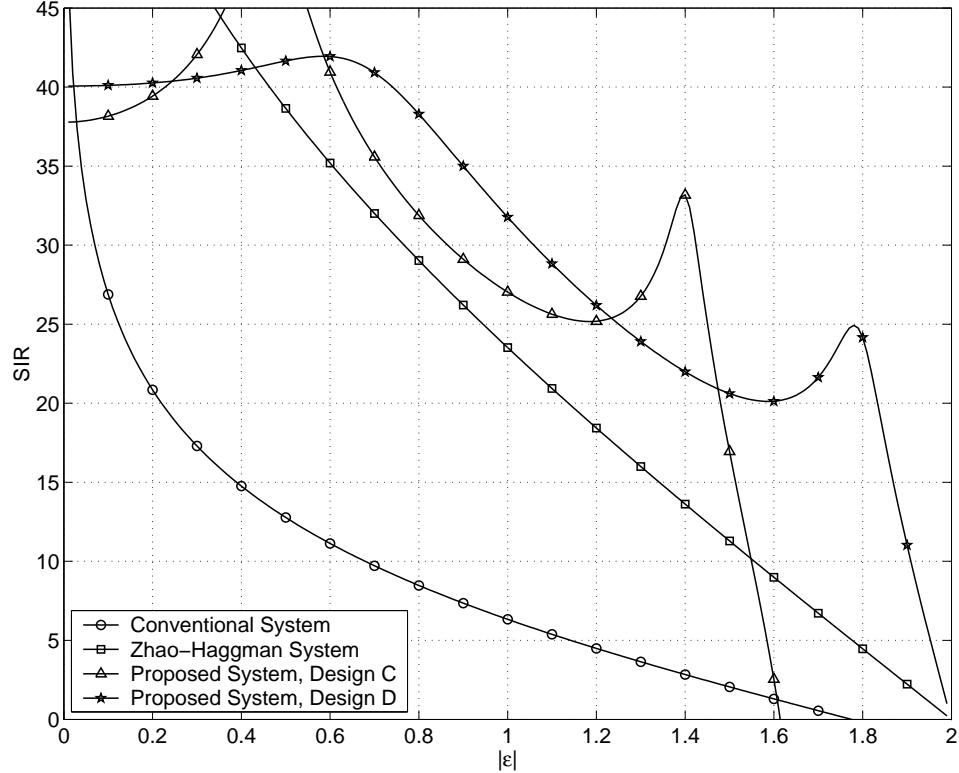


Figure 2.5: SIR of the conventional, Zhao-Haggman and proposed (Designs C and D) systems, for $L = 4$.

this method, for a given BER and a maximum available E_b/N_0 we find the design parameters that maximize the range of tolerable frequency shifts. While this design method is much more computationally complex compared to the SIR based design method, the resulting designs should be more reliable since both noise and interference are considered.

Let us define $\gamma_{\delta, \mathbf{c}}(p, \varepsilon)$ as the value of E_b/N_0 that results in a BER of $P_b = p$ in presence of a normalized frequency shift of ε . Now we can define

$$\varepsilon_{max}(p, \gamma_{max}, \delta, \mathbf{c}) = \max \left\{ \varepsilon \mid \forall \beta, |\beta| < \varepsilon; \gamma_{\delta, \mathbf{c}}(p, \beta) \leq \gamma_{max} \right\}. \quad (2.42)$$

In other words, $[-\varepsilon_{max}(p, \gamma_{max}, \delta, \mathbf{c}), \varepsilon_{max}(p, \gamma_{max}, \delta, \mathbf{c})]$ is the largest symmetric range of ε where an E_b/N_0 less than or equal to γ_{max} is required to result in $P_b = p$. Given the above definitions we can find the design parameters from

$$(\delta_{opt}, \mathbf{c}_{opt}) = \arg \max_{(\delta, \mathbf{c})} \varepsilon_{max}(p, \gamma_{max}, \delta, \mathbf{c}). \quad (2.43)$$

The parameters found based on the above criterion with $L = 2$, $M = 1$, $p = 10^{-4}$ and $\gamma_{max} = 10\text{dB}$ and 13dB are presented in Table 2.3. These γ_{max} values have been chosen assuming that they represent the amount of transmit power the system can afford for the target BER.

Table 2.3: Design parameters obtained from the BER based design method, $N = 64$, $L = 2$, $M = 1$, $p = 10^{-4}$.

Design	γ_{max}	δ_1	c_1	$\max \varepsilon_{max}$
E	10dB	0.72	$-0.50 - 0.63j$	0.45
F	13dB	0.40	$-0.58 + 1.68j$	0.66

Figure 2.6 depicts the required E_b/N_0 for the above designs as a function of ε and compares them to those of the conventional and Zhao-Haggman systems. The figure shows that the proposed system can increase the range of tolerable frequency shifts. From another point of view, we can see that while these designs result in slight loss (about 0.25dB for Design E and 0.5dB for Design F) at low frequency shifts, at higher frequency shifts, they are able to achieve up to 1.5dB gain.

2.7 Results

In this section we present the BER performance of the proposed system under different assumptions and compare them to those of the conventional and Zhao-Haggman systems with $L = 2$. But first, let us compare the BER performance of the proposed system with designs A, B, E and F. Figure 2.7 depicts the BER of the conventional

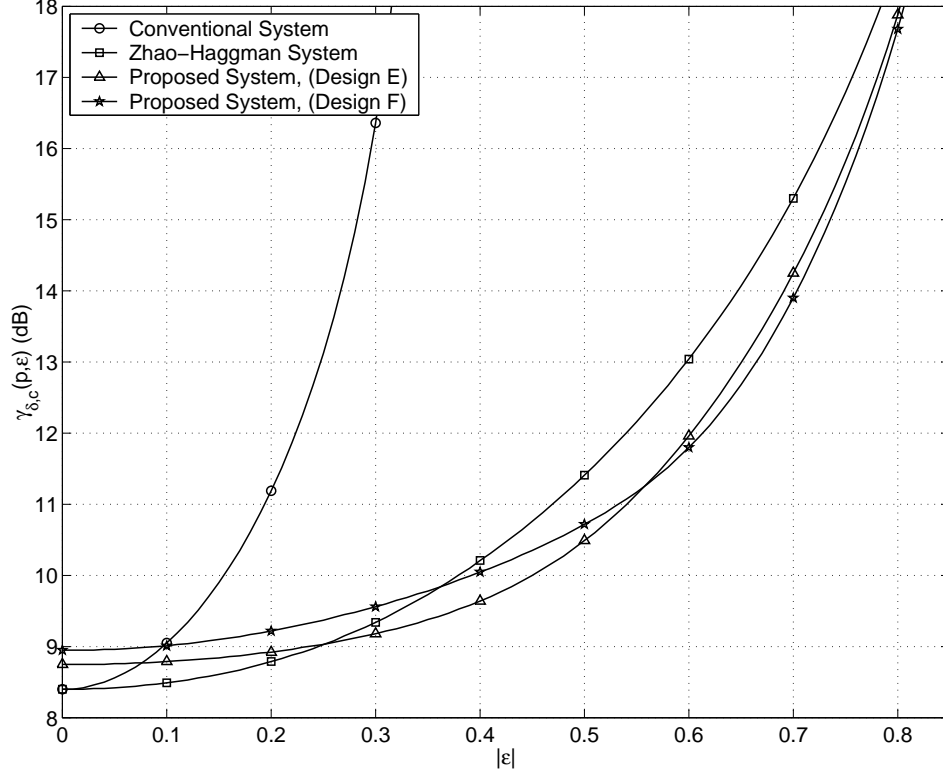


Figure 2.6: Required E_b/N_0 of the conventional, Zhao-Haggman and proposed (Designs E and F) systems for $L = 2$ and $p = 10^{-4}$.

system and the proposed system with designs A, B, E and F, operating over an AWGN channel and in presence of fixed normalized frequency offsets of $\varepsilon = 0$ and 0.5 . Here we have assumed that perfect channel information is available. We can see that as expected, under the above assumptions design E has the best BER performance. However, we should keep in mind that under different circumstances, other designs might perform better.

To compare the proposed system with the conventional and the Zhao-Haggman systems, we consider one of the designs, namely design A. First, we show that when the system operates over a flat AWGN channel and a frequency offset is present, the results obtained from Monte-Carlo simulations match the calculated results if perfect equalization is assumed. We then present the results obtained for the cases where perfect channel equalization is not assumed. The performance of the proposed system operating over frequency selective fading channels is also presented and compared to the conventional and Zhao-Haggman systems. While the proposed system can be employed with any symbol constellation such as M-QAM or M-PSK, here for simplicity we assume that in all cases, symbols are QPSK modulated.

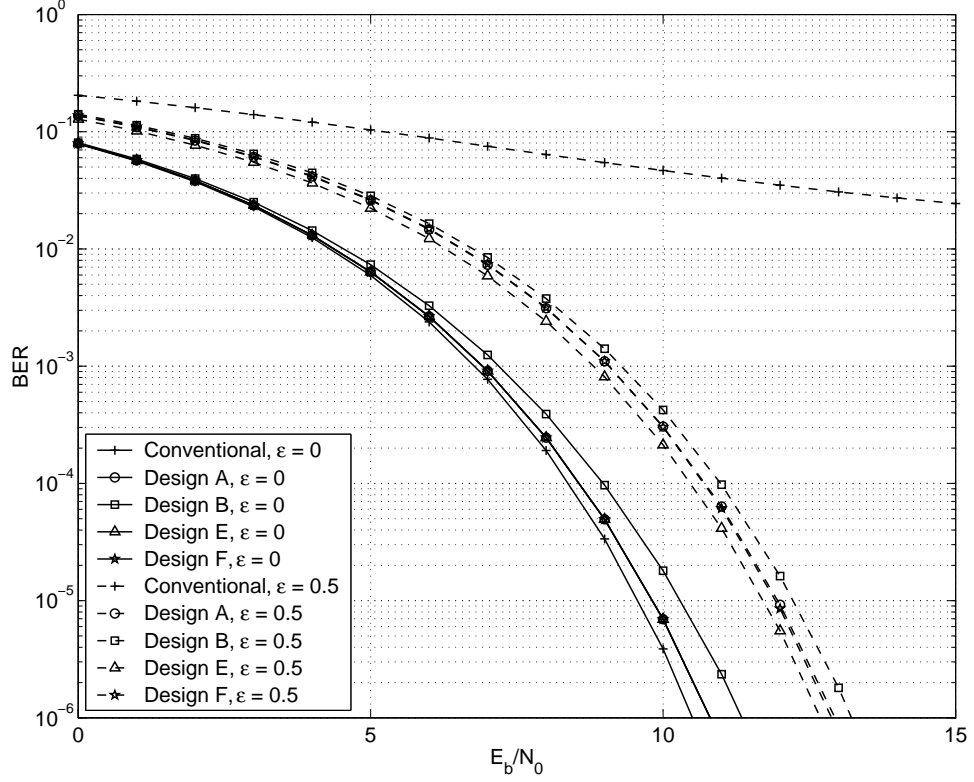


Figure 2.7: BER comparison of designs A, B, E and F, over a flat AWGN channel with perfect equalization.

2.7.1 Mitigation of ICI due to Frequency Offset

When the frequency of the local oscillator at the receiver, f_{RX} , is different from that of the transmitter, f_{TX} , a frequency shift of $\Delta f = f_{TX} - f_{RX}$ exists. Here, we present and compare the BER performance of the proposed, Zhao-Haggman and the conventional systems, for the normalized frequency offsets $\varepsilon = \Delta f T = 0, 0.5$ and 0.7 . Note that if the proposed scheme is used to replace the fine frequency offset estimation, $\varepsilon = 0.5$ represents the worst case.

Coherent System

Figure 2.8 depicts the BER results obtained from the Monte-Carlo simulations as well as the calculations (Section 2.5) for the conventional, Zhao-Haggman and the proposed system (Design A), over a flat AWGN channel. It has been assumed that perfect equalization is performed to correct the phase rotation of the symbols due to the frequency offset. We observe that the theoretical and simulation results agree. Also, we see that, while the proposed system performs slightly (about 0.25dB) worse than the conventional and Zhao-Haggman systems in absence of frequency offset, gains of 1dB or more can be obtained at higher frequency offsets.

The above results have been obtained under the assumption that perfect equalization is performed. However, this assumption is not always realistic. Let us look at the system performance without perfect equalization. We assume that a two dimensional Pilot Symbol Aided Modulation (PSAM) is used [73], i.e. pseudo-random pilot symbols are embedded in the OFDM symbol at the transmitter. At the receiver, since the value of these symbols are known, samples of the channel at the pilot locations can be estimated. These samples are then interpolated to obtain the channel information at other locations. Here an ideal filter has been used for interpolation. In other words, the channel samples have been convolved with a Sinc function to obtain the interpolated values for the channel at non-pilot positions.

Figure 2.9 depicts the BER results when pilot based channel estimation is employed. We have assumed that 25% of the symbols are embedded pilots. We observe that when perfect equalization is not assumed, the advantage of the proposed system over the Zhao-Haggman and conventional systems is more pronounced. For example, considering a BER of 10^{-5} , approximately 7dB gain is achieved at $\varepsilon = 0.7$. This large gain is due to the fact that, in the presence of frequency offset, the pilots are to some degree corrupted by interference. Thus, the channel estimate is not reliable. The

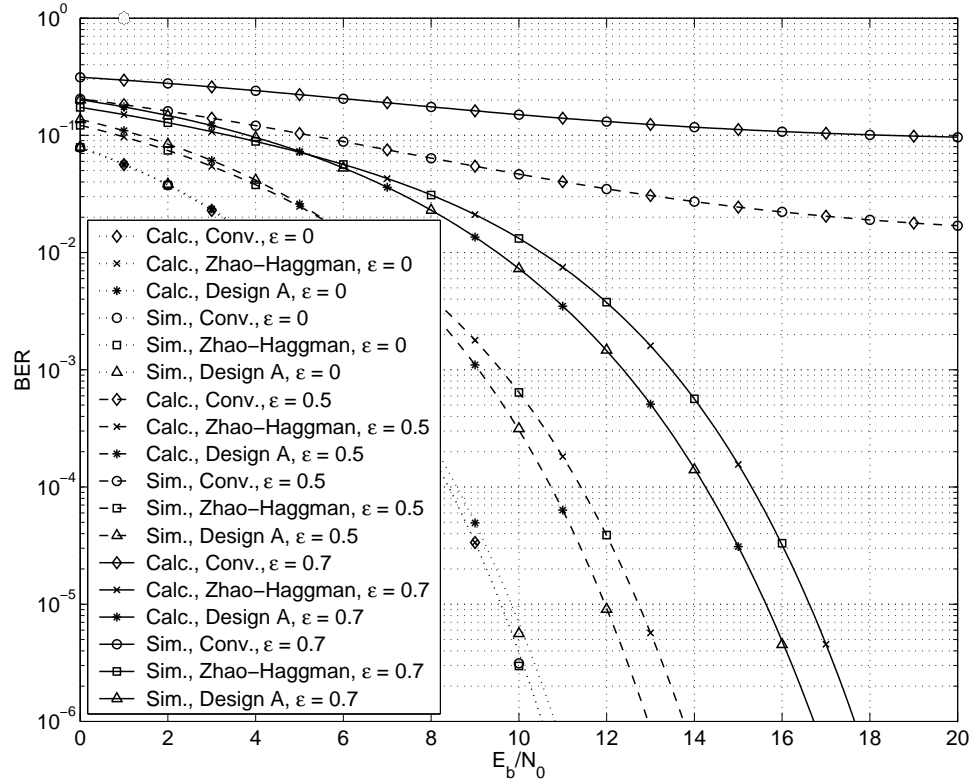


Figure 2.8: Calculated and simulated BER for the conventional, Zhao-Haggman and proposed system (Design A), over a flat AWGN channel with perfect equalization.

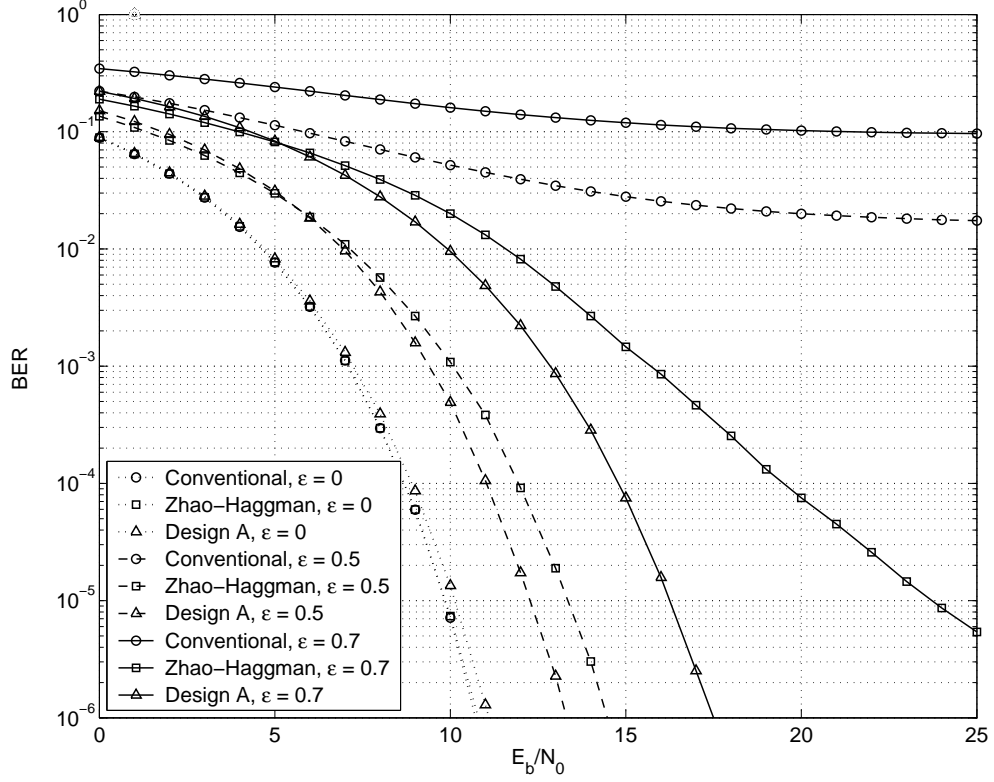


Figure 2.9: BER of the conventional, Zhao-Haggman and proposed system (Design A) with pilot based channel estimation, over a flat AWGN channel.

unreliable channel estimate results in magnification of the effect of the ICI, when it is used in the equalization process. Since the proposed method has less ICI to begin with, its final performance is considerably better.

Non-Coherent System

A non-coherent OFDM system can be implemented if DPSK modulation is used. Such a system is similar to the one depicted in Figure 2.2, if the “equalization” block is removed and DPSK modulation and demodulation are performed in the corresponding blocks. In this case, the information is placed in the phase difference between the symbols modulated on two adjacent sub-carriers, instead of the symbols themselves. In other words, the transmitted symbols S_n are formed from the PSK modulated information symbols s_n by,

$$S_n = \frac{S_{n-1}s_{n-1}}{|s_{n-1}|}, \quad (2.44)$$

and S_0 can be chosen arbitrarily. Therefore, the phase difference between S_n and S_{n-1} is equal to the phase of s_{n-1} . At the receiver, the phase of the information symbols

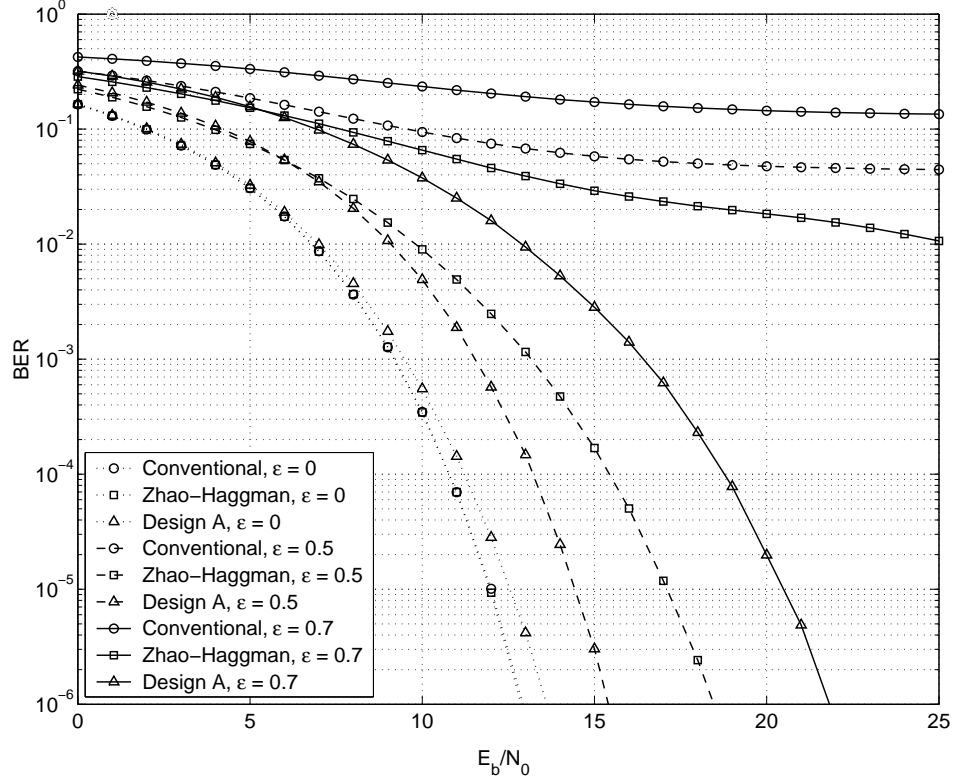


Figure 2.10: BER of the conventional, Zhao-Haggman and proposed system (Design A) with DQPSK modulation, over a flat AWGN channel.

can be recovered by performing

$$\angle s_{n-1} = \angle \left(\frac{s_{n-1}}{|s_{n-1}|} \right) = \angle \left(\frac{S_n}{S_{n-1}} \right). \quad (2.45)$$

If the channel is constant over two consecutive symbols ($2L$ sub-carriers), any channel attenuation and phase shift in the transmitted symbols is removed in the demodulation process, and there is no need for channel estimation and equalization. Figure 2.10 depicts the BER results of the simulated systems when DQPSK is used. We have assumed that the DQPSK coding is reset for each OFDM symbol. Once again we observe that the gain achieved by the proposed system is larger compared to the case where perfect equalization is assumed. For example, at a BER of 10^{-5} and a normalized frequency offset of $\varepsilon = 0.7$, the proposed system performs approximately 3.5dB better than the Zhao-Haggman system, while the conventional system fails.

2.7.2 Mitigation of ICI due to Channel Fading

When the system operates over a fading channel, a spread of frequency shifts is caused by the channel fading, known as the Doppler spread. A Doppler spread can be considered as a combination of many time-varying frequency shifts. Thus, since the proposed scheme does not attempt to estimate the frequency shifts and simply reduces the sensitivity of the system to frequency shifts, we can expect that the system also performs better when a spread of frequency shifts exists. Here we study the proposed and existing systems over a frequency selective Rayleigh fading channel. We use a four tap channel model. The fading coefficient on each tap is a random variable with a Rayleigh distribution and a power spectral density given by Jake's model [44]

$$S(f) = \begin{cases} \frac{K}{[1-(f/f_D)]^{1/2}} & |f| < f_D \\ 0 & \text{otherwise} \end{cases}, \quad (2.46)$$

where K is a constant and f_D is the maximum Doppler frequency. The excess delay and the relative average power of the taps are specified in Table 2.4. We have assumed that a cyclic prefix of length $T/8$ has been used to remove ISI.

Coherent System

The BER results of the proposed and existing systems operating over a frequency selective Rayleigh fading channel are obtained using Monte-Carlo simulations. Let us first compare the performance of our proposed system to that of a convolutionally coded OFDM system with similar rate, over the frequency selective Rayleigh fading channel described above. Figure 2.11 depicts the BER performance of the proposed system with $L = 2$, as well as that of a half rate coded OFDM system, for normalized Doppler frequencies of $\varepsilon_D = f_D T = 0.01, 0.5$ and 0.7 . In the coded OFDM system a $1/2$ rate convolutional code with constraint length of 10 has been used together with a block interleaver of sufficient length. For both systems we assume perfect equalization. We observe that the coded system has better performance at lower Doppler frequencies. However, over fast channels, the proposed system considerably outperforms the coded system.

Figure 2.12 compares the performance of conventional, Zhao-Haggman and pro-

Table 2.4: Delay profile of the frequency selective Rayleigh fading channel.

Tap	Excess Delay	Relative Average Power
1	0	0dB
2	$T/64$	-6dB
3	$T/32$	-12dB
4	$3T/64$	-18dB

posed systems, when perfect equalization is assumed. The BER results have been presented for the normalized Doppler frequencies of $\varepsilon_D = f_D T = 0.01, 0.5$ and 0.7 . No fixed frequency shift has been assumed, i.e. $\varepsilon = 0$. We observe that while at the low Doppler frequency of $\varepsilon_D = 0.01$ the Zhao-Haggman and the proposed systems perform only slightly better than the conventional, at a high Doppler frequencies of $\varepsilon_D = 0.5$ and 0.7 the error floor caused by the ICI is considerably lowered. For example, with $\varepsilon_D = 0.7$, while the Zhao-Haggman system has an error floor equal to 0.008 , the proposed system reaches its floor at 0.0025 . Figure 2.13 shows that when pilot based equalization (as described in Section 2.7.1) is performed, the difference between the error floors is larger. In this case, when $\varepsilon = 0.7$, the Zhao-Haggman and the proposed systems have error floors equal to 0.015 and 0.0025 , respectively.

Non-Coherent System

The advantage of the proposed system at high Doppler frequencies can also be seen if a non-coherent DQPSK system (as described in Section 2.7.1) is considered. Figure 2.14 shows that while neither of the systems have good performance under these

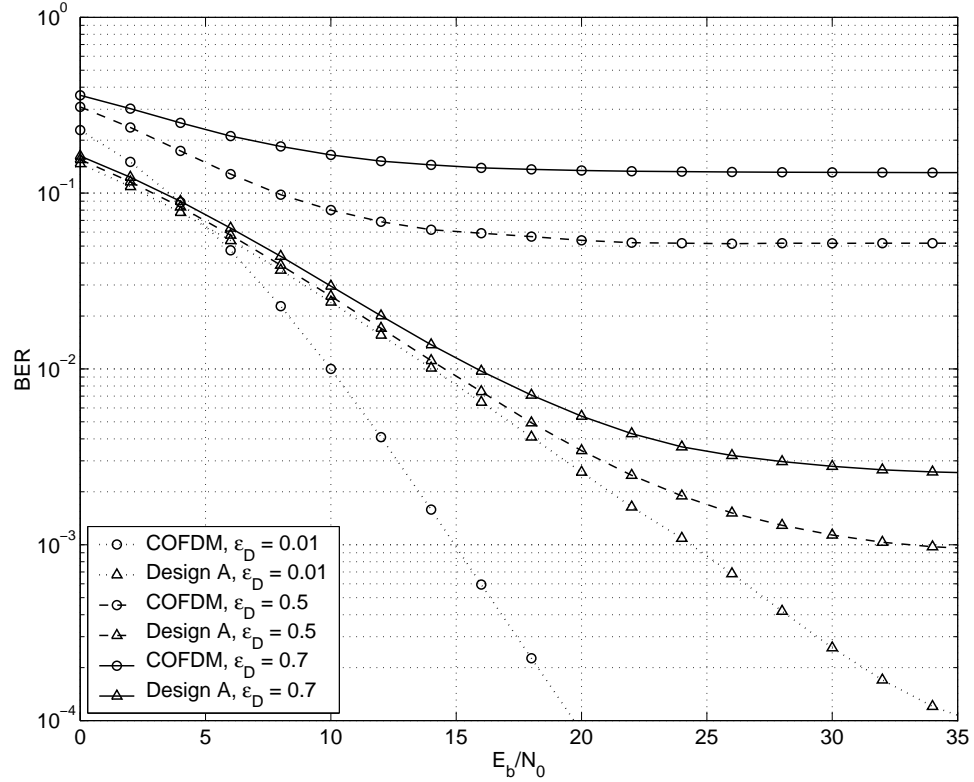


Figure 2.11: BER performance of the proposed system (Design A) and a 1/2 rate coded OFDM system, over a frequency selective Rayleigh fading channel with perfect equalization.

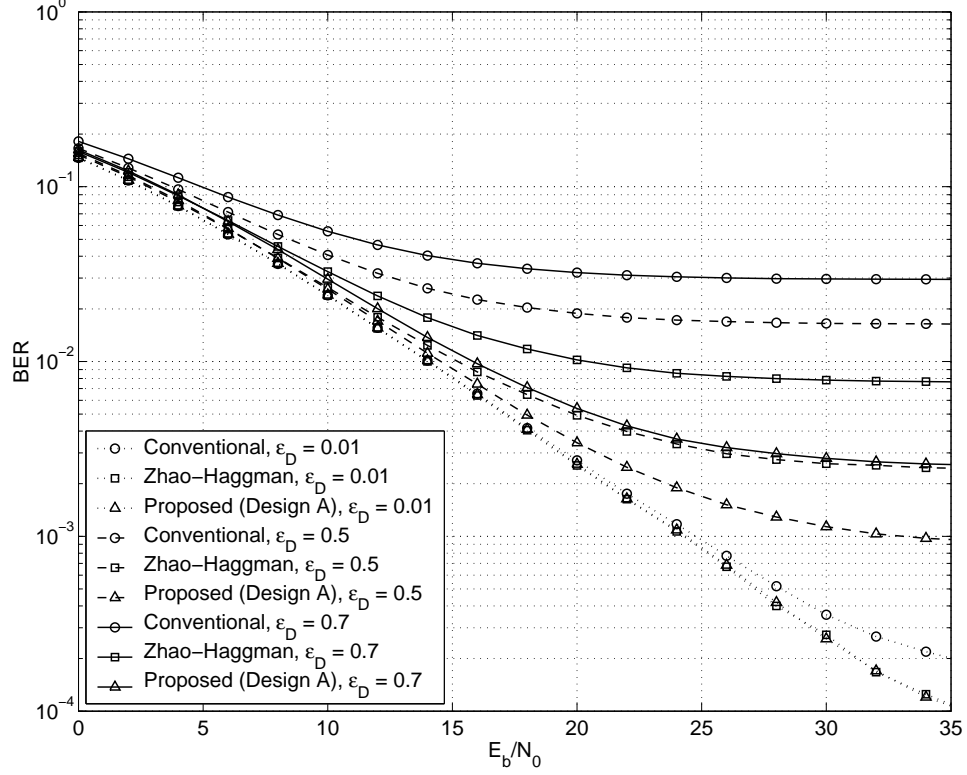


Figure 2.12: BER of the conventional, Zhao-Haggman and proposed system (Design A), over a frequency selective Rayleigh fading channel with perfect equalization.

assumptions, the proposed system has lower error floor compared to the other systems.

The poor performance of all systems under the assumptions above is due to the fact that since the data symbols are modulated on every $L = 2$ sub-carriers, in order for the DPSK to work properly, the phase rotation induced by the channel must stay approximately constant over $2L = 4$ sub-carriers. Therefore, over the assumed channel, all systems perform poorly. High error floors suggest that the non-coherent system must be employed together with a channel coding scheme to result in adequate performance. Figure 2.15 depicts the BER results for the non-coherent conventional and proposed systems when a $1/2$ rate convolutional code is used to code the information bits. We observe that while the conventional system has high error floors at high Doppler frequencies, the proposed scheme has substantially better performance.

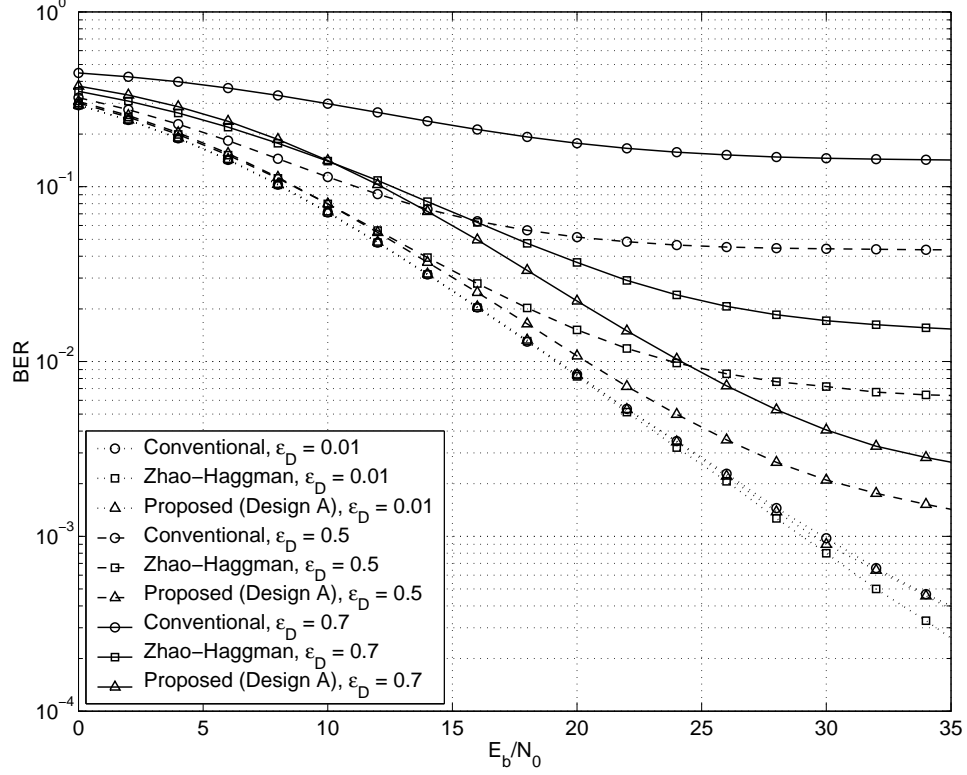


Figure 2.13: BER of the conventional, Zhao-Haggman and proposed system (Design A) with pilot based channel estimation, over a frequency selective Rayleigh fading channel.

2.8 Summary

In this chapter we have proposed a general ICI self-cancellation scheme that can reduce the sensitivity of the OFDM system to frequency shifts. We have shown that Zhao-Haggman's self-cancellation scheme is equivalent to special cases of the proposed scheme. We have provided two parameter design methods, based on SIR and BER. Using these methods, we have obtained approximately optimal designs when an SIR or BER constraint is desired.

Through SIR and BER analysis and Monte-Carlo simulations we have shown that the proposed system has better performance in presence of an oscillator frequency offset or when ICI is created as a result of channel fading. Significantly larger gains are achieved when the equalization process is imperfect.

The proposed general self-cancellation scheme has two major advantages. The first advantage is its very low complexity compared to the estimate and correct methods. The proposed scheme only requires $2N$ additional multiplications. Another advantage of the proposed scheme is that it does not require the frequency shift to be a single value or remain constant for a long period of time. Hence, this scheme can also be

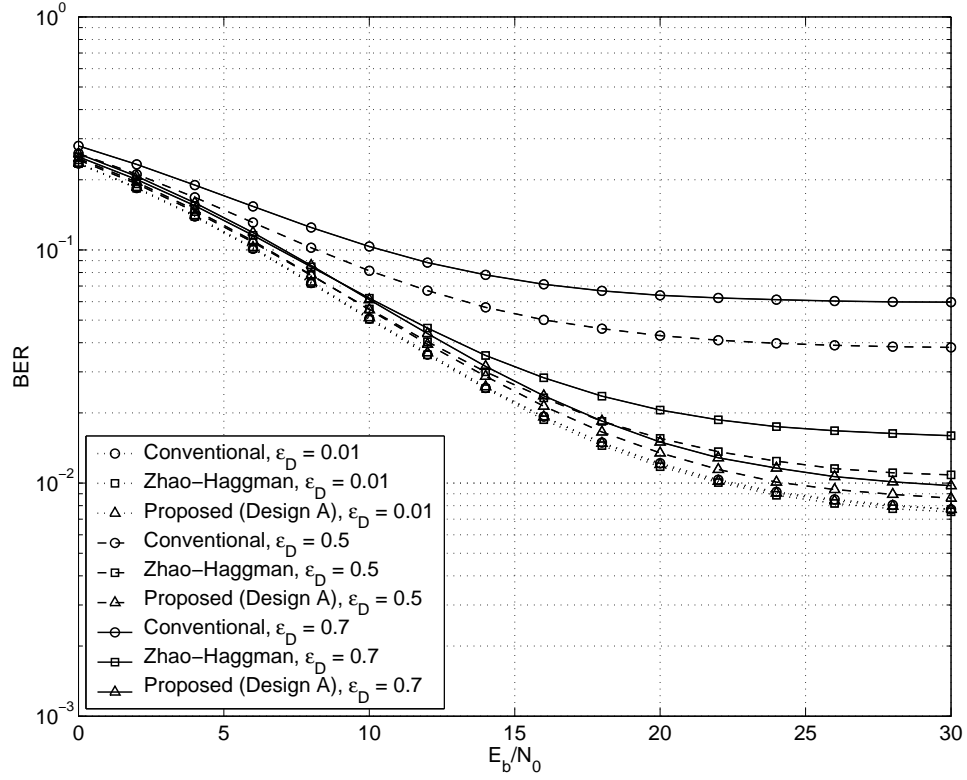


Figure 2.14: BER of the conventional, Zhao-Haggman and proposed system (Design A) with DQPSK modulation, over a frequency selective Rayleigh fading channel.

used to reduce the ICI created as a result of fast channel fading.

In summary, the proposed scheme can be used as a low complexity alternative to fine frequency offset estimation methods, in the applications where the lower rate and increased power consumption can be tolerated. The proposed scheme is also very effective in reducing the ICI when the OFDM system operates over a fast fading channel.

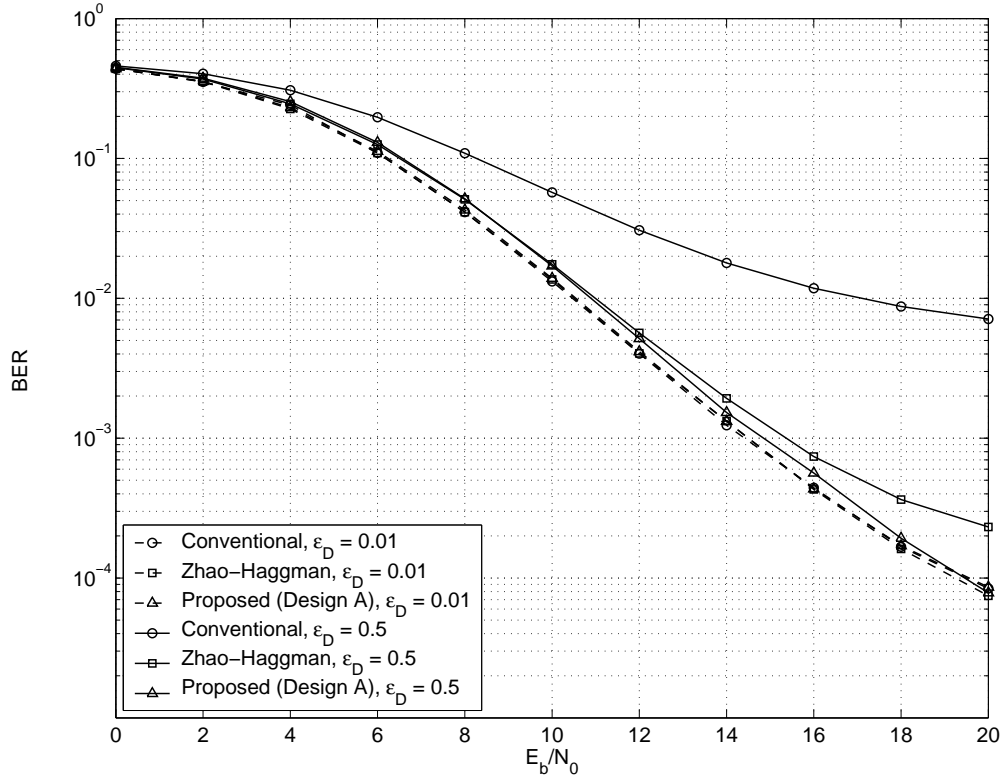


Figure 2.15: BER of the conventional and proposed system (Design A), over a frequency selective Rayleigh fading channel with DQPSK modulation and 1/2 rate convolutional code.

Chapter 3

Sub-Channel Selective MC-SS and MC-CDMA

In this section we propose and analyze the Sub-Channel Selective (SCS) technique for MC-SS and MC-CDMA systems. The proposed technique is a form of sub-optimal bit-loading (chip-loading) for MC-SS and MC-CDMA systems. We also propose a distributed loading algorithm that can be used in an SCS-MC-CDMA system. For the single user case (SCS-MC-SS), we provide an analytical study of the BER performance of the system. We also obtain the BER performance of the system, for both single-user and multi-user cases through Monte-Carlo simulations.

3.1 Motivation

The MC-SS scheme achieves many desired properties by spreading a data symbol over the sub-channels of an OFDM system. These properties include

- Low probability of detection
- Interference and jamming resilience
- Frequency diversity

Also, the MC-SS scheme can be used to implement a MC-CDMA system for multi-user applications.

If the CSI is available at the transmitter, a form of water-filling and bit-loading (chip-loading) can be used to increase the power efficiency of the MC-SS or MC-CDMA systems. It should be noted that in the MC-SS case the bit (chip) assignment is limited to the selection between one or no chips for each OFDM sub-channel. The power, however, can be assigned according to the sub-channel quality.

In an MC-CDMA system the channel estimation process considers both noise and interference in identifying the sub-channel quality. Thus, the use of a bit-loading

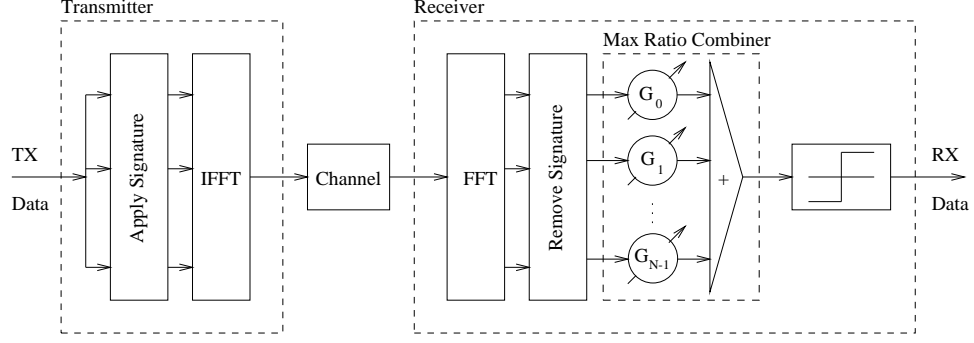


Figure 3.1: Conventional MC-SS system

algorithm helps separate the users and assign sub-channels to each user, loosely similar to an OFDMA system (see Section 1.2.2), where each user is assigned a number of sub-channels.

3.2 System Description

In the conventional MC-SS system copies of a symbol are transmitted on all sub-channels (Figure 3.1). A signature (spreading code) is applied to the chips, i.e. the phase of each sub-channel is adjusted according to the chips of the signature. In the MC-CDMA systems these signatures are user specific and orthogonal. At the receiver, after removing the signature, the output of the different sub-channels are often combined using Maximal Ratio Combining (MRC). The ideal MRC weights, G_i , are the complex conjugate values of the sub-channel gains. In other words, if we model the sub-channel i by

$$y_i = H_i x + n_i, \quad (3.1)$$

where y_i is the output of the sub-channel, x is the transmitted symbol, H_i is the complex sub-channel gain and $n_i \sim \mathcal{N}(0, \sigma^2)$ is the AWGN on sub-channel i , the MRC decision variable is

$$y = \sum_{i=1}^N G_i y_i, \quad (3.2)$$

where ideal MRC weights are given by $G_i = H_i^*$. In practice, the MRC weights are obtained from the estimate of the channel.

Note that the magnitude of the MRC weights, $|G_i|$, are directly related to the SNR of the sub-channel. Thus, we can distinguish the *good* sub-channels (high SNR) from *bad* ones (low SNR), by examining these parameters. From (3.2) we can observe that the outputs of the *bad* sub-channels have a small contribution to the decision variable. Thus, if these sub-channels are turned off at the transmitter and are omitted from the MRC at the receiver, the power spent on these sub-channels will be saved and can be redirected towards the other sub-channels, resulting an overall gain. In other words, if

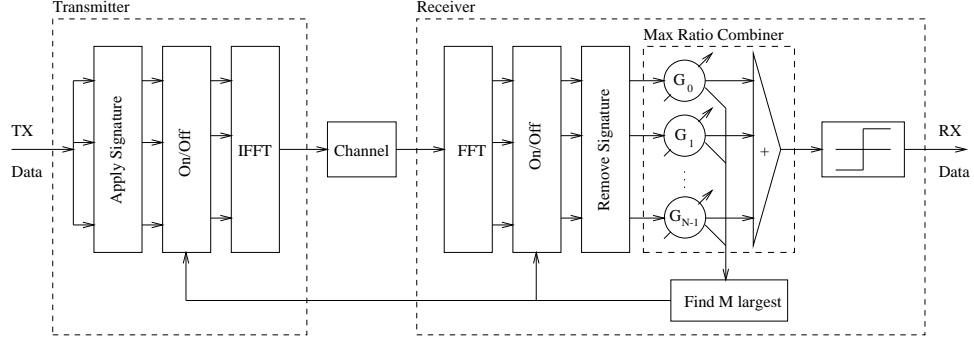


Figure 3.2: Sub-Channel Selective MC-SS system

we select M sub-channels (out of N) that have the M largest $|G_i|$ and turn the other sub-channels off, a better BER performance will be achieved. We call this technique Sub-Channel Selective (SCS) MC-SS. In concept, SCS MC-SS is similar to a Hybrid-Selection/MRC (H-S/MRC) [25], except that power is not wasted on the unselected diversity branches (sub-channels). In other words, SCS MC-SS implements a sub-optimal (on/off) chip-loading solution in which the power spent on a sub-channel is limited to two possible values 0 or P_T/M , where P_T is the total transmitted power.

In practice, the amount of feed-back required can be greatly reduced if the magnitudes of the MRC weights are examined at the receiver and the M best sub-channels are selected and reported to the transmitter via the feed-back channel (Figure 3.2). The transmitter only uses the selected sub-channels to transmit the chips.

The most important advantage of the SCS method will appear in the MC-CDMA system. In a CDMA system the dominant degrading factor is the interference that a user will receive from other users, resulting from imperfect orthogonality of the signatures or the impairments of the channel. Since a sub-channel that has small gain for one user can have a rather large gain for another user, the water-filling algorithm will reduce the interference between the users by loosely assigning different sub-channels to different users.

3.3 Drop and Add Algorithm

Here we provide a distributed algorithm for selection of the best sub-channels, called the Drop and Add (DA) algorithm, and show that it converges to near optimum solution.

3.3.1 Algorithm Description

Since the estimation algorithms use the outputs of the sub-channels to calculate the MRC weights, when a sub-channel is off, the MRC weight for that sub-channel will not be available. When the channel is time variant or when users join or leave the

system, it is possible that one of the off sub-channels will become better than the worst selected (on) sub-channel. Therefore, the off sub-channels must be probed regularly and the on sub-channels must be updated after each probing of the off sub-channels.

Here, we propose a distributed algorithm for periodically probing and updating the selected sub-channels. This algorithm can be used for multi-access, broadcast or interference channels. We call this algorithm the DA algorithm. In the DA algorithm, in each iteration, each user updates its own sub-channels by turning off the worst sub-channel (smallest $|G_i|$) and randomly turning on one of the previously off sub-channels. This procedure is repeated (for the whole system) with time period T . Specifically, user k will perform this step at times $nT + \frac{kT}{K}, n = 1, 2, \dots$ where K is the total number of users in the system. If the newly added sub-channel happens to be a *bad* one it will be dropped in a later step and if it is a *good* sub-channel it will be kept.

Since the MRC weights are available at the receiver, it is more efficient if the algorithm is implemented at the receiver. In this case, after each iteration, the receiver only has to inform the transmitter about the indices of the dropped and added sub-channels, through a feed-back channel.

This algorithm will converge if T is small enough such that the algorithm can track the changes in the channel. On the other hand, T/K should be long enough to allow the channel estimator to produce reliable estimates of the sub-channel gains. Therefore, the convergence of this algorithm is limited by the extent of fading in the channel.

Also, for the multi-user case where different users have different channel profiles, the DA algorithm allows the users to select their best sub-channels, while avoiding the interference generated by the other users. When other users are transmitting on sub-channel i , the interference caused by their transmission will be added to the noise and will result in a low Signal-to-Interference-and-Noise Ratio (SNIR), resulting in a smaller $|G_i|$. Therefore, the user probing this sub-channel is less likely to keep it.

3.3.2 Convergence

For the single-user system, it is easy to show that the DA algorithm will converge. In each iteration, the worse selected sub-channel is dropped. If the randomly chosen added sub-channel happens to be better than the dropped one, the system has approached the optimal sub-channel allocation. On the other hand, if the randomly added sub-channel is worse than the last dropped sub-channel, it is now the worst sub-channel and it will be dropped in the next iteration. Therefore, overall the system will approach the optimal sub-channel allocation and it will reach the optimal solution with exception of one (worst) sub-channel.

For the multi-user case, the analysis of the convergence of the DA algorithm is much more complex and has not been proved. However, we have shown the convergence of the DA algorithm for specific cases through simulation. Figure 3.3 shows

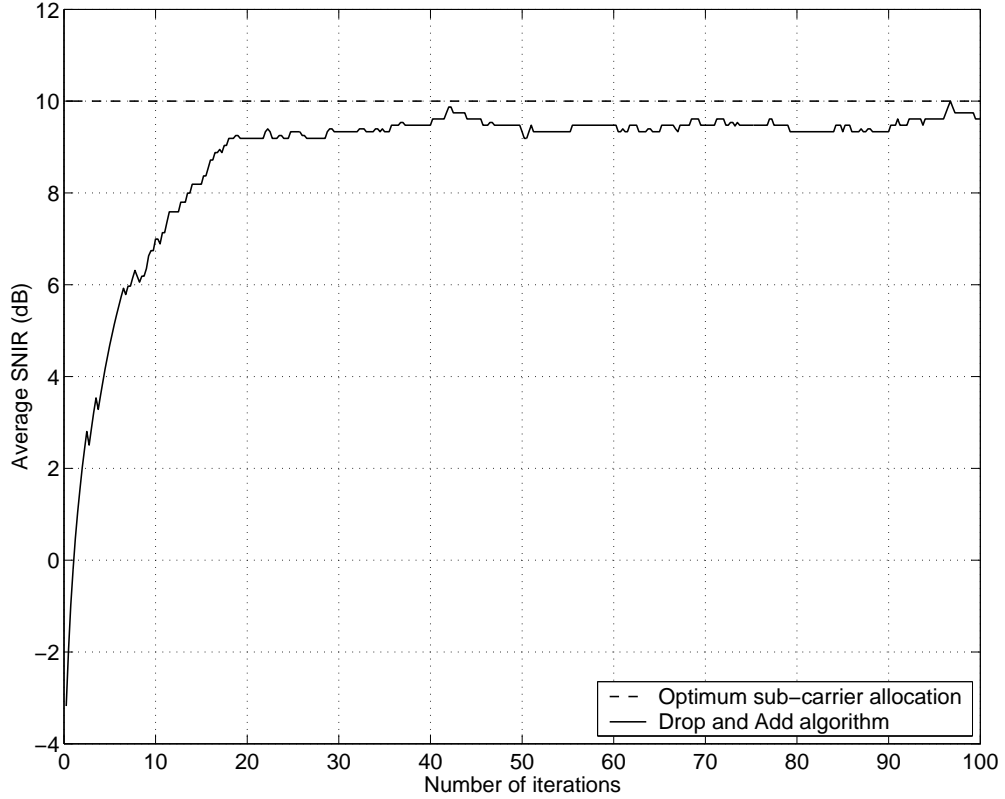


Figure 3.3: Convergence of the DA algorithm for a four user system over a flat multi-access AWGN channel.

the average SNIR as a function of iteration number in a $K = 4$ user SCS MC-CDMA system and compares it to the SNIR when optimal sub-channel allocation is used. We have assumed that the system has $N = 64$ sub-channels and that $M_k = 16$, $k = 1, 2, 3, 4$, where M_k is the number of selected sub-channels for user k . We have also assumed a flat AWGN multi-access channel. Although the channel is flat, the bit-loading will still be useful since it can assign different sub-channels to different users and therefore avoid interference.

Similarly, Figure 3.4 compares the average SNIR for a two user case with $N = 64$ and $M_1 = M_2 = 32$ where each user has a different frequency selective channel profile.

In both cases it can be observed that within 20 to 40 iterations, the DA algorithm reaches within 1dB of the optimum value.

It is also possible to modify the DA algorithm so that it converges faster. In the initial iterations, the selected sub-channels are far from the optimal solution. Therefore, if more than one sub-channel is dropped (and added) in the first few iterations, the convergence will be much faster. However, allowing multiple sub-channels to be dropped and added in each iteration, will cause larger deviation from the optimal allocation after enough time has passed. Therefore, the best way is

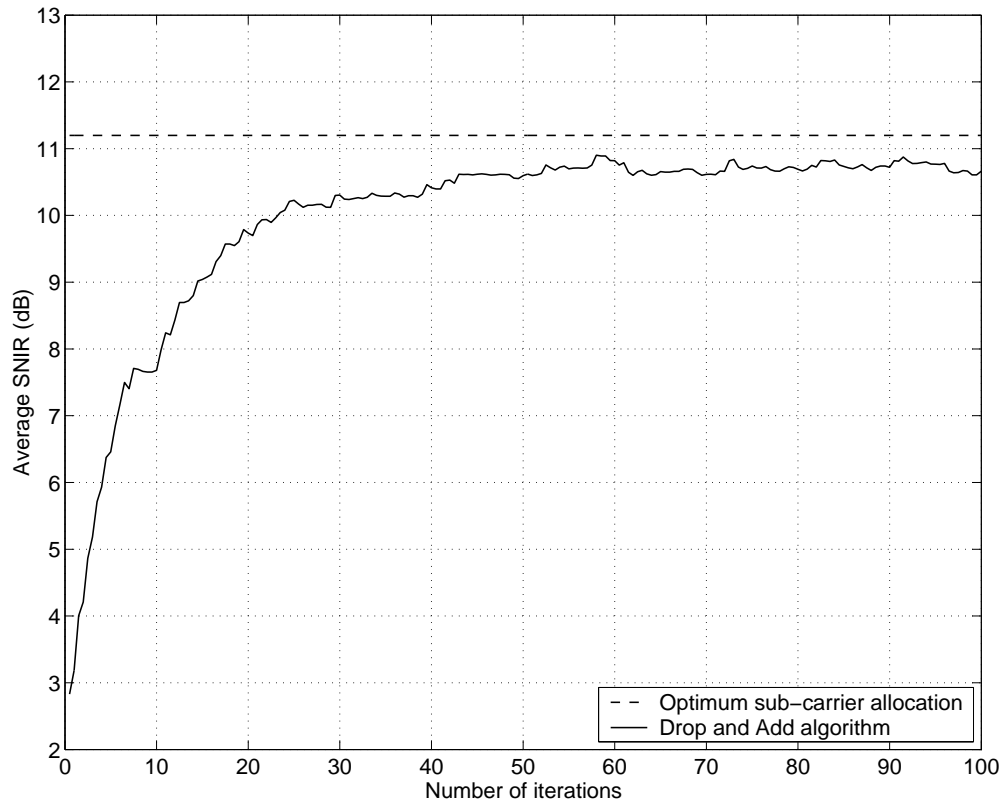


Figure 3.4: Convergence of the DA algorithm for a two user system over a frequency selective multi-access AWGN channel.

to taper off the number of dropped/added sub-channels as time goes on. Also, the number of dropped and added sub-channels in each iteration can be adapted based on the overall SNIR of the system. In such a case, more sub-channels should be dropped and added when the total current SNIR is less than desired, but once the desired SNIR is reached, the number of dropped and added sub-channels can be reduced.

3.4 BER Analysis

In this section we analyze the BER performance of the single user SCS MC-SS system over a frequency selective Rayleigh fading channel. To simplify the analysis of the BER performance of the system we assume that the sub-channels are statistically independent and identically distributed. Furthermore, we assume that the channel weight estimation and the sub-channel selection are perfect, i.e. we assume that the complex channel weights are known at the transmitter. The BER performance of a normal MRC system, with BPSK modulation, is derived in [75]. Here, we provide an analysis (similar to the analysis in [109] and [110]) to obtain the BER performance of the SCS MC-SS system. First the BER is obtained for a fixed set of channel weights. Then, the result is averaged over the probability distribution function of the weights.

The output of the MRC for a system with BPSK modulation can be given as

$$\begin{aligned} \text{Re}\{y\} &= \text{Re}\left\{\sum_{i \in \mathcal{A}} H_i^* y_i\right\} \\ &= \sum_{i \in \mathcal{A}} |H_i|^2 x + \sum_{i \in \mathcal{A}} \text{Re}\{H_i^* n_i\}, \end{aligned} \quad (3.3)$$

where $y_i = H_i x + n_i$ is the received value on sub-channel i and \mathcal{A} is the set of all selected sub-channels ($\mathcal{A} = \{0, 1, 2, \dots, N-1\}$ represents the conventional MC-SS). Since H_i and n_i are independent and n_i are circularly symmetric Gaussian random variables, the signal power is equal to

$$P_S = E_c \left(\sum_{i \in \mathcal{A}} |H_i|^2 \right)^2, \quad (3.4)$$

and the noise power is

$$P_N = N_0 \sum_{i \in \mathcal{A}} |H_i|^2, \quad (3.5)$$

where E_c is the chip energy and N_0 is the power spectral density of the noise. Therefore, the overall signal to noise ratio is

$$\begin{aligned} \gamma_b &= \frac{E_c}{N_0} \sum_{i \in \mathcal{A}} |H_i|^2 \\ &= \sum_{i \in \mathcal{A}} \gamma_i, \end{aligned} \quad (3.6)$$

where

$$\gamma_i = \frac{E_c |H_i|^2}{N_0}. \quad (3.7)$$

For the BPSK modulation, given γ_b , the BER can be given as

$$P_e(\gamma_b) = Q(\sqrt{2\gamma_b}), \quad (3.8)$$

and the overall BER can be computed using

$$P_e = \int_0^\infty P_e(\gamma) f_{\gamma_b}(\gamma) d\gamma. \quad (3.9)$$

Now, we obtain the probability distribution function (pdf) of γ_b for the conventional and SCS systems. Since $|H_i|$ is Rayleigh distributed, the distribution of $\gamma_i = E_c |H_i|^2 / N_0$ is exponential

$$f_{\gamma_i}(\gamma) = \frac{1}{\bar{\gamma}_{sc}} e^{-\gamma/\bar{\gamma}_{sc}}, \quad (3.10)$$

where $\bar{\gamma}_{sc}$ is the average SNR per sub-channel.

For the conventional system,

$$\gamma_b = \sum_{i=0}^{N-1} \gamma_i. \quad (3.11)$$

Since γ_i are statistically independent, γ_b is chi-square-distributed with $2N$ degrees of freedom.

$$f_{\gamma_b}^{\text{Conv.}}(\gamma) = \frac{1}{(N-1)! \bar{\gamma}_{sc}^N} \gamma^{N-1} e^{-\gamma/\bar{\gamma}_{sc}}. \quad (3.12)$$

Using this pdf in (3.8) the BER of the conventional system can be computed.

For the SCS MC-SS system, γ_b is the sum of the M largest γ_i 's. Let $\gamma_{(i)}$ be the order statistics [81] of γ_i . In other words, $(\gamma_{(0)}, \gamma_{(1)}, \dots, \gamma_{(N-1)})$ is a permutation of $(\gamma_0, \gamma_1, \dots, \gamma_{N-1})$, where $\gamma_{(0)} < \gamma_{(1)} < \dots < \gamma_{(N-1)}$. Then the joint pdf of $\gamma_{(i)}, i = 0, \dots, N-1$ is

$$f(\gamma_{(0)}, \dots, \gamma_{(N-1)}) = \begin{cases} N! \prod_{i=0}^{N-1} f_{\gamma_i}(\gamma_{(i)}) & \gamma_{(0)} < \dots < \gamma_{(N-1)} \\ 0 & \text{otherwise} \end{cases}, \quad (3.13)$$

or

$$f(\gamma_{(0)}, \dots, \gamma_{(N-1)}) = \begin{cases} \frac{N!}{\bar{\gamma}_{sc}^N} e^{-\frac{1}{\bar{\gamma}_{sc}} \sum_{i=0}^{N-1} \gamma_{(i)}} & \gamma_{(0)} < \dots < \gamma_{(N-1)} \\ 0 & \text{otherwise} \end{cases}. \quad (3.14)$$

Let us define the auxiliary variables

$$Z_i = \begin{cases} N \cdot \gamma_{(0)} & i = 0 \\ (N-i)(\gamma_{(i)} - \gamma_{(i-1)}) & i > 0 \end{cases}. \quad (3.15)$$

The original variables $\gamma_{(i)}$ can be obtained from Z_i by

$$\gamma_{(i)} = \sum_{j=0}^{i-1} \frac{1}{N-j} Z_j. \quad (3.16)$$

The Jacobian for this change of variables is

$$\begin{aligned} J(Z_i; \gamma_{(i)}) &= \det \left(\begin{bmatrix} N & 0 & \cdot & \cdot & \cdot & 0 \\ -N+1 & N-1 & \cdot & \cdot & \cdot & 0 \\ 0 & -N+2 & N-2 & & & 0 \\ \cdot & \cdot & & & & 0 \\ \cdot & \cdot & & & \cdot & 0 \\ 0 & 0 & \cdot & \cdot & -1 & 1 \end{bmatrix} \right) \\ &= N!. \end{aligned} \quad (3.17)$$

Also,

$$\sum_{i=0}^{N-1} \gamma_{(i)} = \sum_{i=0}^{N-1} Z_i. \quad (3.18)$$

Thus, the joint pdf of Z_i is

$$f(z_0, \dots, z_{N-1}) = \frac{1}{\bar{\gamma}_{sc}^N} e^{-\frac{1}{\bar{\gamma}_{sc}} \sum_{i=0}^{N-1} z_i} \quad 0 < z_i < \infty. \quad (3.19)$$

This means that Z_i are independent and exponentially distributed with mean $\bar{\gamma}_{sc}$. We have

$$\gamma_b = \sum_{i=N-M}^{N-1} \gamma_{(i)}, \quad (3.20)$$

and substituting (3.16) for $\gamma_{(i)}$ yields

$$\begin{aligned} \gamma_b &= \sum_{i=N-M}^{N-1} \sum_{j=0}^{i-1} \frac{1}{N-j} Z_j \\ &= \sum_{k=0}^{N-M-1} \frac{M}{N-k} Z_k + \sum_{k=N-M}^{N-1} Z_k \\ &= \sum_{k=0}^{N-M-1} c_k Z_k + \sum_{k=N-M}^{N-1} Z_k, \end{aligned} \quad (3.21)$$

where $c_k = \frac{M}{N-k}$, $k = 0, \dots, N-M-1$.

Since all the terms in (3.21) are independent, pdf of γ_b can be calculated by convolving the distributions of the components. The second sum has a chi-square distribution with $2M$ degrees of freedom

$$f_2(\gamma) = \frac{1}{(M-1)! \bar{\gamma}_{sc}^M} \gamma^{M-1} e^{-\gamma/\bar{\gamma}_{sc}}. \quad (3.22)$$

The distribution of the first sum does not have a closed form, but it can be expressed as

$$f_1(\gamma) = f_{W_0}(\gamma) * f_{W_1}(\gamma) * \dots * f_{W_{N-M-1}}(\gamma). \quad (3.23)$$

where $*$ is the convolution operator and $W_i = c_i Z_i$. Thus

$$f_{W_i}(\gamma) = \frac{1}{c_i \bar{\gamma}_{sc}} e^{-\frac{\gamma}{c_i \bar{\gamma}_{sc}}}. \quad (3.24)$$

Convolving (3.23) and (3.22) yields

$$f_{\gamma_b}^{\text{SCS}}(\gamma) = f_1(\gamma) * f_2(\gamma). \quad (3.25)$$

Using this pdf in (3.8) the BER of the SCS MC-SS system can be computed.

In the analysis above, we have assumed that the sub-channels have independent fading. This assumption is generally not accurate. In general, the fading coefficient of adjacent sub-channels are correlated. However, this analysis can still provide an approximation if it is performed with the effective number of sub-channels, \tilde{N} , equal to the degree of diversity among sub-channels. This is due to the fact that the sub-channels with equal (strongly correlated) gains do not offer extra diversity. In a multi-path channel with large number of paths, the total number of diversity branches is approximately $\tilde{N} = \frac{N}{B_C T}$, where B_C is the coherence bandwidth and $1/T$ is the sub-channel spacing ($B_C T$ is the number of adjacent sub-channels with strongly correlated gains).

3.5 Results

In this section we study the BER performance of the SCS MC-SS and SCS MC-CDMA systems and compare it to the conventional systems. For the single-user case we show that the simulation results match the calculations, when sub-channels are statistically independent. For both single-user and multi-user cases, through Monte-Carlo simulations, we show that the SCS system significantly outperforms the conventional system in terms of BER. In all of the simulations we have assumed that $N = 64$ sub-channels exist and a cyclic prefix of length $T/2$ has been used to prevent ISI. All the users use random spreading codes. We have also assumed that perfect CSI is available at the transmitter.

3.5.1 Single-user System

In a non-fading channel, the system will converge after a number of iterations of the DA algorithm. After that, the sub-channel selection will not change except for one sub-channel that is used for probing. Figure 3.5 depicts the BER of the conventional and SCS MC-SS systems over a frequency selective AWGN channel, obtained from Monte-Carlo simulations. We have assumed that $M = 32$ sub-channels are on at

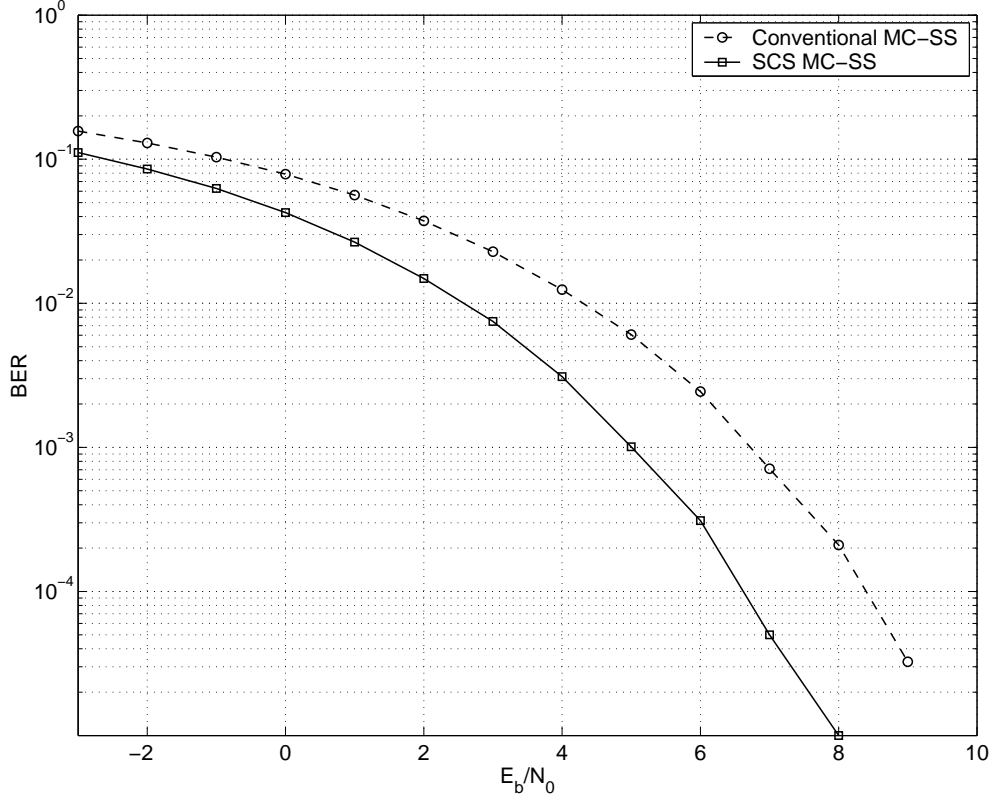


Figure 3.5: BER performance of single user conventional and SCS MC-SS systems over a frequency selective AWGN channel.

each point in time. The frequency selective channel has been modelled by a two ray channel with equal gains and a delay spread of $D_S = T/4$. We can see that an improvement of approximately 1dB has been achieved.

When the system operates over a fading channel, the DA algorithm must find the best M sub-channels as channel changes. If the channel fading is slow, the DA algorithm can successfully track the channel and approximately find the optimal sub-channel selection. In this case, the analysis performed in Section 3.4 is accurate, if the sub-channels experience independent Rayleigh fading. Figure 3.6 depicts the calculated BER of the conventional and SCS systems for this case, and compares them to the results obtained from Monte-Carlo Simulations. Once again, we have assumed that $M = 32$ sub-channels are selected at each time. Furthermore, we have assumed that each sub-channel has a independent Rayleigh fading process with a normalized Doppler frequency of $f_D T = 0.001$. We can see that the calculation results match the simulation results. We can also observe that the SCS system performs better than the conventional system. For example, at a BER of 10^{-5} a gain of approximately 2dB gain is achieved.

Figure 3.7, shows the BER of the conventional and SCS systems over a two-ray

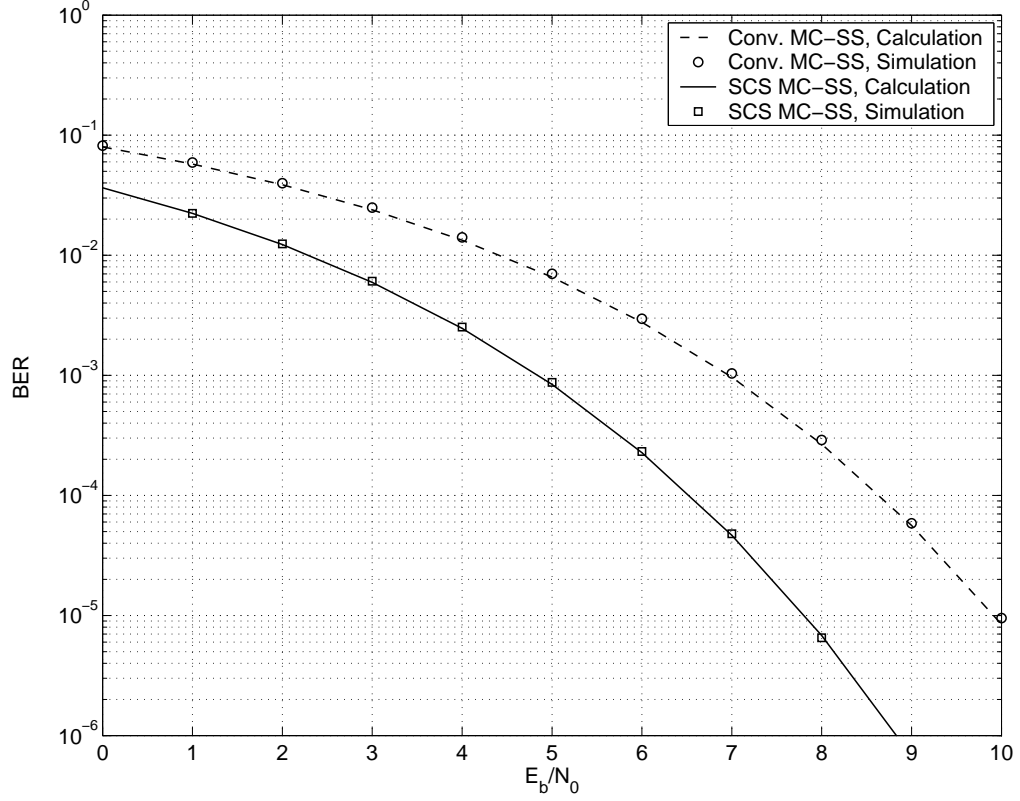


Figure 3.6: Calculation and simulation results for conventional and SCS MC-SS systems with independent sub-channel fading.

Rayleigh fading channel, where equal average power has been assumed for the two rays. Also, each ray has a normalized Doppler frequency of $f_D T = 0.001$. The delay spread is equal to $D_S = T/4$. As it can be seen, while compared to the independent sub-channel assumption, the lower degree of diversity results in worse BER results, we can still observe that the SCS system has about 2dB advantage with respect to the conventional system.

3.5.2 Multi-user System

In the multi-user case, the SCS system can perform better than the conventional system even when the channel is not frequency selective. In this case, although all the sub-channel gains are equal, the DA algorithm will still lead to an optimal sub-channel distribution where the interference between users are minimized. In other words, although the channel is flat, the estimated MRC weights can be different, since the interference is also considered. If the interference is assumed to be Gaussian, the

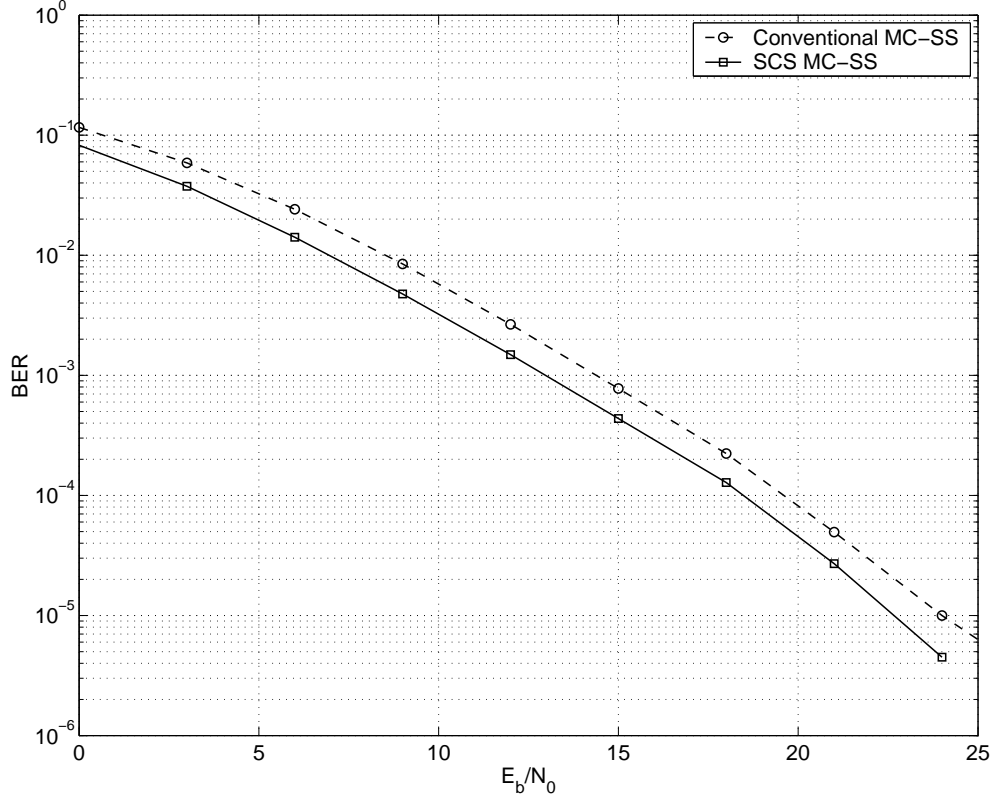


Figure 3.7: BER performance of single user conventional and SCS systems over a frequency selective fading channel.

ideal estimated sub-channel gain on sub-channel i for user k_0 is

$$G_i^{(k_0)} = \frac{[H_i^{(k_0)}]^*}{\sum_{k=0, k \neq k_0}^{K-1} m_i^{(k)} |H_i^{(k)}|^2 + \sigma^2}, \quad (3.26)$$

where $H_i^{(k)}$ is the sub-channel gain between transmitter k and receiver k_0 , σ^2 is the power of AWGN per sub-channel and $m_i = 0$ if sub-channel i is off and $m_i = 1$ if it is on. It is obvious that even if $H_i^{(k)}$ are equal, G_i^k can still be different.

The advantage of the SCS system in such a scenario has also been shown through simulations. Figure 3.8 depicts the BER performance of the conventional and SCS systems with $K = 4$ users in a multi-access channel, where $M_k = 16, k = 1, 2, 3, 4$. Since $N = 64$, with these values of M_k , the optimal sub-channel assignment avoids any interference. As we expect, we see that the SCS system has superior performance compared to the conventional system.

In a more general setting, Figure 3.9 presents the BER of the conventional and the SCS systems in a frequency selective multi-access channel with $K = 2$ users and

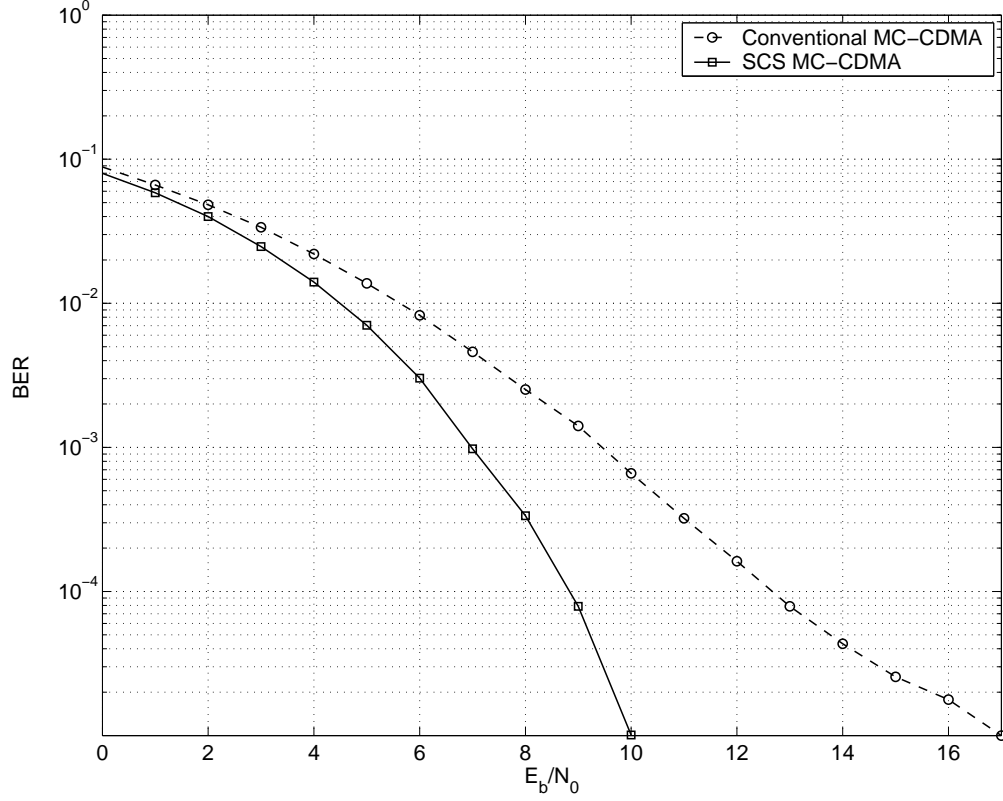


Figure 3.8: BER performance of $K = 4$ user conventional and SCS systems over a flat multi-access AWGN channel.

$M_1 = M_2 = 32$. Both channels have been modelled with two rays with equal gains and delay spreads $D_{S_1} = T/16$ and $D_{S_2} = T/4$, respectively.

As we expect, the performance of the SCS system is considerably better than that of the conventional system.

3.6 Summary

In this chapter we proposed the SCS MC-SS and SCS MC-CDMA methods. These methods only use the sub-channels with better quality for chip transmission and avoid the sub-channels with bad quality. We proposed the distributed DA algorithm and showed that it converges to near optimum solutions. We provided an analysis for the BER of the SCS MC-SS system and showed that the analytical and simulated results agree. Our results show that for slow fading frequency selective channels, the proposed techniques outperform their conventional counterparts.

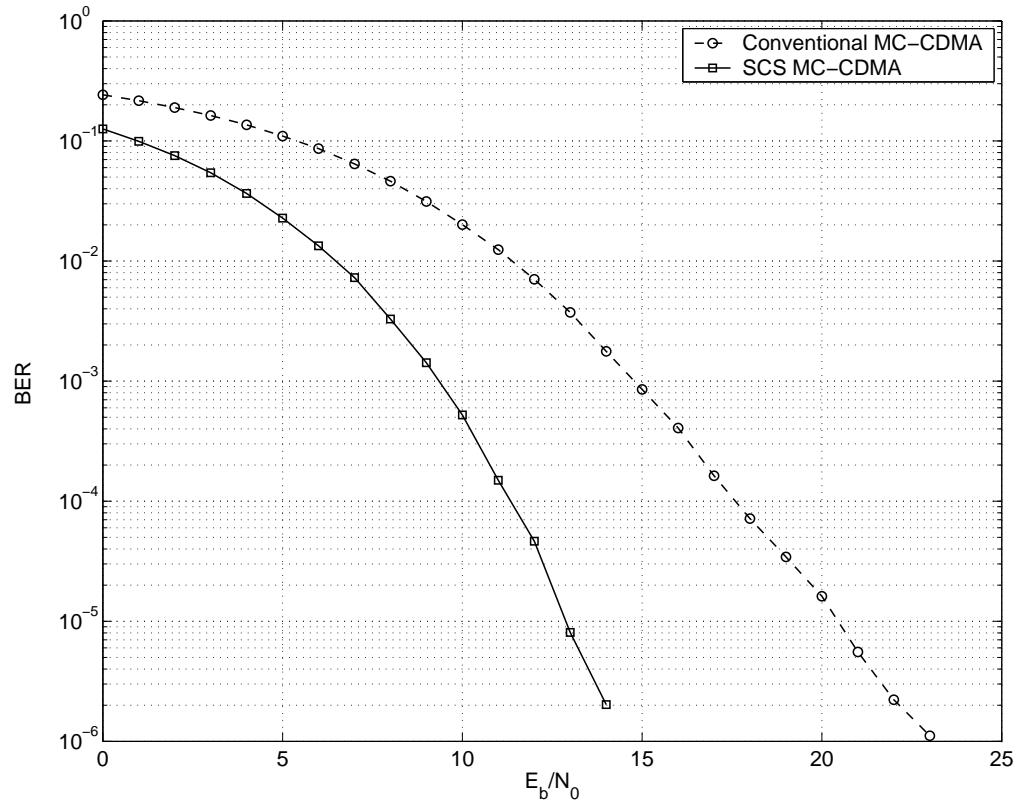


Figure 3.9: BER performance of $K = 2$ user conventional and SCS systems over a frequency selective multi-access AWGN channel.

Chapter 4

Robust Bit-Loaded OFDM

In this section we first study the sensitivity of a bit-loaded OFDM system to unreliability of CSI. Then, we propose a robust bit-loaded OFDM system that employs Code Division Multiplexing (CDM) to achieve frequency diversity and mitigate unreliable CSI.

4.1 Motivation

Bit-loading algorithms can greatly improve the performance of an OFDM system in terms of power efficiency, transmission rate or BER, by achieving water-filling gain. These algorithms require the availability of CSI at the transmitter. If the CSI available to the transmitter is not reliable, the bit-loading algorithm results in sub-optimal assignment of bits and power to sub-channels. As a result, the performance of the system is degraded.

Availability of accurate CSI at the transmitter is not hard to achieve in wired systems. However, in a wireless system obtaining perfect CSI at the transmitter is not always trivial. This is mainly due to the time variations of the channel and bandwidth scarcity in the feedback channel.

To battle the CSI unreliability, diversity must be used together with bit-loading. Here, after looking at the sensitivity of a bit-loaded OFDM system to unreliable CSI, we propose a robust bit-loaded system that achieves frequency diversity by spreading the symbols in frequency using a CDM scheme. The use of CDM allows us to achieve frequency diversity without any loss in transmission rate.

4.2 Sensitivity of Bit-Loaded OFDM to Unreliable CSI

Before introducing our robust bit-loaded system let us look at the sensitivity of a bit-loaded OFDM system to unreliable CSI.

4.2.1 Causes of Unreliable CSI

When a bit-loaded OFDM system operates over a fading channel, three major factors contribute to the unreliability of CSI at the transmitter.

- **Channel estimation error:** The channel estimate can be inaccurate as a consequence of noise, assumption of an incorrect channel model at the receiver or inadequate training. Error in the estimate of the channel results in sub-optimal bit-loading at the transmitter and sub-optimal detection at the receiver. Leke and Cioffi [59] consider the effect of the channel estimation error on detection, but do not study its effect on bit-loading.
- **Limited capacity in the feedback channel:** If the bit-loading algorithm is implemented at the transmitter, the CSI must be fed back from the receiver. On the other hand, if the bit-loading algorithm is implemented at the receiver, the bit and power allocation must be fed back to the transmitter. In either implementation, if the available bandwidth in the feedback channel is limited, either the feedback information must be reduced [16], or this information must be updated less frequently. In either case, the CSI present at the transmitter becomes less reliable.
- **Feedback delay:** Even if accurate CSI is available at the receiver and no limit on the amount of feedback exists, a delay is always present in the feedback channel. This delay is equal to the total time between the time when CSI is sensed and the time when the bit-loaded OFDM symbol, using this CSI, is transmitted. Such delay causes the information at the transmitter to be outdated with regards to the current condition of the channel. This problem has been previously noted [98][115] and it has been mentioned that a form of diversity can potentially be the solution.

We consider the feedback delay as the major factor in the unreliability of the CSI at the transmitter. In other words, we assume that perfect CSI is available at the receiver and that there is no limit on the amount of information returned on the feedback channel. However, we assume that a total delay of k_τ OFDM symbols exists between the CSI available to the transmitter and the current CSI. Furthermore, we assume that the receiver is aware of the delay value and, thus, can detect the symbols correctly.

4.2.2 Effect of Unreliable CSI

Before we proceed to describe the robust bit-loading algorithm let us look at the effect of outdated CSI on a bit-loading algorithm.

Modelling

Let us describe the impulse response of a frequency selective fading channel at time t as

$$h_t(\tau) = \sum_i \alpha_i(t) \delta(\tau - \tau_i), \quad (4.1)$$

where $\alpha_i(t)$ are the complex gains and τ_i are the corresponding delays. We assume a Rayleigh fading channel, i.e. we assume that $\alpha_i(t)$ are complex Gaussian random variables. If the channel remains constant for the duration of one OFDM symbol, the channel gain for the n th sub-channel of the k th OFDM symbol can be given by

$$H_{n,k} = \sum_i \alpha_i(kT) e^{j2\pi\tau_i n/NT} \quad (4.2)$$

where T is the duration of the OFDM symbol. Based on this model we assume that the bit and power allocation of an OFDM symbol transmitted at time k , is obtained using $H_{n,k-k_\tau}$.

Let us define ρ as the normalized autocorrelation of channel gains at times k and $k - k_\tau$, i.e.

$$\begin{aligned} \rho &= E[\alpha_i(k(T + T_{CP})) \alpha_i^*((k - k_\tau)(T + T_{CP}))] \\ &= R_{\alpha\alpha}(k_\tau(T + T_{CP})), \end{aligned} \quad (4.3)$$

where $R_{\alpha\alpha}(\cdot)$ is the autocorrelation function of $\alpha_i(\cdot)$ and T_{CP} is the length of the cyclic prefix. We assume that the Power Spectral Density (PSD) of α_i is described by the Jakes' model [44],

$$S_{\alpha\alpha}(f) = \begin{cases} \frac{1}{\sqrt{1-(f/f_D)^2}} & |f| < f_D \\ 0 & \text{otherwise} \end{cases}, \quad (4.4)$$

where f_D is the maximum Doppler frequency. Hence,

$$\begin{aligned} \rho &= R_{\alpha\alpha}(k_\tau(T + T_{CP})) \\ &= J_0(2\pi f_D k_\tau(T + T_{CP})) \\ &= J_0(2\pi \varepsilon_D k_\tau), \end{aligned} \quad (4.5)$$

where $J_0(\cdot)$ is the Bessel function of the first kind and $\varepsilon_D = f_D(T + T_{CP})$ is the normalized maximum Doppler frequency. Note that here the normalization of the Doppler frequency is different compared to the one in preceding chapters. We can see that the correlation between the current and outdated CSI is a direct function of the Doppler-delay product.

Effect of Outdated CSI on Bit-Loaded System

We assume that the CSI available at transmitter is outdated. In other words, we assume that H_{n,k_0-k_τ} , where k_0 is the current time, is used for bit-loading. At the receiver both the current and outdated channel weights, H_{n,k_0} and H_{n,k_0-k_τ} are available. In other words, we assume that the bit-loading algorithm uses H_{n,k_0-k_τ} to assign the bit and power allocation. However, the OFDM symbol actually experiences H_{n,k_0} . Also, we assume that the receiver uses the current CSI to equalize and detect the received data. Thus, the feedback delay does not affect the detection.

Using the model presented above we have obtained the BER performance of a bit-loaded OFDM system with Fischer's algorithm [27] (see Appendix A), for different values of Doppler-delay product, using Monte-Carlo simulations. We have assumed that the channel remains constant for the duration of one OFDM symbol and that a cyclic prefix of sufficient length removes any ISI and ICI. Furthermore, we have assumed that $N = 256$ sub-channels, each with bandwidth $1/T = 10\text{kHz}$, exist and that a total of $B_T = 2N$ convolutionally coded bits are modulated on each OFDM symbol. We have used a half rate convolutional code with a constraint length of 6, and a random interleaver. At the receiver, a hard-decision Viterbi algorithm is used to decode the convolutional code. The delay profile of the channel has been modelled by the 12 tap Hilly Terrain model (HTx) provided by the GSM standard [24], also presented in table 4.1.

Figure 4.1 demonstrates the sensitivity of this bit-loading algorithm to outdated CSI, for Doppler-delay values $\varepsilon_D k_\tau = 0.072$ ($\rho = 0.95$), $\varepsilon_D k_\tau = 0.102$ ($\rho = 0.90$) and $\varepsilon_D k_\tau = 0.126$ ($\rho = 0.85$). We observe that the performance quickly degrades as

Table 4.1: Delay profile of the GSM 12 tap Hilly Terrain (HTx) channel model.

Tap Number	Excess Delay	Relative Average Power
1	$0.0\mu S$	-10.0dB
2	$0.1\mu S$	-8.0dB
3	$0.3\mu S$	-6.0dB
4	$0.5\mu S$	-4.0dB
5	$0.7\mu S$	0.0dB
6	$1.0\mu S$	0.0dB
7	$1.3\mu S$	-4.0dB
8	$15.0\mu S$	-8.0dB
9	$15.2\mu S$	-9.0dB
10	$15.7\mu S$	-10.0dB
11	$17.2\mu S$	-12.0dB
12	$20.0\mu S$	-14.0dB

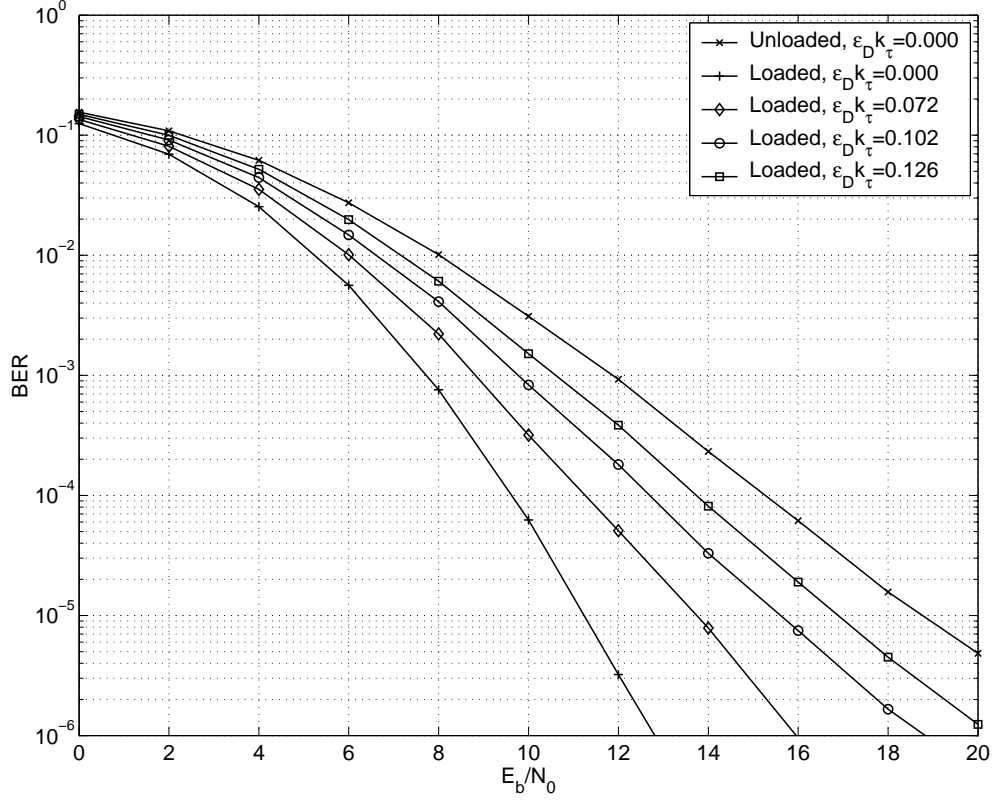


Figure 4.1: BER of bit-loaded OFDM in presence of outdated CSI.

the CSI becomes less up-to-date. For example, we can see that at a BER of 10^{-5} , approximately 2.25dB loss is introduced at $k_{\tau}\varepsilon_D = 0.072$ and more than 4dB loss occurs at $k_{\tau}\varepsilon_D = 0.102$.

4.3 CDM based Robust Bit-Loaded OFDM

The use of frequency domain CDM has previously been studied by Kaiser [47]. When frequency domain CDM is used, frequency diversity is achieved without any loss in transmission rate. Our proposed CDM based bit-loaded OFDM system uses the frequency diversity achieved from the use of CDM to combat unreliability in CSI. To describe our proposed system and obtain the results we assume that Fischer's bit-loading algorithm has been used. However, with minor modifications the proposed system can also be employed with other bit-loading algorithms.

4.3.1 System Description

In our CDM based bit-loaded system, first the sub-channels are sorted according to $|H_{n,k_0-k_{\tau}}|$. The sorted sub-channels are then grouped into K groups of $L = N/K$

sub-channels. Then, using a conventional bit-loading algorithm $R \leq L$ symbols are assigned to each group. Within each group, the R symbols are spread using orthogonal Hadamard codes. In other words, if $\mathbf{x} = [x_0, \dots, x_{N-1}]^T$ is the vector of data symbols modulated according to the sorted sub-channel gains, the spread symbols are obtained by

$$\mathbf{y} = \mathbf{C}\mathbf{x} \quad (4.6)$$

where the code matrix, \mathbf{C} , is an $N \times N$ block-diagonal matrix, and all diagonal components of \mathbf{C} are equal to the $L \times L$ Hadamard matrix [1], \mathcal{H}_L , defined by

$$\mathcal{H}_{2^m} = \begin{cases} [1] & m = 0 \\ \begin{bmatrix} \mathcal{H}_{2^{m-1}} & \mathcal{H}_{2^{m-1}} \\ -\mathcal{H}_{2^{m-1}} & \mathcal{H}_{2^{m-1}} \end{bmatrix} & \text{otherwise} \end{cases}, \quad (4.7)$$

where $L = 2^m$. Note that when $R < L$, before spreading, $L - R$ symbols in each group are set to zero.

Since the symbols within each group are spread over all L sub-channels in that group, they experience an equivalent channel gain equal to

$$|H'_{kL+l}| = \sqrt{\frac{1}{L} \sum_{i=0}^{L-1} |H_{kL+i}|^2}, \quad (4.8)$$

where k is the group index and l is the index of the sub-channel within its group. Therefore, this equivalent channel gain must be used in the bit-loading algorithm to determine the appropriate bit and power allocation.

The spread symbols are then transmitted through the channel. Thus the received values can be expressed as

$$\mathbf{r} = \mathbf{H}\mathbf{y} + \mathbf{n}, \quad (4.9)$$

where $\mathbf{H} = \text{diag}(H_0, \dots, H_{N-1})$, $H_n = H_{n,k_0}$ and \mathbf{n} is the AWGN noise vector with covariance matrix $\sigma_n^2 \mathbf{I}_N$. Note that to simplify the notation, here we assume that H_n are sorted. In practice, \mathbf{y} must be unsorted before transmission.

If $R = 1$, for optimum noise performance, the received values must be combined at the receiver using Maximal Ratio Combining (MRC). In other words, the received values are then equalized by the equalization matrix \mathbf{G}_{MRC} , i.e.

$$\hat{\mathbf{y}} = \mathbf{G}_{MRC}\mathbf{r}, \quad (4.10)$$

where $\mathbf{G}_{MRC} = \text{diag}(G_{MRC,0}, \dots, G_{MRC,N-1})$ and

$$G_{MRC,kL+l} = \frac{H_{kL+l}^*}{\frac{1}{L} \sum_{i=0}^{L-1} |H_{kL+i}|^2}. \quad (4.11)$$

The sum in (4.11) is performed within each symbol's group. The estimates of the data symbols can then be found by despreading $\hat{\mathbf{y}}$, or

$$\begin{aligned}\hat{\mathbf{x}}_{MRC} &= \mathbf{C}^T \hat{\mathbf{y}} \\ &= \mathbf{C}^T \mathbf{G}_{MRC} \mathbf{H} \mathbf{C} \mathbf{x} + \mathbf{C}^T \mathbf{G}_{MRC} \mathbf{n}.\end{aligned}\quad (4.12)$$

If $R > 1$, although the spreading codes are orthogonal, due to the difference in the channel gains in the sub-channels used for spreading, the received signals are not orthogonal.

If MRC is used to combine the received values, noise performance is optimized, but self interference is created. On the other hand, if Zero-Forcing (ZF) combining is used, i.e.

$$\hat{\mathbf{y}} = \mathbf{G}_{ZF} \mathbf{r}, \quad (4.13)$$

and

$$\begin{aligned}\hat{\mathbf{x}}_{ZF} &= \mathbf{C}^T \hat{\mathbf{y}} \\ &= \mathbf{C}^T \mathbf{G}_{ZF} \mathbf{H} \mathbf{C} \mathbf{x} + \mathbf{C}^T \mathbf{G}_{ZF} \mathbf{n}.\end{aligned}\quad (4.14)$$

where $\mathbf{G}_{ZF} = \text{diag}(G_{ZF,0}, \dots, G_{ZF,N-1})$ and

$$G_{ZF,kL+l} = \frac{H_{kL+l}^*}{|H_{kL+l}|^2}, \quad (4.15)$$

the self-interference between the symbols can be avoided. However, ZF combining results in noise enhancement and, therefore, does not result in desirable performance.

To deal with this problem we use an iterative Multi User Detection (MUD) technique known as *multi-stage detection with decorrelating first stage* [106]. In this technique, first the received values are combined using both ZF and MRC. Then, the data bits are detected and decoded using the symbol estimates obtained from the ZF combining, $\hat{\mathbf{x}}_{ZF}$. These bits are then re-encoded and remodulated to result in a more accurate estimate of the original symbols, $\hat{\mathbf{x}}_1$. Using these estimates the amount of self interference created in the MRC process is calculated

$$\mathbf{s}_1 \approx (\mathbf{A} - \text{diag}(\mathbf{A})) \hat{\mathbf{x}}_1, \quad (4.16)$$

where

$$\mathbf{A} = \mathbf{C}^T \mathbf{G}_{MRC} \mathbf{H} \mathbf{C}. \quad (4.17)$$

This self-interference is then subtracted from the symbol estimates obtained from MRC to obtain a better estimate

$$\hat{\mathbf{x}}_{MUD,1} = \hat{\mathbf{x}}_{MRC} - \mathbf{s}_1. \quad (4.18)$$

This process can be iteratively repeated by using the symbol estimates obtained from (4.18) in (4.16). Figure 4.2 depicts two iterations of this technique.

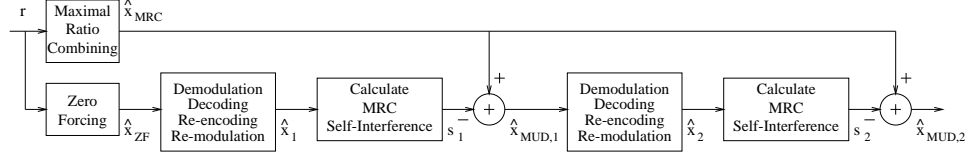


Figure 4.2: Multi-stage detector with decorrelating first stage for CDM.

In summary, one possible implementation of the the proposed algorithm can be described in the following steps. These steps are also depicted in Figure 4.3. Here the bit-loading algorithm is implemented at the receiver and the bit and power allocation as well as the sort permutation is sent back to the transmitter via the feedback channel.

- **At the transmitter:**

1. Modulate the coded data bits, according to the bit and power allocation received from the feedback channel.
2. Spread the symbols.
3. Unsort the sub-channels using the permutation received from the feedback channel.
4. Perform OFDM modulation (IFFT and cyclic prefix) and transmit.

- **At the receiver:**

1. Bit-loading:
 - (a) Sort the sub-channels according to the available CSI, and divide the sub-channels into groups.
 - (b) Within each group of L sub-channels, calculate the effective channel gain.
 - (c) Use a conventional bit-loading algorithm to find the bit and power allocation.
 - (d) Send the bit and power allocation and the sort permutation to the transmitter.
2. Detection:
 - (a) Perform OFDM demodulation (FFT and removal of the cyclic prefix)
 - (b) Sort the sub-channels using the (delayed) permutation.
 - (c) Employ the MUD technique to detect the data, using current CSI.
 - (d) Demodulate the symbols and decode.

The proposed scheme is less sensitive to CSI error since, although the sub-channel coefficients in each group are relatively equal in magnitude, the CSI errors on these

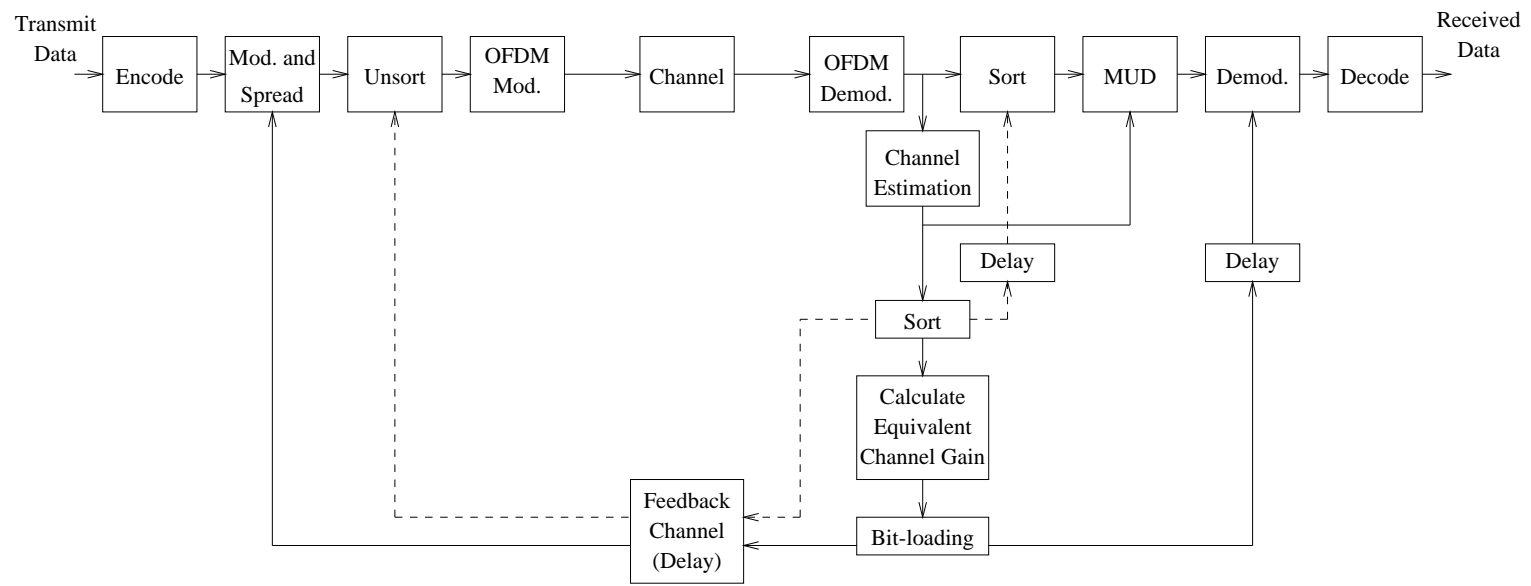


Figure 4.3: OFDM system with CDM based robust bit-loading.

sub-channels are not necessarily similar. This is due to the fact that the sub-channels are shuffled when they are sorted according to their quality. The shuffling effect happens specially when the channel is strongly frequency selective and large number of sub-channels exist. In this case sub-channels with similar quality exist at different places in the total bandwidth. While these sub-channels have similar magnitude, since they are not correlated, they have different magnitude errors. Therefore, the diversity obtained from the spreading the symbols can reduce the effect of CSI errors.

4.3.2 Computational Complexity

The calculation of the exact computational complexity of the system is complicated and strongly depends on the specific implementation details. Here we provide a very loose approximate calculation of the order of the additional computational complexity required to implement the proposed robust systems. For simplicity, compared to the complexity of complex multiplications, we neglect the addition operations.

The number of comparison operations required for sorting the sub-channels is of the order of $N \log N$. This operation is only performed once. Other “sort” and “un-sort” blocks in Figure 4.3 are merely reordering (or re-indexing) of the data according to the permutation obtained from the sort operation.

In the matrix form, spreading and despreading operations appear to require $L^2K = LN$ multiplications each. However, since the components of the Hadamard matrices are limited to 1’s and -1 ’s, multiplications are not necessary and only the signs of the variables must be changed before summations. Therefore, these operations require additions and less than LN sign changes that do not involve considerable computational complexity.

Calculation of each MRC weight only requires summations and one division. Note that $|H_l|^2$ have to be calculated to be used in the bit-loading algorithm, even when CDM is not used. Similarly, to calculate each ZF weight only one division is used. Multiplication of the symbols by these weights also require N multiplications each.

The main factor in computational complexity is the iterative MUD technique. In calculation of matrix \mathbf{A} , the calculation of \mathbf{GH} only requires N multiplications. Thus, the calculation of matrix \mathbf{A} only requires additions, sign changes and N multiplications. However, to calculate the self-interference using (4.16), $IL^2K = ILN$ multiplications are required, where I is the number of iterations. Besides, for each iteration, the data bits must be decoded and re-encoded. The computational complexity of this operation is dominated by the Viterbi algorithm. Here we have used hard-decision decoding, thus the calculation of the metrics only requires XOR operations, which is negligible compared to complexity of the other operations. The Viterbi algorithm also requires S comparisons per coded-bit or $ISMN$ comparisons per OFDM symbol, where S is the number of states and M is the number of coded bits per OFDM sub-carrier.

Thus, overall we can say that the implementation of the proposed system requires

$O(ILN)$ additional complex multiplications and $O(N \log N + ISMN)$ additional comparisons.

4.4 Robust Bit-Loaded MIMO OFDM

The proposed system can be extended to a MIMO OFDM system for bit-loading in frequency and space.

4.4.1 Space-Frequency Sub-Channels

In a MIMO OFDM system, each sub-channel must be modelled in vector form. In other words, if M_T transmitter antennas and M_R receiver antennas are used, for the i th sub-channel we can write

$$\mathbf{r}_i = \mathbf{H}_i \mathbf{s}_i + \mathbf{n}_i, \quad (4.19)$$

where $\mathbf{s}_i = [s_0, \dots, s_{M_T-1}]^T$ and $\mathbf{r}_i = [r_0, \dots, r_{M_R-1}]^T$ are the vector of transmitted symbols and received values on all antennas, $\mathbf{n}_i = [n_0, \dots, n_{M_R-1}]^T$ is a zero mean AWGN vector with covariance matrix $\mathbf{K}_n = \sigma^2 \mathbf{I}_{M_R}$ and \mathbf{H}_i is an $M_R \times M_T$ matrix containing the channel coefficients for each pair of transmit and receive antennas. For simplicity, let us assume $M_T = M_R = M_A$. With minor modifications the following can be extended to the case where $M_T \neq M_R$.

If the matrix \mathbf{H}_i is decomposed using a Singular Value Decomposition (SVD) [21], we have

$$\mathbf{H}_i = \mathbf{U}_i \mathbf{\Sigma}_i \mathbf{V}_i^\dagger, \quad (4.20)$$

where $\mathbf{\Sigma}_i$ is a diagonal matrix containing the singular values of \mathbf{H}_i , and \mathbf{U}_i and \mathbf{V}_i are column orthogonal matrices and $(\cdot)^\dagger$ represents the Hermitian transpose. Hence, if the spread symbol vector $\mathbf{y}_i = [y_0, \dots, y_{M_A-1}]^T$ is pre-coded to produce

$$\mathbf{s}_i = \mathbf{V}_i \mathbf{y}_i, \quad (4.21)$$

and the received symbols are post-processed by

$$\mathbf{z}_i = \mathbf{U}_i^\dagger \mathbf{r}_i, \quad (4.22)$$

we have

$$\begin{aligned} \mathbf{z}_i &= \mathbf{U}_i^\dagger \mathbf{r}_i \\ &= \mathbf{U}_i^\dagger \mathbf{U}_i \mathbf{\Sigma}_i \mathbf{V}_i^\dagger \mathbf{V}_i \mathbf{y}_i + \mathbf{U}_i^\dagger \mathbf{n}_i \\ &= \mathbf{\Sigma}_i \mathbf{y}_i + \mathbf{n}'_i. \end{aligned} \quad (4.23)$$

This means that with this pre-coding and post-processing, each sub-channel is equivalent to M_A parallel sub-channels in space, with gains equal to the singular values of

\mathbf{H}_i . Obviously, if $\text{rank}(\mathbf{H}_i) < M_A$ some of the (space) sub-channel gains will be equal to zero. Furthermore, we note that

$$\begin{aligned}
\mathbf{K}_{\mathbf{n}'} &= \mathbb{E}[\mathbf{n}_i'^\dagger \mathbf{n}_i'] \\
&= \mathbb{E}[\mathbf{n}_i^\dagger \mathbf{U}_i \mathbf{U}_i^\dagger \mathbf{n}_i] \\
&= \mathbb{E}[\mathbf{n}_i^\dagger \mathbf{n}_i] \\
&= \sigma^2 \mathbf{I}_{M_A}.
\end{aligned} \tag{4.24}$$

In other words, the post-processing does not result in any change in the noise characteristics. Overall, if this pre-coding and post-processing is used for all OFDM sub-channels, a MIMO OFDM system can be seen to have a total of NM_A space-frequency sub-channels.

4.4.2 Robust Bit-loading in Space and Frequency

Given the concept of space-frequency sub-channels, any bit-loading algorithm can be used to assign the number of bits and transmission power to these sub-channels [76][112]. However, such a system will be even more sensitive to unreliable CSI since not only the bit-loading is sub-optimal, the pre-coding does not match the channel. In other words,

$$\begin{aligned}
\mathbf{z}_i &= \mathbf{U}_{k_0,i}^\dagger \mathbf{r}_i \\
&= \mathbf{U}_{k_0,i}^\dagger \mathbf{U}_{k_0,i} \boldsymbol{\Sigma}_{k_0,i} \mathbf{V}_{k_0,i}^\dagger \mathbf{V}_{k_0-k_\tau,i} \mathbf{y}_i + \mathbf{U}_{k_0,i}^\dagger \mathbf{n}_i \\
&= \boldsymbol{\Sigma}_{k_0,i} \mathbf{V}_i' \mathbf{y}_i + \mathbf{n}_i',
\end{aligned} \tag{4.25}$$

where $\mathbf{V}_i' = \mathbf{V}_{k_0,i}^\dagger \mathbf{V}_{k_0-k_\tau,i}$. This means that the components of \mathbf{y}_i interfere with each other, which in turn causes more performance degradation.

Another important point is that the spreading and despreading must be performed on sorted space-frequency sub-channels. But the sub-channels must be unsorted before they can be transmitted over the proper sub-channels. Thus, the vector of received values are

$$\mathbf{z} = \boldsymbol{\Sigma} \mathbf{V}' \mathbf{P}^{-1} \mathbf{C} \mathbf{x} + \mathbf{n}, \tag{4.26}$$

where \mathbf{z} , \mathbf{x} and \mathbf{n} are vectors of length NM_A , \mathbf{H} , \mathbf{V}' and \mathbf{C} are block diagonal matrices with components \mathbf{H}_i , \mathbf{V}_i' , and \mathcal{H}_L , respectively, and \mathbf{P} is a permutation matrix modelling the sort process. Now, if we define

$$\tilde{\mathbf{H}} = \boldsymbol{\Sigma} \mathbf{V}' \mathbf{P}^{-1} \mathbf{C}, \tag{4.27}$$

The ZF and MRC combining results can be found from (see Appendix B)

$$\hat{\mathbf{x}}_{ZF} = \tilde{\mathbf{H}}^{-1} \mathbf{z}, \tag{4.28}$$

and

$$\hat{\mathbf{x}}_{MRC} = \text{diag}(\tilde{\mathbf{H}}^\dagger \tilde{\mathbf{H}})^{-1} \tilde{\mathbf{H}}^\dagger \mathbf{z}. \quad (4.29)$$

and the matrix \mathbf{A} , used in the MUD technique is now

$$\mathbf{A} = \text{diag}(\tilde{\mathbf{H}}^\dagger \tilde{\mathbf{H}})^{-1} \tilde{\mathbf{H}}^\dagger \tilde{\mathbf{H}}. \quad (4.30)$$

Although the computational complexity of this method is high, the computation of these matrices are practical since

$$\tilde{\mathbf{H}}^{-1} = \mathbf{C}^T \mathbf{P} \mathbf{V}'^\dagger \mathbf{\Sigma}^{-1} \quad (4.31)$$

and

$$\tilde{\mathbf{H}}^\dagger = \mathbf{C}^T \mathbf{P} \mathbf{V}'^\dagger \mathbf{\Sigma}. \quad (4.32)$$

Note that $\mathbf{P}^{-1} = \mathbf{P}^\dagger$, $\mathbf{V}'^{-1} = \mathbf{V}'^\dagger$, and $\mathbf{\Sigma}$ is diagonal and has real components. Also, we note that the \mathbf{C} and \mathbf{V}' are sparse. Thus, these computations can take place using sparse matrices, where the permutation can also be performed with little additional complexity.

4.5 Results

In this section we present the simulation results for the performance of the proposed systems and compare them to the conventional ones.

4.5.1 Robust Bit-Loaded OFDM

Similar to Section 4.2.2, we assume that the OFDM system has $N = 256$ sub-channels and each sub-channel has a bandwidth of 10kHz. The data bits are coded using a half rate convolutional code with constraint length 6, and interleaved using a random interleaver. The decoding is performed using a hard-decision Viterbi algorithm. We use the 12 tap Hilly Terrain model (HTx) provided in the GSM standard [24]. Furthermore, we have assumed that the channel remains constant during one OFDM symbol and that a cyclic prefix of sufficient length removes ISI and ICI.

Let us first look at the case where $R = 1$. This case is of interest, since the absence of self interference allows the use of MRC. Hence, the iterative MUD technique is not required and the system can be implemented with much lower complexity. Figure 4.4 compares the proposed system with $L = 4$ and $R = 1$, to a conventional system ($L = 1$), for different values of Doppler-delay product. In both systems a total of $B_T = N/2$ coded data bits have been modulated on each OFDM symbol. We observe that as expected, the performance degradation in the conventional system is much more severe compared to that of the proposed system. However, the performance of the proposed system is worse in presence of perfect CSI. Hence, the performance gain only appears at higher Doppler-delay products and at lower BER values.

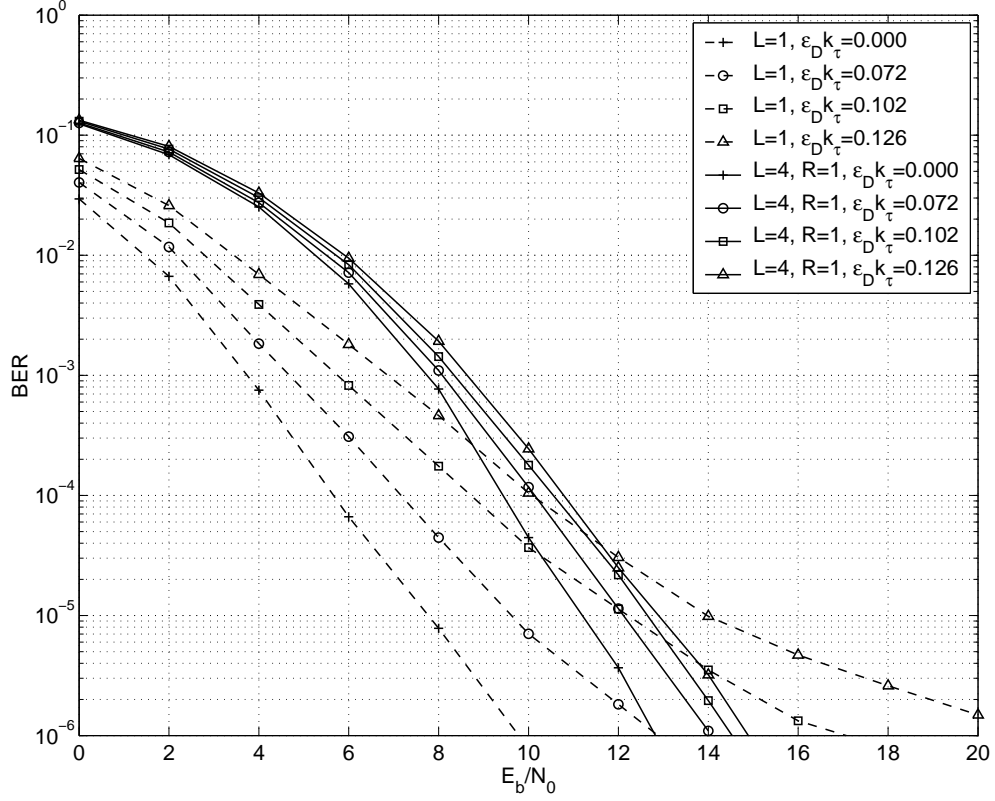


Figure 4.4: BER performance of the proposed system with $L = 4$ and $R = 1$ compared to that of a conventional system.

When perfect CSI is available, the proposed system has a inferior performance compared to the conventional system. This is because spreading forces the proposed system to use the sub-channels with bad quality, to provide the same transmission rate. This problem does not exist when $L = R$. However, in such a case, the more complex MUD detection technique must be used to remove the self interference, and higher computational complexity is required.

Figure 4.5 depicts the BER performance of the proposed system with $L = R = 4$ and compares it to that of the conventional system ($L = 1$). In both systems, a total of $B_T = 2N$ coded bits are modulated. We have assumed that a Doppler-delay product of $\varepsilon_D k_\tau = 0.102$ exists. The BER results are presented for three cases where $I = 1, 2$ and 3 iterations are performed in the detection process. Also, the BER results for a genie aided MUD, where correct symbols are used instead of $\hat{\mathbf{x}}_{ZF}$. The genie aided system has a performance equivalent to an MRC scheme without any self-interference.

We observe that even with $I = 1$ iteration, the proposed algorithm considerably outperforms the conventional one. Furthermore, we observe that $I = 2$ iterations result in BER performance approximately equal to that of the genie aided case and

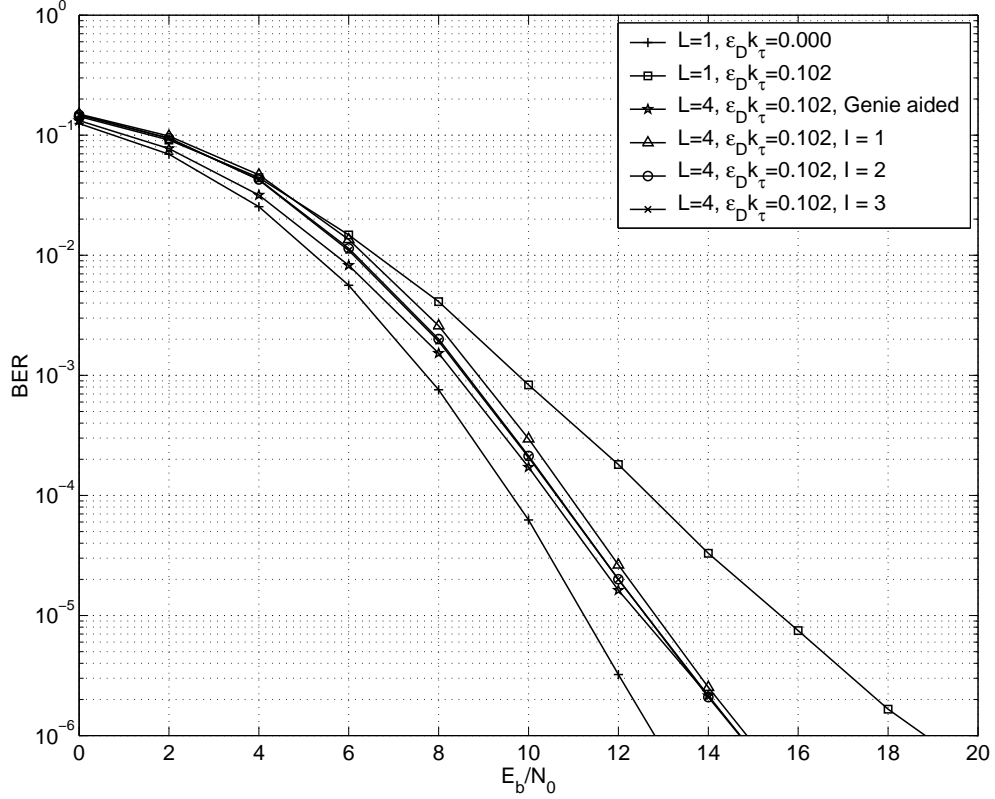


Figure 4.5: BER performance of the proposed system with different numbers of iterations of the MUD scheme.

using larger number of iterations does not result in additional gain. Compared to the conventional system we can see that approximately 3dB gain is achieved at a BER equal to 10^{-5} .

Figure 4.6 compares the BER performance of the proposed algorithm for group sizes $L = 1, 2, 4$ and 8 , when a Doppler-delay product of $\varepsilon_D k_\tau = 0.102$ exists. As expected, we can see that a larger group size allows a larger degree of diversity, and thus, a better performance is achieved. However, we note that the computational complexity of the system quickly increases with L and the achieved incremental gain decreases with L . The results suggest that groups larger than $L = 4$ unjustifiably increase the complexity of the system while providing marginal performance gain.

4.5.2 Robust Bit-Loaded MIMO OFDM

First we look at the sensitivity of a space-frequency bit-loaded MIMO system, without CDM. We assume that the OFDM system has $N = 64$ sub-channels, each with a bandwidth of 10kHz. Also, we assume that $M_A = 2$ receive and transmit antennas are used. Thus, a total of $NM_A = 128$ space-frequency sub-channels are available. Furthermore, similar to our previous simulations, we assume that the data bits are

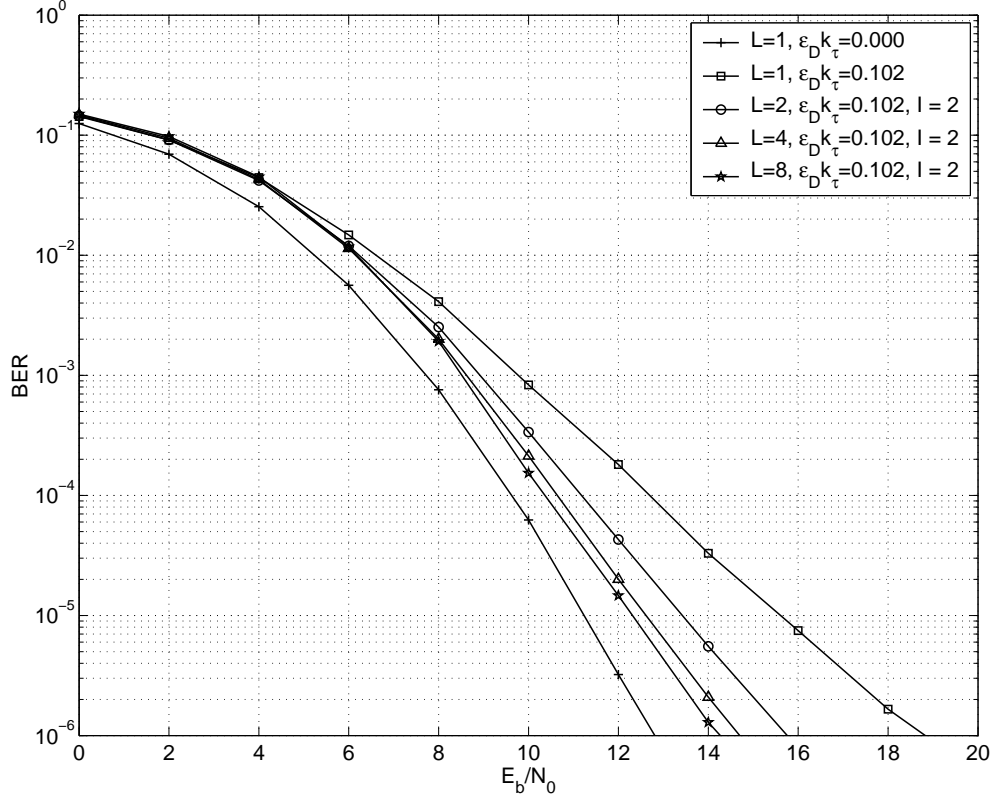


Figure 4.6: BER performance of the proposed algorithm with different group sizes.

coded using a half rate convolutional code and interleaved using a random interleaver. A hard-decision Viterbi algorithm is used for decoding. We use the 12 tap Hilly Terrain model (HTx) provided in the GSM standard [24]. We have assumed that the channel remains constant during one OFDM symbol and that a cyclic prefix of sufficient length removes ISI and ICI.

Figure 4.7 shows that as discussed in Section 4.4.2, this system is even more sensitive to outdated CSI compared to a single antenna OFDM system studied in Section 4.2.2. We can see that at a BER of 10^{-4} , Doppler-delay products of 0.045 and 0.072 result in 3.5dB and 6.5dB loss, respectively.

Figure 4.8 compares the proposed robust system with $L = R = 4$, with a conventional system ($L = 1$), for a Doppler-delay product of $\epsilon_D k_\tau = 0.072$. The MUD technique described above has been used and the results are presented for $I = 1$ and 2 iterations, as well as the genie aided case. We observe that the proposed scheme is considerably less sensitive to outdated CSI. For example, we can see that at a BER of 10^{-4} the MUD with $I = 1$ iteration results in approximately 3dB gain. If $I = 2$ iterations are used, this gain is increased to about 5dB. In the genie aided case 6dB gain is achieved. We expect that with increasing the number of iterations, the BER

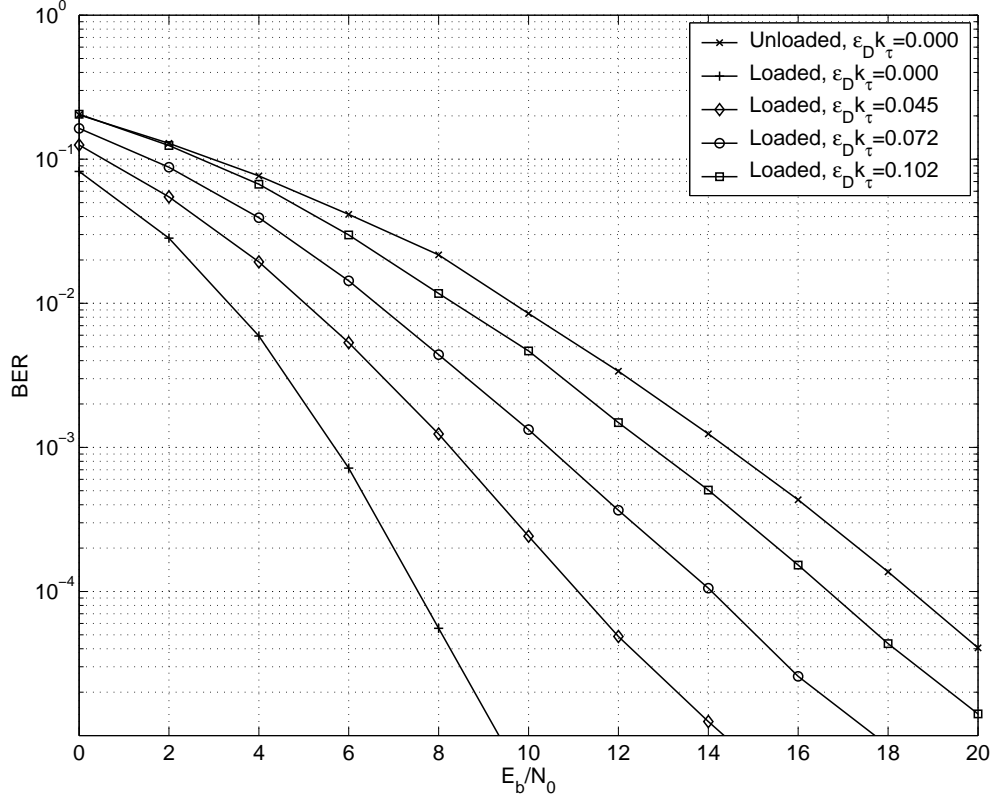


Figure 4.7: BER of bit-loaded MIMO-OFDM in presence of outdated CSI.

performance of the MUD technique approaches that of the genie aided case.

4.6 Summary

In this chapter after considering the sensitivity of a bit-loaded OFDM system to outdated CSI, we offered a robust bit-loaded OFDM system where frequency domain CDM has been used to achieve frequency diversity, without any loss in transmission rate. Our simulation results show that the proposed system is considerably less sensitive to outdated CSI than the conventional system, and can tolerate larger Doppler-delay products, which means that the system can be used for high data rate communications over channels with higher degree of time variations. This robustness is achieved at the price of increased complexity.

We also looked at the sensitivity of a MIMO OFDM system where by employing pre-coding and post-processing, the bit-loading is performed in space and frequency. We saw that this system is even more sensitive to unreliable CSI, since unreliability in CSI also leads to sub-optimal pre-coding. We then extended our proposed method to such a system where the bit-loading and CDM are performed on space-frequency sub-channels. Our results show that our proposed system also provides robustness in

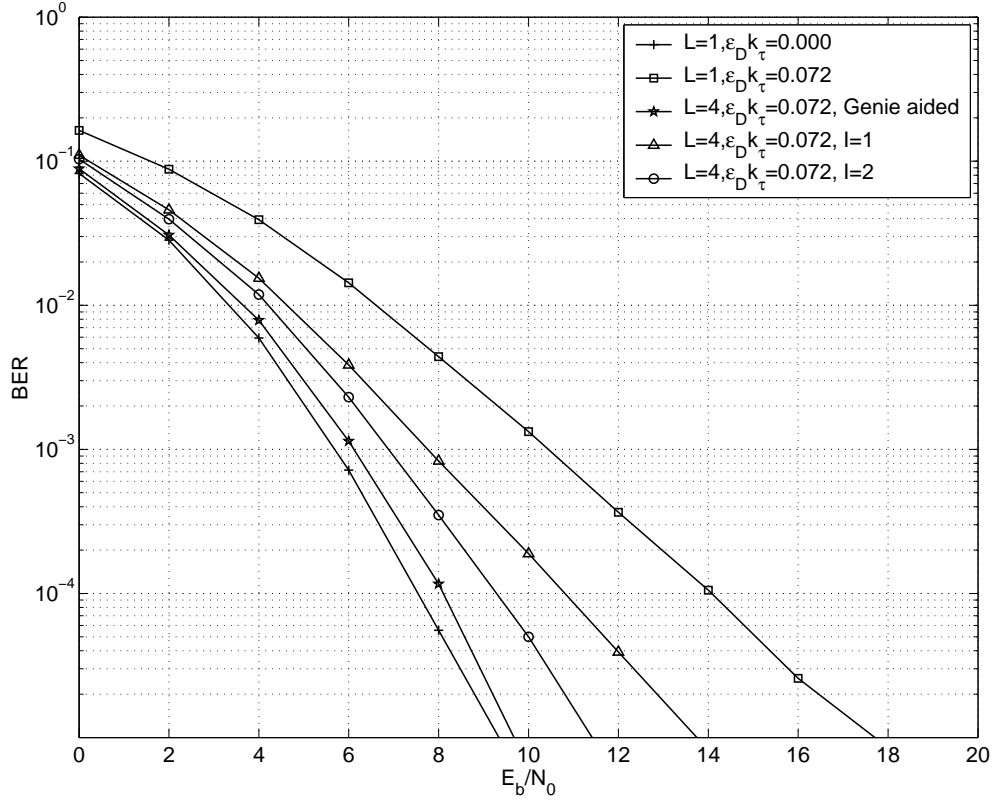


Figure 4.8: BER performance of the proposed MIMO OFDM system with different numbers of iterations of the MUD technique.

a bit-loaded MIMO OFDM system, at the price of higher computational complexity.

Chapter 5

Conclusion and Future Direction

In this part of the report we have considered some of the important issues arising from the use of OFDM and MC modulation schemes over wireless channels.

In Chapter 2 we improved the performance of the Zhao-Haggman's ICI self-cancellation scheme by generalizing it. We proposed the general self-cancellation scheme that uses windowing operations at the transmitter and the receiver to reduce the amount of ICI. We demonstrated that the Zhao-Haggman's method is a special case of the general self-cancellation scheme. After analyzing the SIR and BER of the proposed system, we proceeded to design windows based on an SIR or a BER constraint. Our results showed that the proposed scheme outperforms the Zhao-Haggman and the conventional OFDM systems.

In Chapter 3 we proposed the sub-channel selective MC-SS and MC-CDMA as a sub-optimal, on/off, bit-loading (chip-loading) technique, where the transmitter only uses a fraction of the sub-channels to transmit the data chips. We also provided the drop and add distributed algorithm that requires very small amount of feedback. We showed that this algorithm converges to near optimum selection of the sub-channels. Our performance results show that the sub-channel selective MC-SS system has considerably better power efficiency. This gain was also shown in the sub-channel selective MC-CDMA system, where both noise and interference has been considered in selecting the sub-channels.

In Chapter 4 we considered the problem of unreliability in CSI when a bit-loaded OFDM system operates over a time-variable channel. We focused on the feedback delay as the major cause of CSI unreliability and showed that the existing bit-loaded systems are very sensitive to unreliable CSI. Then, we proposed a robust bit-loaded OFDM system where the data symbols are spread over a group of sub-channels using CDM. This allows the system to achieve frequency diversity without any loss in transmission rate. At the receiver an iterative MUD algorithm is used to detect the spread symbols and remove self-interference. We also extended our proposed method to bit-loaded MIMO OFDM systems where bit-loading is performed in frequency and space. Our results show that the proposed system can tolerate higher degree of

unreliability in CSI. Therefore, it can be employed over channels with considerably faster time variations.

Overall we have considered some of the most important problems of high data rate OFDM and MC modulation systems operating over wireless channels. In doing so we have proposed solutions and novel systems that can improve the performance of the high data rate communications over frequency selective fading channels. Hence, we have helped making the implementation of such systems more practical and more feasible.

5.1 Future Direction

In regard to the general self-cancellation scheme, many possible directions can be followed in future research.

In our window design process, we have limited ourself to windows that are constructed as sum of complex exponentials. Although any window of length N can be described as a summation of N complex exponentials, the computational complexity of the window design using an exhaustive search becomes prohibitively large. With a more general look at the windows, and considering other window design methods, potentially better windows may be designed.

Also, the proposed general self-cancellation scheme provides better performance in presence of frequency shifts, at the price of lowering the data rate by a factor of L . Although Zhao and Haggman have shown that their half rate scheme performs better than a half rate convolutional code, in general a combination of coding and a self-cancellation scheme might be used. Hence, a study of the trade-off between the coding rate and L is needed.

Another issue is channel estimation. When a self-cancellation is used, the power of each data symbol is distributed over more than one sub-channel. Therefore, when a pilot-symbol aided channel estimation is used, more information is available since the power of each pilot is also distributed over more than one sub-channel. Thus, the channel estimation should take this into account by combining all of the power from pilot symbols for channel estimation.

In our window design process we forced the windows to have symmetrical spectrum, but we did not force them to be symmetrical in time. This means that our designed windows are not real in the frequency domain. Thus, a phase shift is introduced to the frequency components of the signal. However, since an unknown phase shift is already introduced by the channel, this additional phase shift does not cause any problem in the design of the system, since it can be corrected together with the channel phase shift. To the best knowledge of the author, in most applications of windowing in communication systems standard windows are employed. These windows generally have very good side-lobe characteristics. However, they have been designed under the constraint that they must be symmetric in time. This leads us to believe

that potentially better windows can be designed for other applications of windowing in communication systems, by relaxing the requirement of symmetry in time.

Research on the robust bit-loaded OFDM systems using CDM can also be continued in several directions.

One possible direction is the study of other causes of unreliability in CSI, namely channel estimation error and limited bandwidth in the feedback channel. While we have focused on the feedback delay as the main cause of unreliability in CSI, it is conceivable to believe that the frequency diversity gained by the CDM bit-loaded scheme can mitigate unreliable CSI regardless of its source. However, other causes lead to different models for unreliable CSI. Furthermore, channel estimation error affects the detection at the receiver as well as the bit-loading. Hence, a study of the effectiveness of the proposed method in mitigation of unreliability in CSI caused by other causes is needed.

Also, in obtaining our results we have used Fischer's bit-loading algorithm in conjunction with our CDM scheme. Fischer's algorithm minimizes the symbol error rate for given power and data rate for each OFDM symbol. Other bit-loading algorithms where the power consumption or the transmission rate are optimized should also be considered.

In our study we have used a multi-user detection technique called the *multi-stage detection with decorrelating first stage*. While this technique has proved to be successful in detection of the CDM modulated symbols, it is computationally complex. Other detection and interference cancellation techniques may be able to achieve equal performance with lower computational complexity. Thus, the detection of the CDM modulated signals with other MUD techniques can be studied.

Another angle in future research is an attempt to remove the sorting of the sub-channels according to their quality. Besides reducing the complexity, this would allow the system to operate on channels with larger coherence bandwidths. The proposed system achieves frequency diversity, since if the channel coherence bandwidth is much smaller than the group width, the CSI error of the sub-channels in each group will be uncorrelated. However, if the sort precess is removed, the sub-channels of each group can be chosen using an interleaving process. Thus, such a system would not necessarily require the above assumption. On the other hand spreading the symbols on groups consisting of sub-channels with very different qualities is expected to lower the bit-loading gain. Hence, the performance of such a system and its ability to combat CSI unreliability must be studied.

Part II

**JOINT SOURCE-CHANNEL
CODING**

Chapter 6

SPIHT Source Coding

6.1 Introduction

This part of the report treats joint source and channel coding. We shall present extensive results for transmission of 2-D and 3-D SPIHT encoded images and video at various transmission rates and various multipath spread and Doppler frequency for various multi-antenna systems. The basis of our performance results throughout this section is the development of a new real-time operational source code distortion-rate (D-R) estimator. If the transmitter does not have any knowledge of the channel, then a joint source-channel coding (JSCC) algorithm must naturally be designed for a worst case scenario. We will also give results of the PSNR degradation using the worst case scenario. Later results will establish that by using MIMO OFDM and a real time JSCC algorithm under a transmission rate constraint, a higher PSNR can be achieved relative to the SISO system for image and image sequence transmission at low signal-to-noise (SNR) ratio. We will also use time and frequency interleaving when more protection is needed against fading.

In the following sections, we give an overview of the SPIHT compression algorithm and introduce the new D-R estimator. In Chapter 3, we employ a real-time near optimum JSCC method over the binary symmetric channel (BSC) and BPSK modulation over the flat fading channel. In Chapter 4, both analytic and simulation results, based on our own MATLAB simulator, are generated for the single-input, single-output (SISO) OFDM system. Chapter 5 treats the MIMO channel in which orthogonal space-time block codes (OSTBC) are employed. We develop a nearly optimum real-time JSCC algorithm for SISO and OSTBC MIMO and present both analytic and simulation results for various multipath delays and Doppler spreads.

6.2 SPIHT Image Compression

SPIHT is an embedded wavelet compression algorithm, and as such, it admits special properties for resistance to channel errors. In this section, we review the algorithm and give compression results for our implementation in MATLAB.

6.2.1 Performance measures

Two popular distortion metrics are the Mean Squared Error(MSE) and the Peak Signal to noise Ration(PSNR). Given an image X of size $M_r * M_c$ and it's lossy compressed version \tilde{X} , the MSE and PSNR are defined as

$$MSE = \frac{1}{M_r M_c} \sum_{i=1}^{M_r} \sum_{j=1}^{M_c} (X(i, j) - \tilde{X}(i, j))^2 \quad (6.1)$$

$$PSNR = 10 \log_{10}(255^2 / MSE) \quad (6.2)$$

PSNR will be used to evaluate the simulation results throughout this report.

transformed into another domain, and then quantized and subsequently coded. This process is referred to as Transform Coding. The transforms which are usually linear, exploit the interpixel correlation in the image for the purpose of compression. One measure of performance of a particular transform is how well it decorrelates the signal. The discrete wavelet transforms(DWT) we will be looking at are Biorthogonal and Separable. The main observation is that as a result of having the biorthogonality condition, the squared norm in the transform domain is not preserved but it is very close for the filters we will be using.

Chapter 7

The SPIHT Algorithm

An overview of the SPIHT [139] algorithm is given in this chapter in order to enhance understanding of error sensitivities of different kinds of bits in the SPIHT codestream. We shall distinguish between the two classes of bits, the value bit class (VBC) and the location bit class (LBC). In a later chapter, we shall derive formulas for the contribution of bits in the VBC toward lowering the distortion. We shall also see that channel errors affecting the VBC cause only graceful degradation of performance, while channel errors affecting the LBC cause loss of synchronization and catastrophic failure.

First the source image is transformed via a discrete wavelet transform of three or more levels of decomposition. Figure 7.1 shows the subband structure of a three-level two-dimensional decomposition and the so-called spatial orientation tree structures upon which the SPIHT algorithm searches. For the LL band, each coefficient in a 2 by 2 block with the exception of the upper left coefficient is a parent of four coefficients in the same subband. For other subbands, each coefficient is a parent of four coefficient at the next lower level. This process continues until we reach the first subband level and since there are no more levels, the first level has no descendants. With the exception of the LL band which links a parent to four children on the same level, every other parent coefficient is linked to its children in the next lower subband. In these bands each coefficient at the pixel (i,j) is a root for the pixels $(2i, 2j)$, $(2i+1, 2j)$, $(2i, 2j+1)$, $(2i+1, 2j+1)$. Following the notation in [139] let us denote by $\mathcal{O}(i,j)$ the set of coordinates of the offsprings of the wavelet coefficient at location (i,j) . In Figure 7.1 $\mathcal{O}(0,1)$ consists of the coordinates of the coefficients B1, B2, B3 and B4. We definite $\mathcal{D}(i,j)$ as the set of all descendants of the coefficients at location (i,j) . Descendants include the children, the grandchildren and so on all the way down to the first subband level. As seen in Figure 7.1, the size $\mathcal{D}(i,j)$ is either zero or is a sum of powers of four. By \mathcal{H} we denote the set of all nodes in the LL band. Finally by $\mathcal{L}(i,j)$ we mean the set of coordinates of all descendants of the coefficient at location (i,j) except for the immediate children of the coefficient at location (i,j) . By definite $\mathcal{L}(i,j) = \mathcal{D}(i,j) - \mathcal{O}(i,j)$. In Figure 2.1 the set $\mathcal{L}(0,1)$ is

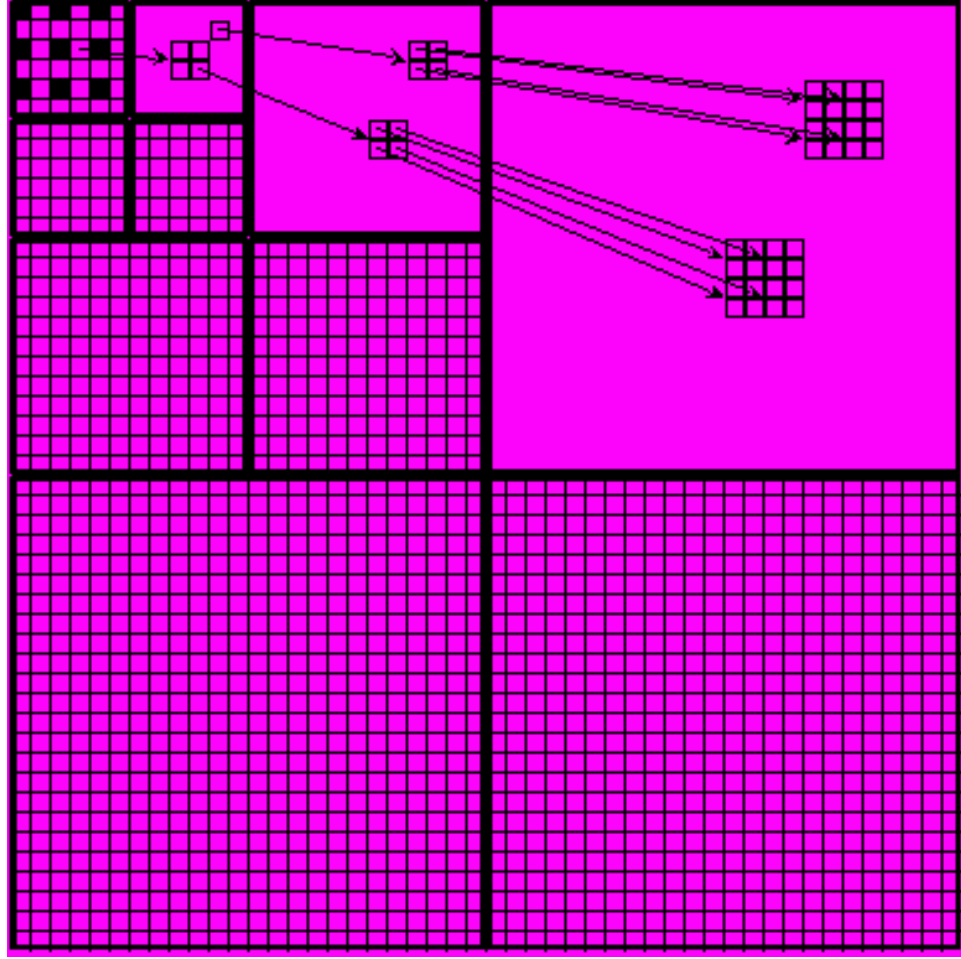


Figure 7.1: Tree structure in the two-dimensional wavelet transform

composed of the coordinates of the coefficients B11,..., B14,...,B44.

With the exception of the first iteration which has a single pass, there are two passes for SPIHT. First the *sorting pass* is applied to every iteration. The initial threshold level is $\tau = 2^{\lfloor \log_2(\max_{(i,j)} |y_{i,j}|) \rfloor}$ for the first iteration. After each pass of the SPIHT algorithm the value of the threshold is halved. All coefficients whose magnitudes are larger than or equal to the threshold and smaller than twice the threshold are considered significant. Such a coefficient is called a significant coefficient. During this pass, the significant coefficients that have magnitudes larger than or equal to the threshold and smaller than twice the threshold are found. Once such a coefficient is found, its position and approximate magnitude which is about one and half times the threshold level are inferred from the significance map by one bit of information and its sign is coded using one additional bit of information. After the sorting pass, there is the *refinement pass* where the next *most significant bit*(MSB) of each coefficient that was previously found significant is stored. Then threshold is halved and the next set

of significant coefficients are coded and the previous set of coefficients are refined. As the SPIHT algorithm iterates to reach the threshold level $\tau = 0$, the approximation for the magnitude of a previously found significant coefficient becomes more exact after each pass due to the refinement bits. The *progressive image quality* means that the quality of image goes from low to high as more bits are sent and *embeddedness property* means that given a coarser image with L bits and a finer image with M bits, then the first L bits of the finer image is the same as the bitstream of the coarser image.

To implement this algorithm, SPIHT makes use of three lists. The *list of insignificant pixels* (LIP), the *list of significant pixels* (LSP), and the *list of insignificant sets* (LIS). The initial threshold τ is set to $\tau = 2^{\lfloor \log_2(\max_{(i,j)} |y_{i,j}|) \rfloor}$. The LIP and LSP are sets that contain the coordinates of the coefficients of Y . The LIS on the other hand is a set of sets whose elements are the coordinates of the roots of sets of type \mathcal{D} or \mathcal{L} . The LIP is initialized to \mathcal{H} . The elements of \mathcal{H} that have descendants are also placed in the LIS as type \mathcal{D} components. The LSP is initially an empty set. In each iteration, the sorting pass part processes the members of LIP and then the members of LIS. This is the significance map encoding step which contains information on the position and magnitude of coefficients at each threshold. After the sorting pass, the elements of the LSP are processed in the refinement step and in this way the uncertainty in the magnitude of a coefficient gets smaller and the image quality becomes progressively better.

The algorithm starts by examining each coordinate in the LIP. If the coefficient at that coordinate is significant, then we output a 1 followed by a bit representing the sign of the coefficient. The algorithm then appends the coefficient to the end of the LSP list. If the coefficient at that coordinate is not significant, we transmit a 0. After the algorithm examines all of the elements of the LIP, it then begins processing the elements of the LIS. The elements of the LIS as we mentioned before are sets that contain many coordinates of coefficients. If a set at coordinate (i,j) is not significant, then SPIHT transmits a 0. If a set is significant, the algorithm outputs a 1. The binary output is based on the binary decision about the significance of a set. We append this decision value to the output stream.

If an LIS element tests as significant at (i,j) then the algorithm checks the type of the element. If the element is of type \mathcal{D} then the SPIHT coder checks each offspring coefficient $\mathcal{O}(i,j)$. For each child that is significant, the algorithm outputs a 1 and the sign of the coefficient and appends the coefficient to the end of the LSP. If a child is not significant, then the algorithm outputs a zero and appends this zero to the LIP. The coordinates of $\mathcal{O}(i,j)$ then are removed from the LIS and appended to the end of the LIS as type \mathcal{L} to denote the set of descendants of children. This new set $\mathcal{L}(i,j)$ is examined again during the same pass of the SPIHT algorithm. If $\mathcal{L}(i,j)$ is empty, then we remove the coordinate (i,j) from the list. Now suppose the element

of the LIS to be examined at (i,j) is of type \mathcal{L} . Then we add each coordinate in $\mathcal{O}(i,j)$ to the end of the LIS as the root of a set of type \mathcal{D} . These new entries in the LIS have to be examined during the same pass. After examining them, we remove the coordinate (i,j) from the LIS.

With the exception of the first pass of the SPIHT algorithm, each sorting pass is followed by the refinement pass. In the refinement pass we are at threshold $\tau = 2^n$ and thus the n th most significant bit of the magnitude of all previous LSP entries with the exception of the current pass is appended to the output bit stream. The reason for excluding the current pass is because we have already sent the significance information and the sign bit in the sorting pass. So with the exception of the pixels added to LSP during the current pass, all other pixels that were found to be significant during prior passes are refined. Finally after the sorting pass and the refinement pass, the threshold τ is halved and the whole process is repeated. This can continue until the threshold is equal to 1.

The bits in a SPIHT codestream can be divided into two classes: one that conveys coefficient value, called the value bit class (VBC); and the other that conveys location only called the location bit class (LBC). The VBC consists of the significant '1' decisions and signs of individual coefficients and the bits gathered in the refinement passes. The LBC consists of the significance decisions on sets of more than one coefficient. The bits of these classes can be sent to separate sub-bitstreams during the encoding process.

The decoding of SPIHT is identical to the encoding process of SPIHT. Since the output bit stream shows the path and order of the way the lists are manipulated, we can reconstruct the exact state of the encoder if both streams are present. So the decoder retraces the step of the encoder and the values that have been found significant are reconstructed. Assuming that a significant coefficient found at the threshold τ is uniformly distributed between the values $[\tau, 2\tau)$, we assign the initial value 1.5τ to that coefficient. As we receive more of the refinement bits from the VBC, the true value of that significant coefficient is approximated more closely.

Although the algorithm was presented for encoding a two-dimensional wavelet transform of an image, it applies also to a three-dimensional wavelet transform of an image sequence. The only difference is the that branching of the spatial orientation tree to the third dimension usually gives eight children for each node. The sorting and refinement passes use the same procedure.

7.1 SPIHT simulator for MATLAB

A binary uncoded SPIHT codec for MATLAB has been developed for the purpose of image transmission. As far as we know, this is the first SPIHT coder for MATLAB. Given the popularity of the MATLAB environment and the ease of variable

Image	bpp	SPIHT	MATLAB SPIHT
Lena	.2	32.73	32.66
	.5	36.84	36.77
	1	39.98	39.88
Barbara	.2	26.29	26.15
	.5	30.94	30.83
	1	35.94	35.79
Goldhill	.2	29.53	29.35
	.5	32.71	32.53
	1	36.00	35.81

Table 7.1: Performance of MATLAB and original SPIHT

manipulation in such an environment, the codec is useful for the purpose of simulation. Although the results are similar to that of original binary uncoded SPIHT written in C++, the decoding and coding time takes much longer. For example to code Lena up to .25 bpp(bits per pixel) it took us about 30 seconds on a Pentium IV 2.0 Ghz machine with 256 megabytes of ram, whereas the C++ SPIHT code takes less than a second to code Lena up to 2 bpp. The relative speed can be attributed to the fact that MATLAB is not a compiled language like C++. Furthermore our algorithm was not optimized and the slowest portion was the LIS where the algorithm needs to search through a set of coordinates for significant coefficients. Of course all the analysis done in this report is valid for the binary uncoded SPIHT codec in C++ as well as other similar compression schemes. The program is useful for researchers who are concerned with PSNR performance and want to use available functions of MATLAB including the Communications, Wavelets, Signal Processing and Image Processing toolboxes in a single environment. Table 7.1 shows the relative performance of MATLAB SPIHT and the C++ SPIHT used in [139].

7.2 Distortion-Rate Profile of SPIHT

Wheeler [144] analyzed the reduction in distortion for each received bit. We will expound on that work and then design an accurate distortion-rate (D-R) curve estimator for the SPIHT coder. Recall from [139] that at each iteration of the SPIHT coder, all coefficients that are greater than the threshold τ at that pass and are less than 2τ are considered significant by the SPIHT coder. All other transformed coefficients which are not significant are deemed insignificant. Once a significant coefficient is found, its position and approximate magnitude, which is about one and half times the threshold level, are inferred from the significance map by one bit of information and its sign is coded using one additional bit of information. So a newly found transformed

coefficient $Y(i, j)$ at location (i, j) found to be significant at a threshold $\tau = 2^n$ is assigned a magnitude value of $\tilde{Y}(i, j) = 1.5\tau$. For simplicity, we have assumed a uniform distribution for the magnitude of the coefficients at each threshold. Nevertheless, excellent results in terms of D-R estimation have been obtained by assuming a uniform distribution. After a coefficient has been found to be significant at τ , then it is put in a special list for further refinement at each subsequent SPIHT pass. Each refinement pass effectively halves the region of uncertainty relative to the previous refinement pass.

Initially before any decoding, each coefficient of the image is assumed to be zero. When a coefficient $Y(i, j)$ is found to be significant at τ , then a sign bit and a significance bit are sent. The mean of the lowest frequency subband is also zero, because the image mean is subtracted before coding. Assuming that the coefficient is positive and uniformly distributed between $[\tau, 2\tau)$, then the expected square error in assuming a zero value for the coefficient is

$$E\{(Y(i, j) - 0)^2\} = \int_{\tau}^{2\tau} \frac{1}{\tau} y^2 dy = \frac{7}{3} \tau^2 \quad (7.1)$$

For most images, a probability distribution biased toward the smaller values in the interval would be more accurate, but the uniform distribution proves to be accurate enough for our work and also satisfies the minimax criterion. If we reproduce the coefficient $\tilde{Y}(i, j) = 1.5\tau$ then the expected squared error becomes

$$E\{(Y(i, j) - \tilde{Y}(i, j))^2\} = \int_{\tau}^{2\tau} \frac{1}{\tau} (y - 1.5\tau)^2 dy = \frac{1}{12} \tau^2 \quad (7.2)$$

Since the quantization interval reduces by a factor of 2 and the MSE by a factor of 4 at each lower bit plane then if k refinement bits were received for the (i, j) coefficient and the coefficient was found at a significance level τ , the MSE between the actual and estimated coefficient value is

$$E\{(Y(i, j) - \tilde{Y}(i, j))^2\} = \frac{1}{12} \left(\frac{1}{4}\right)^k \tau^2 \quad (7.3)$$

We will keep track of the number of the newly found significant bits for each pass of the bit plane coder as well as the total number of bits per each pass. We assume that the bit plane decoding starts at the level $\tau = 2^n$. Let us denote by $N_{SBS}(i)$ as the number of sign bits in pass i and by $Nd_{SBS}(i)$ the number of sign bits decoded in pass i . Note that $N_{SBS}(i)$ is equal to the number of coefficients found significant at pass i . These quantities are easily generated by the SPIHT coder at virtually no cost in the computational complexity of the algorithm.

Since SPIHT finds all the coefficients that are significant relative to a threshold at each pass, then $N_{SBS}(i)$ is equivalent to the number of transformed coefficients whose magnitude is greater than or equal to 2^i and less than 2^{i+1} . Assuming that we stopped decoding during the sorting pass of the significance level $\tau = 2^k$, an approximation for $D(R)$, denoted by $\hat{D}(R)$ is given by

$$\begin{aligned} \hat{D}(R) = & \frac{1}{K} \left[\sum_{i=k+1}^n N_{SBS}(i) \frac{2^{2i}}{12} \left(\frac{1}{4}\right)^{i-(k+1)} + \right. \\ & \frac{2^{2(n-k)}}{12} N d_{SBS}(n-k) + \\ & \left. [N_{SBS}(n-k) - N d_{SBS}(n-k)] \frac{7}{3} 2^{2(n-k)} + \right. \\ & \left. \sum_{m=0}^{n-k-1} N_{SBS}(m) \frac{7}{3} 2^{2m} \right] \end{aligned} \quad (7.4)$$

R , the rate, is a sum of location, sign and refinement bits. The first component of Equation (7.4) takes into account the reduction of distortion after $n - k$ passes by decoding all the sign bits found from significance level n all the way down to significance level $k + 1$ and is given by Equation (7.3) per sign bit. The second term is a result of the number of sign bits decoded at the significance level k . The remaining two terms are the mean square error given by Equation (7.1) for not yet found non-zero coefficients. In order to have $\hat{D}(R)$ for every obtainable R , we need $N_{SBS}(m)$ for every threshold level.

We have calculated some of the estimated $D(R)$ values for threshold levels 12 down to 3 ($\tau = 2^{12}$ to 2^3) in Table 7.2 for two popular images. These results verify that $\hat{D}(R)$ is a good approximation for the actual $D(R)$ in all cases. We have also used the same approximation for 3-D SPIHT [2] and Table 7.2 lists the same results obtained for the luminance Y components of two video sequences. Based on these results the model we propose for a fast computation of the SPIHT D-R characteristic is a linear interpolation between the $\hat{D}(R)$'s at each pass of the SPIHT algorithm. A more exact model could have been obtained had we considered the decrease in distortion due to each refinement bit. But this would make our model too complex to be suitable for real-time applications.

7.2.1 SPIHT Error Response

Errors in reception of bits in the LBC cause catastrophic decoding failure, while those in the VBC cause only graceful degradation. In order to verify and illustrate

Level	Lena		Goldhill		Football		Susie	
	$\hat{D}(R)$	$D(R)$	$\hat{D}(R)$	$D(R)$	$\hat{D}(R)$	$D(R)$	$\hat{D}(R)$	$D(R)$
12	5594	6241	7185	7671	19225	16883	15804	12293
11	1222	1181	1102	978	1547	1163	1750	1639
10	724	642	636	511	900	957	366	363
9	457	383	468	379	631	605	174	173
8	284	237	329	268	429	395	116	107
7	157	130	218	177	285	260	80	72
6	83	67	132	107	165	155	51	46
5	42	33	72	58	80	79	29	27
4	22	16	34	26	34	34	14	14
3	11	7	12	9	11	12	6	6

Table 7.2: Actual and estimated D-R points of SPIHT images and video at the end of each threshold

the impact of these kinds of errors, we simulate the situation using the following simple algorithm. The pseudo code for this algorithm is

```

decode image up to ith bit, then
flip ith bit
decode till the 14000th bit
calculate PSNR

```

Figure 7.2 illustrates the discontinuity of the PSNR depending on the type of bit error. For this figure, the Lenna image is decoded up the first 14000 bits. We have shown the effect of having a single bit error for up the first 6000 bits. The figure shows that having a bit error anywhere in the LBC is catastrophic. For the VBC, we can see that we need more error protection for the beginning of the VBC stream relative to the end of the VBC stream. We also note that there are sharp jumps and variations depending on type of error that has occurred.

Summary

In this chapter, we presented an overview of the SPIHT codec and developed an estimator for average mean-squared-error based on counting bits in the value bit class (VBC). We have also simulated the effects of errors versus bit stream location in the LBC and VBC bitstream classes. The SPIHT codec has been cited in most of the recent literature that deals with JSCC methods. The codec is very fast, easily implementable and provides high quality compression ratio. The codec also provides a general paradigm for modern progressive bit-plane wavelet coders and so the results achieved throughout this report will carry over to other codecs. We have developed our own SPIHT coder in MATLAB, which will be used for our simulations.

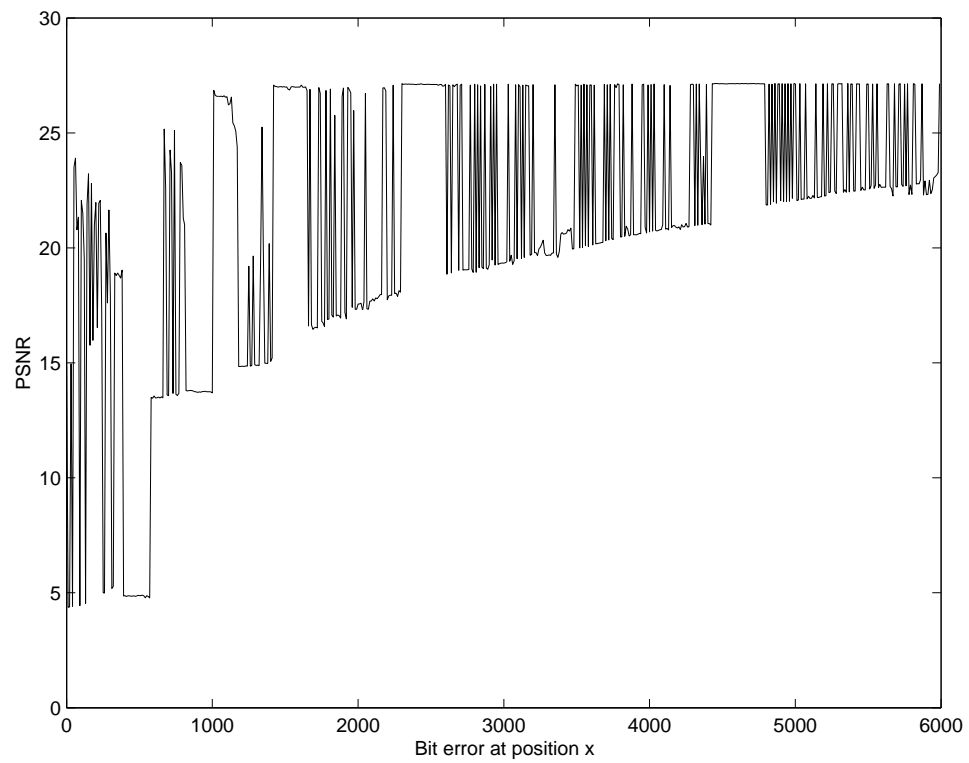


Figure 7.2: Variation of PSNR as a function of different bit errors

Chapter 8

Joint Source and Channel Coding for Binary Symmetric and Fading Channels

This chapter is composed of five sections. In Section 1 we introduce Reed-Solomon (RS) codes. In Section 2 we discuss why most JSCC require the D-R function and the current work and drawbacks that has been done with regards to the estimation of D-R for SPIHT and progressive embedded wavelet coders. The drawback of some of these methods will also be discussed. In Section 3 we will discuss the JSCC problem over BSC and apply both optimum EEP and optimum UEP. In section 4, we will give a summary of the work done on this chapter. The basis of this chapter is from our recent work [154] [155], but more extensive simulation results as well an assessment of the probability of decoding will be provided.

8.1 Approximating the Performance of Reed Solomon Codes

Reed Solomon(RS)[150] codes are a popular type of forward error correction(FEC) employed in fading channel environments. Their wide usage is due to their powerful burst error correction capabilities. FEC is a technique that enhances channel reliability by adding parity symbols to the information message that is to be transmitted. The RS codeword that we will use is of block size of $N_{code} = 2^q - 1$ code symbols, where each code symbol is a q bit binary sequence. Each RS codeword will be used as a transmission block. Assuming we feed the coder a sequence of k_{code} code symbols, each RS code word will have a redundancy of $N_{code} - k_{code}$ for a total RS code word size of N_{code} . The minimum distance of the code d_{min} is no less than $N_{code} - k_{code} + 1$. The parity bits are used by the receiver to detect and correct errors.

A coder/decoder pair can correct up to $t \leq \lfloor (d_{\min} - 1)/2 \rfloor$ q -bit symbols bytes that have been corrupted and detect all errors between t and $(d_{\min} - 1)$. If the number of symbol errors exceeds t , the decoder will either declare failure or commit an error and decode the RS code incorrectly. If the block is decoded erroneously, the error can be detected using a cyclic redundancy checks(CRC).

We are interested in the error correction capability of each RS block and the probability of block failure P . We denote the probability of code symbol error by P_{cs} . We also assume that the probability of code symbol error for each code symbol is independent of other code symbols in each RS block. If the channel has memory then we may use time and/or frequency interleaving to make sure that the code symbol errors are independent. Then $B(N_{code}, P_{cs})$, the number of symbol errors in a block, is a binomial random variable with parameters N_{code} and P_{cs} . Then P , the probability of more than t symbol errors, is given by [150]

$$P = \Pr(B(N_{code}, P_{cs}) \geq t + 1) = \sum_{i=t+1}^{N_{code}} \binom{N_{code}}{i} P_{cs}^i (1 - P_{cs})^{N_{code}-i} \quad (8.1)$$

The binomial random variable $B(N_{code}, P_{cs})$ has a mean $N_{code}P_{cs}$ and variance $N_{code}P_{cs}(1 - P_{cs})$. When N_{code} is large and $N_{code}P_{cs}(1 - P_{cs})$ is moderate [151] we may use the Central Limit Theorem and the Gaussian approximation for the binomial to approximate P_{bl}

$$P_{bl} \simeq \int_{t+1}^{\infty} \frac{1}{\sqrt{2\pi N_{code}P_{cs}(1 - P_{cs})}} \exp\left(\frac{-(v - N_{code}P_{cs})^2}{2N_{code}P_{cs}(1 - P_{cs})}\right) dv \quad (8.2)$$

An almost exact approximation for P_{bl} is of the form

$$P_{bl} \simeq \exp(k_n t^n + k_{n-1} t^{n-1} + \dots k_0 t^0) \quad (8.3)$$

What is useful about Equation 8.3 is that the Hessian and gradient of any objective function can be formed. We have found that a 2nd order approximation in exponent for P_{bl} gives an excellent match for many different values including the case of $N_{code} = 63$ and $N_{code} = 255$ and for a wide ranges of P_{cs} . Table 8.1 lists some of the coefficients that were calculated using optimization methods.

8.2 Distortion-Rate Function and JSCC

Progressive image and video transmission is problematic in the presence of noisy channels. Progressive source coders like Image SPIHT [139] and Video SPIHT [138]

N_{code}	P_{cs}	$[k_2 \ k_1 \ k_0]$
63	.1	[-0.04112149323789 0.09343048654548 0.02152057588701]
63	.05	[-0.05242151327609 -0.33512894009818 0.37661990557610]
63	.01	[-0.08449549527332 -1.50034722186712 -0.49889161205900]
63	.001	[-0.14592854199996 -3.40738752058987 -2.78235783192835]
255	.1	[-0.01084053699139 0.29721930874216 -1.33972367997743]
255	.05	[-0.00275274032862 -0.50233442376517 4.15717599307081]
255	.01	[-0.04768622392018 -0.52650437332400 0.42696753006915]
255	.001	[-0.09445869061940 -2.26015352713813 -1.32706293362521]

Table 8.1: Coefficients for approximation of RS block failure

use a variable length format where the correct decoding of future bits depend upon the correct transmission of past bits. Decoding after the first single bit error can increase the expected distortion at the receiver and the best strategy is to stop decoding before the first bit error. We assume that the decoder has the capability to detect all block errors. Let us denote by $D(R)$ the mean square error distortion per sample remaining after R bits have been correctly decoded. Due to the progressive nature of the source coder bitstream, we stop decoding prior to the first decoding failure. Since all blocks after an erroneous block are corrupted due to their dependency on the incorrect block, the expected distortion $E(D)$ depends on the location of the first block error. If we successfully decode all blocks up to and not including block m , the distortion per sample is denoted by $D_b(m)$. This probability of first block failure is equal to $P(1)$ for $m = 1$ and $P(m) \prod_{j=1}^{m-1} (1 - P(j))$ for $m = 2, 3, \dots, N_d$, where $P(j)$ is the probability of losing block j which has a total of $2t_j$ parity symbols. So the expected end to end distortion $E(D)$ under a bit budget constraint of N_d equal sized blocks and a total source rate R_s bits is given by:

$$E(D) = D(0)P(1) + \sum_{m=2}^{N_d} D_b(m)P(m) \prod_{j=1}^{m-1} (1 - P(j)) + D(R_s) \prod_{j=1}^{N_d} (1 - P(j)) \quad (8.4)$$

The optimization of Equation (8.4) forms the objective function of the joint source channel coding scheme analyzed in [141] [162] [142] [159] [160] [143] amongst many other papers. The distortion in decoding up to block m , $D_b(m)$, depends on the number of bits received for $m - 1$ blocks. Therefore the optimal parity allocation across different blocks depends greatly on the D-R characteristics of the source coder. One method to estimate the D-R curve is to decode at certain number of points at the receiver and interpolate the D-R function. The drawback to such a method is that it might not be realizable for a real-time application. Furthermore such a method is not always accurate because the points that are decoded may not accurately capture

the slope variation to estimate an accurate D-R function. The major benefit of using parametric models is that they allow Equation (101) to be solved using optimization techniques.

In [163] Mallat and Falzon proposed a model of the form

$$D(R) = CR^{1-2\gamma} \quad (8.5)$$

where C is a constant positive number and γ is of order 1. The model approximates the MSE of a zerotree-based wavelet coder at bit rates under 1 bit-per-pixel (bpp). In [141], Appadwedula *et al.* used a piecewise exponential model with different decay parameters. Their parametric model was proposed for a class of images. The drawback of such models is that they are not particularized to a specific image and video sequence. The model proposed by them is given by:

$$D(R) = \sum_{k=1}^4 c_k \exp(-l_k R) \quad (8.6)$$

The constants c and l are used for a class of images. Charfi *et al.* [161] have recently proposed a more accurate parametric Weibull model where the parameters are estimated from the particular image. In order to fit their D-R estimator to the actual D-R curve, they required decoding four and sometimes eight exact points on the actual D-R curve. Their model has a form of:

$$D(R) = a - b \exp(-cR^d) \quad (8.7)$$

where a , b , c , and d are constants that are fitted using the decoded points on the D-R curve.

By analyzing the SPIHT coder and bit plane coders in general, we offer an accurate piece-wise linear model for individual image and video coders. Furthermore by using our D-R estimator, other parametric models can be fitted more accurately for a particular image or video sequence. The advantage of our model is that no decoding is required in order to estimate the D-R function. This makes it well suited for real time applications relative to parametric models that require actual D-R points.

8.3 JSCC over BSC using EEP and UEP

Unequal error protection signifies that we are using different amount of parity symbols per each transmission block. Optimum unequal error protection(UEP) is the parity symbol per packet configuration that yields the minimum transmission distortion. If for example we are only sending three transmission blocks, then we may imagine

a cube lattice whose corner is centered at the origin. The x,y and z-axis of this cube denote the number of parity symbols we will be using per each block. The optimization algorithm in order to find the optimum UEP could be any point on this lattice. On the other in the optimum equal error protection (EEP) we are constraining ourselves on the diagonal of the lattice. It is reasonable to expect that the optimum UEP point on this lattice is not too far off from one of diagonal points on the lattice. The error correction code is Reed Solomon (RS) [150] (255, k), blocks of size 255 bytes, where the number of information symbols k varies per block. Assuming independent byte errors, the number of errors is binomially distributed and the block error probability is equal to the probability of more than t_j byte errors.

For solving the UEP, we want to solve the following minimization problem:

$$\begin{aligned} \min_{\mathbf{t}} E(D) = D(0)P(1) &+ \sum_{m=2}^{N_d} D_b(m)P(m) \prod_{j=1}^{m-1} (1 - P(j)) \\ &+ D(R_s) \prod_{j=1}^{N_d} (1 - P(j)) \end{aligned} \quad (8.8)$$

$$\begin{aligned} \Pr(B(N_{code}, P_{cs}) \geq t + 1) \\ \approx \int_{t+1}^{\infty} \frac{1}{\sqrt{2\pi N_{code} P_{cs} (1 - P_{cs})}} \exp \frac{-(v - N_{code} P_{cs})^2}{2N_{code} P_{cs} (1 - P_{cs})} dv \end{aligned} \quad (8.9)$$

$$\begin{aligned} P(m) &= \Pr(B(N_{code}, P_{cs}) \geq t + 1) \\ &\approx 1 - \Phi((t_m - N_{code} P_{cs}) / (\sqrt{N_{code} P_{cs} (1 - P_{cs})})) \end{aligned} \quad (8.10)$$

where $\mathbf{t} = [t_1, t_2, \dots, t_{N_d}]$.

$$D_b(m) = CR_m^{1-2\gamma} \quad (8.11)$$

$$R_m = ((m - 1) * N_{code} - \sum_{i=1}^m 2 * t_i) \quad (8.12)$$

Using $\hat{D}(R)$ and Equation (8.4), we have solved for the optimal unequal error protection using a gradient based algorithm. We have assumed that we are operating over a binary symmetric channel(BSC) with a cross-over probability of 0.01. We have solved the algorithm for different transmission rate constraints from 0.1089 bpp with

14 RS blocks to 0.755 bpp with 97 RS blocks. In Figure 8.1 we have plotted in the transform domain PSNR based on the expected MSE given by Equation (8.4) for the UEP and EEP case. At the optimal trade-off point between the source rate and the channel rate, the UEP performance at the transmission rate of 0.1089 bpp (bits per pixel) is 0.17 dB better than the best value obtained using EEP. Only when the average error correction capability per block is constrained, then UEP yields a significant improvement over EEP. Figure 8.1 illustrates that when the source rate and channel rate are fixed and only the parity allocation per block is allowed to vary, UEP allows for graceful degradation when the average number of parity bits per block is reduced. In Table 8.2 and Table 8.3 we have listed the *PSNR* based on the expected MSE for the optimal UEP and the optimal EEP for the Lena and Goldhill images and Susie image sequence at various rates. In these two tables the entries UEP and EEP signify the optimal UEP and EEP when the exact D-R function is used and the entries UEP- $\hat{D}(R)$ and EEP- $\hat{D}(R)$ signify the optimal parity allocation achieved via Equation (7.4) and subsequently then applied to Equation (8.4) with the exact D-R curve. Note that there is no more than 0.01 dB difference between PSNR's of the exact and estimated $D(R)$ functions. Furthermore, the maximum difference between the optimal UEP and the optimal EEP is 0.24 dB and the minimum difference is 0.03 dB. We conclude that $\hat{D}(R)$ is as good as the exact $D(R)$ in solving for the optimal parity allocation and that optimal EEP attains almost as good performance as optimal UEP.

Using our simple D-R estimator, we can always obtain the optimal EEP at any transmission rate. Chande and Farvardin [160] used rate compatible convolutional codes. They noticed that for some transmission rates, one of their EEP schemes, which may not necessarily be the optimal EEP, has a small performance loss relative to the optimal UEP. Our results not only confirm this fact, but our method provides the optimal EEP at every transmission rate. All we have to do is to evaluate Equation (101) via Equation (7.4) at several equal code rates and get the minimum value. In Tables 8.5, 8.6, 8.7 and 8.8 we have done this for the luminance Y components of four popular video sequences. Note that for a BSC with a cross-over probability of .001, the optimum EEP is very close to the noise-less channel. This important observation is very beneficial because the advantage of the MIMO system is that with increase number of antennas, the probability of raw bit error reduces greatly over a similar SISO system for the same transmission signal to noise ratio(SNR).

Figure 8.3 displays the optimal UEP and the optimal EEP for the Susie sequence over 131 different transmission rates over a BSC with cross-over probability of 0.01. The transmission rates start from 120 blocks and ends at 250 blocks. It is explicit that the optimal EEP follows the optimal UEP closely and suffers a negligible performance loss. In fact the minimum PSNR difference between the two curves over all the rates is 0.05 dB and the maximum PSNR difference is 0.137 dB.

The probability of decoding failure is defined as the event that all intended trans-

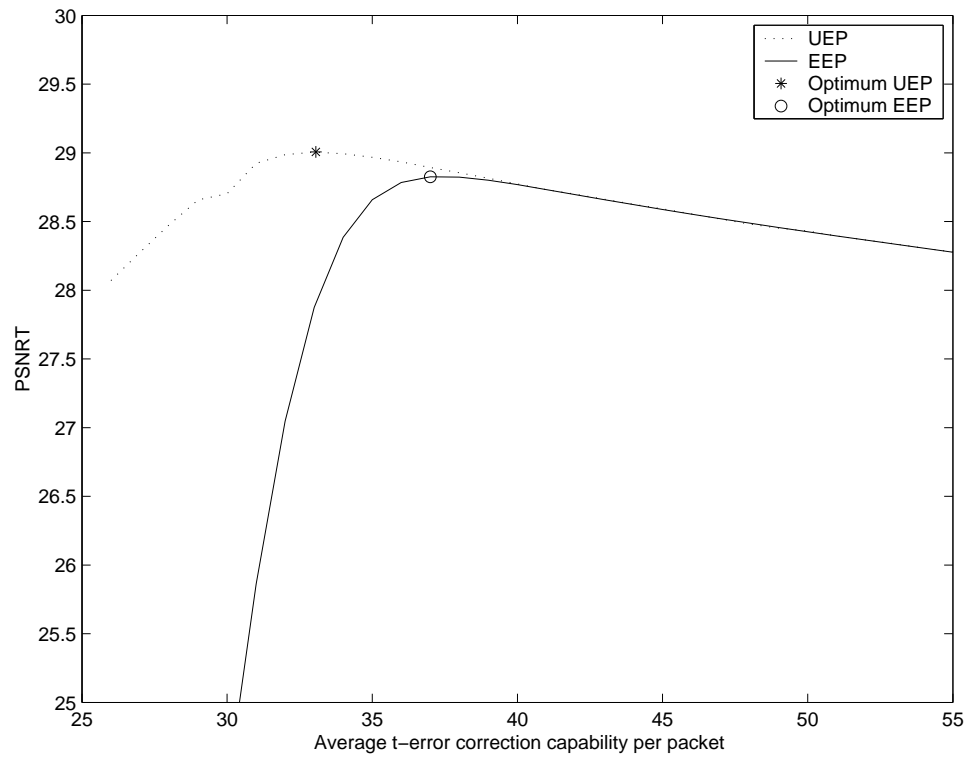


Figure 8.1: EEP vs. UEP for Lenna at transmission rate of .1089 bpp

mission blocks are not decoded correctly. This probability ε_{fail} is defined as:

$$\varepsilon_{fail} = 1 - \prod_{j=1}^{N_d} (1 - P_{bl}(j)) \quad (8.13)$$

Intuitively, a low ε_{fail} signifies that the instantaneous PSNR is close to the average PSNR. Otherwise if ε_{fail} large, the variance around the expected average PSNR is more spread. Since the optimal EEP scheme on average uses more parity bits per block, the probability of decoding failure is less than the probability of decoding failure for the optimal UEP scheme. In Figure 8.3 we have plotted the decoding failure for the same Susie simulation over 131 different transmission rates. It is clearly seen that the optimum EEP has a smaller decoding failure relative to the optimum UEP. It is also obvious that the decoding failure increases as the transmission rate is increased. The jumps in the optimum EEP curve can be ascribed to the fact that at different rates, even very close, the optimum EEP scheme could choose different coding rates.

Despite the slight performance loss in PSNR, the optimal EEP has some advantages over the optimal UEP. First, it does not require any extra header information pertaining to the D-R estimation for the receiver. For the optimal UEP, there exist two options for the receiver to have the necessary header information. Option one is to code and transmit the parity allocation per block. This can potentially be a large amount of information at high transmission rates. Option two entails sending the side information that is needed to calculate $\hat{D}(R)$ at the receiver. This is the number of total bits and sign bits at the end of each SPIHT pass. Considering that without the header information the decoding of the image can not correctly occur, the header information must be extremely well protected. On the other hand, for the optimal EEP the receiver just needs to know a single number that achieves the optimal EEP for a large group of blocks. The second advantage of the optimal EEP is that it does not require optimization techniques like those that employ gradient based methods or dynamic programming to obtain the optimal or near optimal UEP. For real time applications, the time delay to run such programs for every image or video sequence may be intolerable. For systems with power constraints like mobile phones, the use of an optimization program for every image or image sequences could potentially be an obstacle for the system designer. A third advantage of the optimal EEP is that the probability of decoding failure is lower relative to the optimal UEP. Finally the optimal EEP is simpler to implement since the code rate is the same for each block over a large group of blocks whereas for an UEP scheme the parity per each block may vary.

	Lena			
	0.1089 (14 blocks)	0.249 (32 blocks)	0.498 (64 blocks)	0.755 (97 blocks)
Noiseless	30.52	33.91	36.94	38.49
UEP	29.00	32.44	35.24	37.06
EEP	28.83	32.20	35.01	36.78
UEP $\hat{D}(R)$	29.00	32.44	35.23	37.05
EEP $\hat{D}(R)$	28.82	32.20	35.01	36.78

Table 8.2: PSNR for average MSE for Lena image over a memoryless BSC with BER 0.01

	Goldhill			
	0.1089 (14 blocks)	0.249 (32 blocks)	0.498 (64 blocks)	0.755 (97 blocks)
Noiseless	28.15	30.34	32.74	34.70
UEP	27.03	29.25	31.51	32.84
EEP	26.97	29.08	31.49	32.70
UEP $\hat{D}(R)$	27.03	29.25	31.50	32.84
EEP $\hat{D}(R)$	26.97	29.07	31.48	32.69

Table 8.3: PSNR for average MSE for Goldhill image over a memoryless BSC with BER 0.01

Rate	Noiseless	UEP	EEP	UEP $\hat{D}(R)$	EEP $\hat{D}(R)$
0.1811 (120 blocks)	35.95	34.81	34.71	34.81	34.71
0.1962 (130 blocks)	36.18	35.01	34.89	35.01	34.89

Table 8.4: PSNR for average MSE for Susie sequence over a memoryless BSC with BER 0.01 using 3-D SPIHT

Rate (Blocks)	Susie				
	100	200	400	800	1200
Noiseless	35.09	37.62	40.86	45.03	47.96
.01	33.96	36.02	38.82	42.39	44.96
.001	34.83	37.25	40.38	44.37	47.24

Table 8.5: PSNR for average MSE for Susie sequence over a memoryless BSC with BER 0.01 and .001 using 3-D SPIHT

Rate (Blocks)	Table Tennis				
	100	200	400	800	1200
Noiseless	28.56	31.99	36.03	40.08	43.33
.01	27.49	29.99	33.84	37.52	40.06
.001	28.29	31.54	35.50	39.48	42.41

Table 8.6: PSNR for average MSE for Table tennis sequence over a memoryless BSC with BER 0.01 and .001 using 3-D SPIHT

Rate (Blocks)	Football				
	100	200	400	800	1200
Noiseless	26.79	28.95	31.79	35.73	38.95
.01	25.73	27.67	30.12	33.28	35.79
.001	26.56	28.64	31.36	35.03	38.09

Table 8.7: PSNR for average MSE for Football sequence over a memoryless BSC with BER 0.01 and .001 using 3-D SPIHT

Blocks	Flower garden				
	100	200	400	800	1200
Noiseless	20.15	21.99	24.94	29.60	33.66
.01	19.36	20.88	23.26	26.87	29.72
.001	19.98	21.70	24.53	28.85	32.62

Table 8.8: PSNR for average MSE for Flower garden sequence over a memoryless BSC with BER 0.01 and .001 using 3-D SPIHT

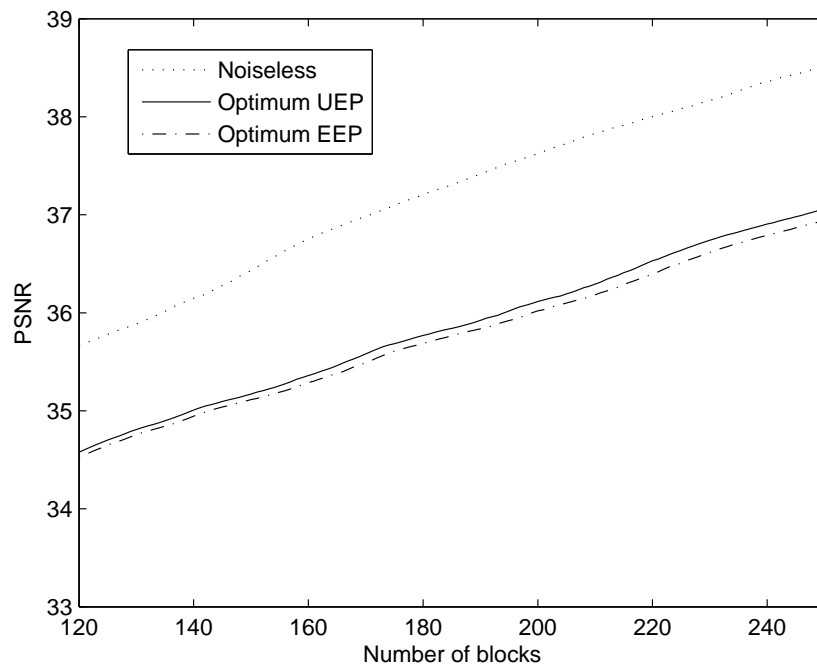


Figure 8.2: Optimum UEP vs Optimum EEP for the Susie sequence over a BSC of 0.01

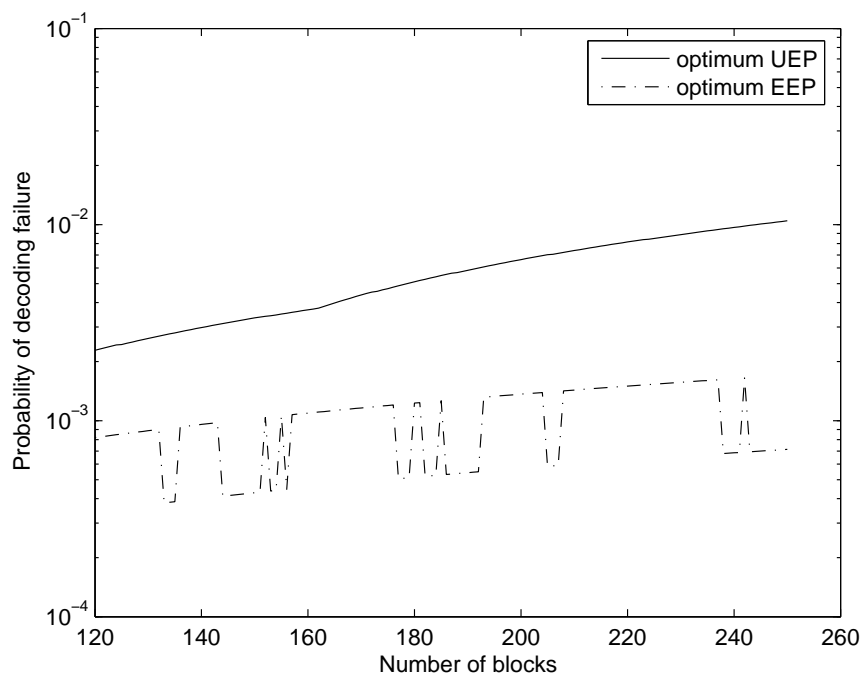


Figure 8.3: Probability of decoding failure for the Susie sequence using the optimum UEP and optimum EEP schemes over a BSC of .01

8.4 Energy and Rate Constrained Transmission over Rayleigh Fading Channels

Now we switch to BPSK transmission over a multipath additive white Gaussian noise (AWGN) channel. One popular model for the cellular multipath propagation medium is to assume that the signal amplitude fades according to the Rayleigh probability distribution. The average bit error rate BER for each bit under Rayleigh fading is given by:

$$p(E) = \frac{1}{2} \left(1 - \left[\frac{E/N_o}{1 + E/N_o} \right]^{1/2} \right), \quad (8.14)$$

where $N_o/2$ is the noise power and E is the energy expended per transmission of each bit. Further simplification of $p(E)$ when $E/N_o \gg 1$ is given by:

$$p(E) \simeq \frac{1}{4(E/N_o)} \quad (8.15)$$

Thus we have

$$P_{cs} \simeq 1 - \left(1 - \frac{1}{4(E/N_o)} \right)^q \quad (8.16)$$

We now consider joint source-channel coding (JSCC) for this channel under an energy constraint. The optimization problem can be formulated as:

$$\min_{t_1, \dots, t_N, E_1, \dots, E_N} \left\{ E(D) + \lambda \left(\sum_{i=1}^N E_i - N E_{avg} \right) \right\} \quad (8.17)$$

Where $E(D)$ was defined in Equation (1), $2t_i$ is the number of parity symbols used in block i , E_i is the energy expended per bit for the i th block, E_{avg} is the constrained average energy per bit for all blocks, N is the number of equal sized blocks transmitted and λ is a Lagrange multiplier. The optimum UE-UEP (Unequal Energy-Unequal Error Protection) solution denoted by Ω^* , must satisfy

$$\Omega^* = \left[\frac{\partial L}{\partial t_1}, \dots, \frac{\partial L}{\partial t_n}, \frac{\partial L}{\partial \lambda}, \frac{\partial L}{\partial E_1}, \dots, \frac{\partial L}{\partial E_n} \right] = 0 \quad (8.18)$$

The Quasi-Newton method can be used to obtain the optimal solution. The error correction code we used are RS codes (N_{code}, k) , where the blocks are of size N_{code} and the number of transmission symbols k , varies per block. Since the number of parity bytes is an integer, we must round the parity byte portion of the optimal UE-UEP solution to the nearest integer. In Figure 8.5 we have graphed the optimum UE-UEP and optimum EEP solutions for the number of information bytes per block and $E - b/N_o$ per block for the first 16 frames of the y-component of the Susie image sequence at the rates of 0.1 bpp and 0.0453 bpp. Notice that at the lowest E_b/N_o of 7.78 dB and a total transmission budget of 0.0453 bpp, we have a 1.09 dB improvement over

EEP in the PSNR. Also note that if the transmission energy constraint is increased, then the PSNR difference between optimum EEP and optimum UE-UEP is about 0.2 dB. This is an important result to consider for energy constrained transmission systems. In Figure 8.6, we have graphed the UE-UEP t_i and E_i for Susie with a rate constraint of 0.0453 bpp and energy constraint of 10 dB per bit. Because the D-R function is a monotonically decreasing function, the energy for each progressive block decreases monotonically. Also since the beginning blocks are more important than the ending blocks, the parity bytes allocation is also a decreasing function. Hence the information symbol allocation for each progressive block increases as shown in Figure 3. In Figure 4 we have plotted the results for the optimum UE-UEP Lena image transmission at 1 bpp. In comparison with the results of Figure 3 in [141], our results show a 0.4 dB improvement at E_b/N_o 8.82 dB. We believe this improvement is due to a more accurate D-R function as well perhaps a different value of N_{code} used in [141].

8.4.1 Conclusion

We considered the problem of joint source-channel coding with energy and bit budget constraints. We used 2-D and 3-D SPHT, the R-S channel coder and the BPSK modulator in order to obtain the optimal energy and parity allocation for each transmission block. By varying the energy for each block at low energy constraints, gains of 0.60 to 1.1 dB in PSNR for image and image sequences were obtained. At higher transmission energy constraints, a variable energy system yields only a modest improvement in PSNR. The results establish that significant improvement in PSNR can be obtained by varying the energy in the low transmission energy region. This can be used to improve cellular system capacity in energy constrained multi-user CDMA systems. Finally, we remark that the methodology used in this paper can be applied to a wide range of progressive source-coders and also to a wide range of channel coders and modulators.

8.5 Summary

We have introduced a new method to estimate the operational D-R characteristics of image and video SPIHT accurately at a very small computational cost. Our method, which is particularized for individual image and image sequences does not require any decoding at the receiver in order to estimate the operational D-R. Although the source coding algorithm used is SPIHT, the D-R estimation method is easily generalizable to any modern progressive coder that employs progressive bit-plane coding. The match between the estimated D-R function and the actual D-R function for both 2-D and 3-D SPIHT verifies that our estimate is an excellent approximation. For the optimal UEP we used a gradient based method to solve for the optimal parity allocation. For the EEP case we did not need any optimization technique and evaluating Equation

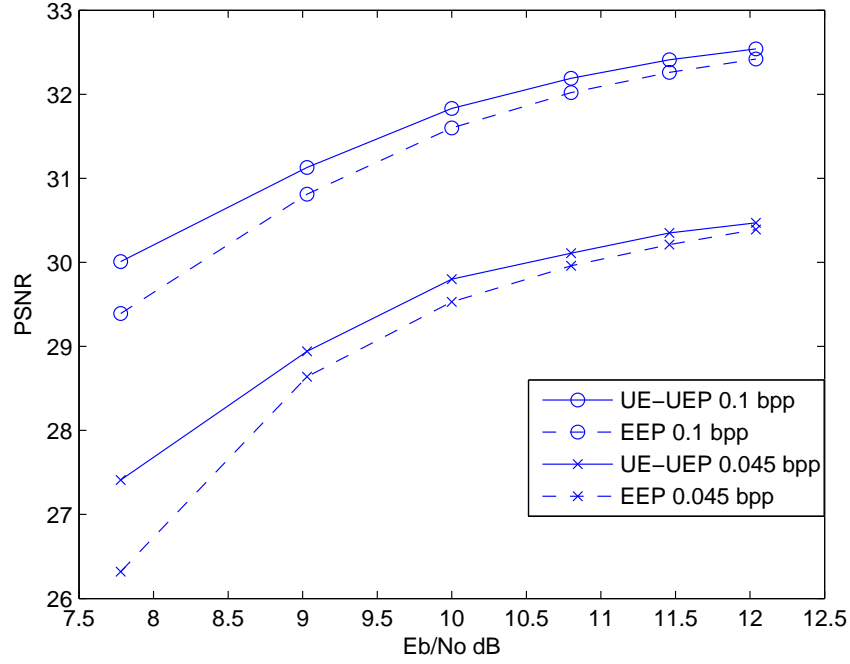


Figure 8.4: Optimum UE-UEP and EEP for Lena.

(101) at several points was sufficient to obtain the optimal EEP. The accurate D-R estimation can bridge the gap between theory and actual real time implementation of joint source channel coding for image and video transmission systems. Finally another major result is that the optimum UEP is only slightly superior to the optimum EEP. It was also mentioned that the optimum EEP offers some substantial practical advantages for real-time applications over the optimum UEP. The major advantages are simpler implementation, a significantly smaller header information and independence from any type of optimization procedure as a consequence of our fast D-R estimation.

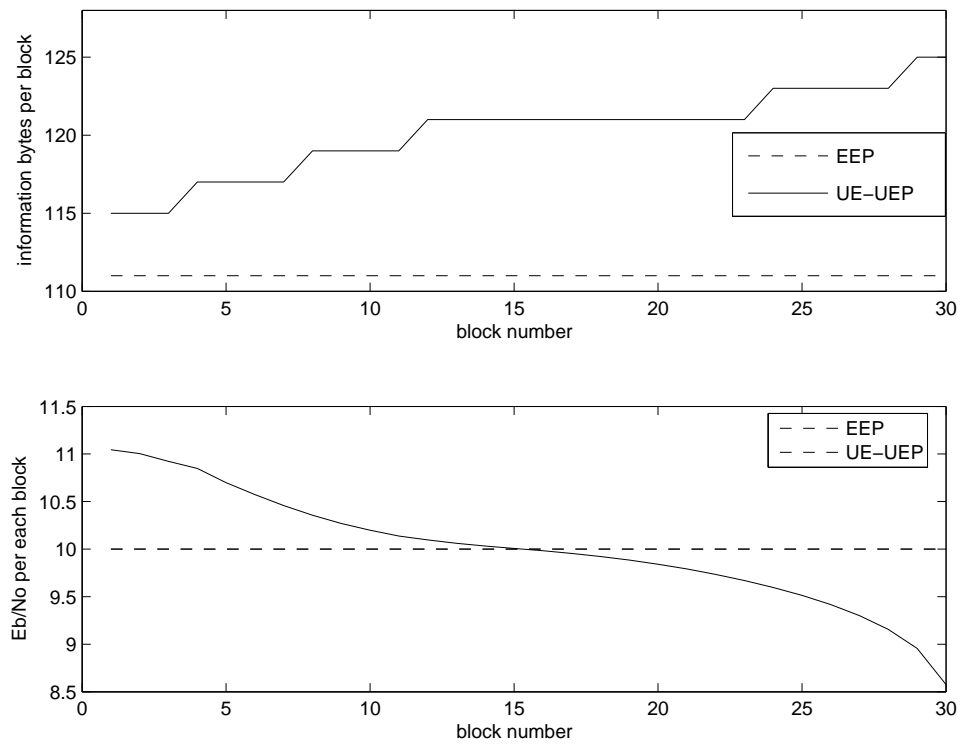


Figure 8.5: Information and Energy Allocation per block for Susie at 0.0453 bpp

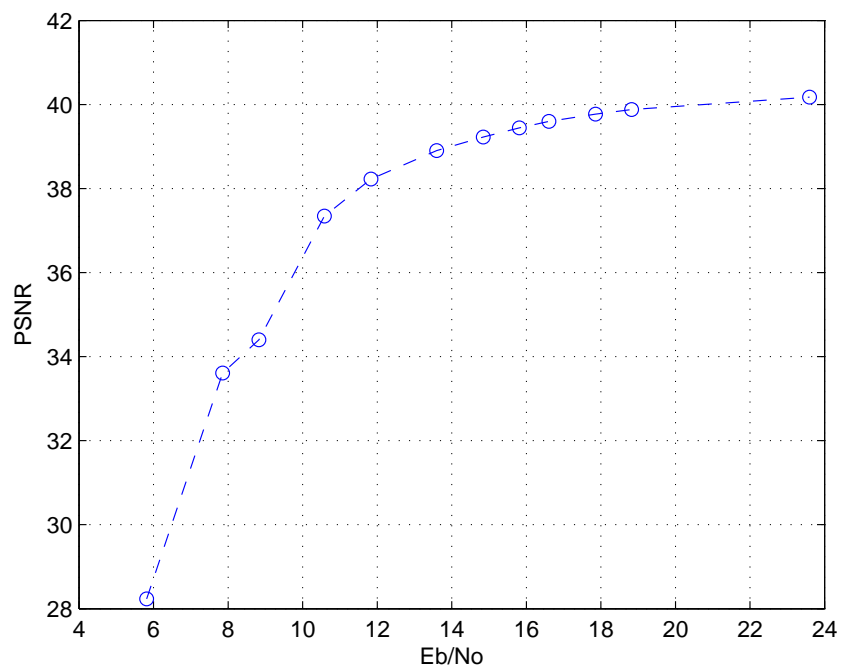


Figure 8.6: Analytic simulation results for optimum UE-UEP for Lena at 1.00 bpp

bpp	nl	7.78	9.03	10.00	10.80	11.46	12.04
hline 30	31.87	27.41	28.94	29.80	30.11	30.35	30.47
34	32.20	28.13	29.47	30.087	30.42	30.62	30.76
38	32.46	28.23	29.82	30.37	30.67	30.86	31.02
42	32.66	28.46	30.06	30.59	30.89	31.13	31.39
46	32.88	28.70	30.28	30.78	31.133	31.48	31.66
50	33.07	29.16	30.47	30.98	31.46	31.72	31.87
54	33.25	29.38	30.64	31.24	31.68	31.90	32.08
58	33.43	29.67	30.78	31.50	31.85	32.09	32.26
62	33.66	29.84	30.96	31.67	32.04	32.26	32.41
66	33.89	30.01	31.13	31.83	32.19	32.41	32.54
70	34.08	30.1432	31.36	31.99	32.34	32.53	32.65

Table 8.9: optimal UE-UEP PSNR obtained for y-component of SUSIE

rate / Eb/No	7.78	9.03	10.00	10.80	11.46	12.04
30	26.32	28.64	29.53	29.96	30.21	30.39
34	27.15	29.00	29.90	30.29	30.50	30.67
38	27.72	29.47	30.15	30.51	30.75	30.89
42	28.00	29.79	30.41	30.74	30.95	31.14
46	28.26	30.01	30.61	30.93	31.22	31.50
50	28.46	30.22	30.79	31.15	31.53	31.75
54	28.65	30.38	30.94	31.45	31.76	31.95
58	28.88	30.54	31.14	31.67	31.94	32.13
62	29.19	30.69	31.41	31.85	32.11	32.29
66	29.39	30.81	31.60	32.02	32.26	32.42
70	29.57	30.94	31.76	32.16	32.39	32.54

Table 8.10: optimal EEP PSNR obtained for y-component of SUSIE

Chapter 9

Robust OFDM Transmission over Fading Channels

In this chapter, we consider the problem of robust image coding and packetization for the purpose of communications over slow fading frequency-selective channels. Toward this end, is presented a novel and analytically based joint source channel coding (JSCC) algorithm to assign unequal error protection to a SPIHT codestream. Under a block budget constraint, the image bitstream is de-multiplexed into two classes with different error responses. In order to minimize the expected mean square error at the receiver, the algorithm assigns unequal protection to the value bit class (VBC) stream. In order to minimize the probability of decoding failure, the algorithm assigns more protection to the location bit class (LBC) stream than the VBC stream. The major advantage of our technique is that the worst case instantaneous minimum peak signal to noise ratio (PSNR) is very close to the average PSNR, while this is not the case for the optimal single stream Unequal Error Protection (UEP) system. The coded image is sent via orthogonal frequency division multiplexing (OFDM), which is an effective modulation scheme to combat ISI (Inter Symbol Interference) and impulsive noise. Using dual adaptive energy OFDM, we use the minimum energy necessary to send each bit stream at a particular probability of bit error.

9.1 Introduction

One of the main challenges of the wireless channels is that signals will suffer intersymbol interference (ISI) caused by the multipath environment [137]. The recent advances in digital signal processing has renewed interest in OFDM (Orthogonal Frequency Division Multiplexing) [167], a multi-carrier technique that is robust against ISI. OFDM has been adopted in many standards for both wireline and wireless applications such as asymmetric digital subscriber line (ADSL), European digital audio broadcasting (DAB), European digital video broadcasting (DVB), Japanese terrestrial integrated services digital broadcasting (ISDB-T), short-range wireless access and wireless LAN

standards (IEEE802.11a).

The rate required to send an uncompressed natural image may not be supported in real time due to bandwidth constraints and naturally the need for compression is realized. Furthermore, due to the error prone nature of the wireless channel, coding techniques must be utilized for reliable transmission. The Set Partitioning in Hierarchical Trees (SPIHT) [139] [168] is extremely popular because of its low computational complexity as well as its progressive nature and its ability to achieve high compression ratios. The SPIHT coder produces one bit stream that contains both value bit class (VBC) and location bit class (LBC) bits. The VBC information is the result of the SPIHT quantizer and entropy coding. The LBC stream holds essential synchronization information and a single error in this stream can cause a catastrophic error. This means that after the first single error in the LBC component, the decoder should stop decoding. As for the VBC bits, the importance of the bit-stream varies because of the SPIHT bit plane progressive quantizer and the need for Unequal Error Protection (UEP) arises. For the purpose of maximizing expected image quality at the receiver, various schemes have been proposed for choosing the channel code rate carefully to match the rate-distortion profile of the source bit-stream. Some of these algorithms incorporate other components including modulation. The common theme within all these schemes is a tight integration between the elements of the source coder and channel coder. Alatan *et al.* [169] used three bitstreams and assigned different coding rates of the rate compatible convolutional coder [170] for each stream. Sherwood and Zeger [171] protected SPIHT images transmitted over a memoryless binary symmetric channel using rate compatible punctured convolutional codes (RCPC) . By separating the SPIHT bitstream Alatan *et al.* [169] were able to get a slight average PSNR improvement over Sherwood and Zeger's work [171].

In this chapter, we introduce a new joint source-channel coding (JSCC) algorithm for OFDM modulation in a fading channel environment that is applicable to bit-plane progressive wavelet coders. In succeeding sections, we describe the joint source and channel coding system, present the fading channel model, solve the adaptive power loading for the OFDM subcarriers, and present simulation results.

9.2 The Joint Source-Channel Coding System

Figure 9.1 shows a detailed description of the OFDM-SPIHT system. The input image is encoded with SPIHT and the compressed bit-stream is divided into the two different classes, LBC and VBC. An error in the VBC class causes only graceful degradation, but an uncorrectable error in the LBC bit-stream causes a catastrophic failure. If an LBC error can not be corrected, it must at least be detected to halt decoding. Using our JSCC algorithm and a fixed bit budget, appropriate error correction is assigned to each stream such that certain quality constraints are met. Both streams need to be sent concurrently in order to maintain partial progressiveness. So bits from both streams are taken at a fixed rate and are assigned to the sub-carriers

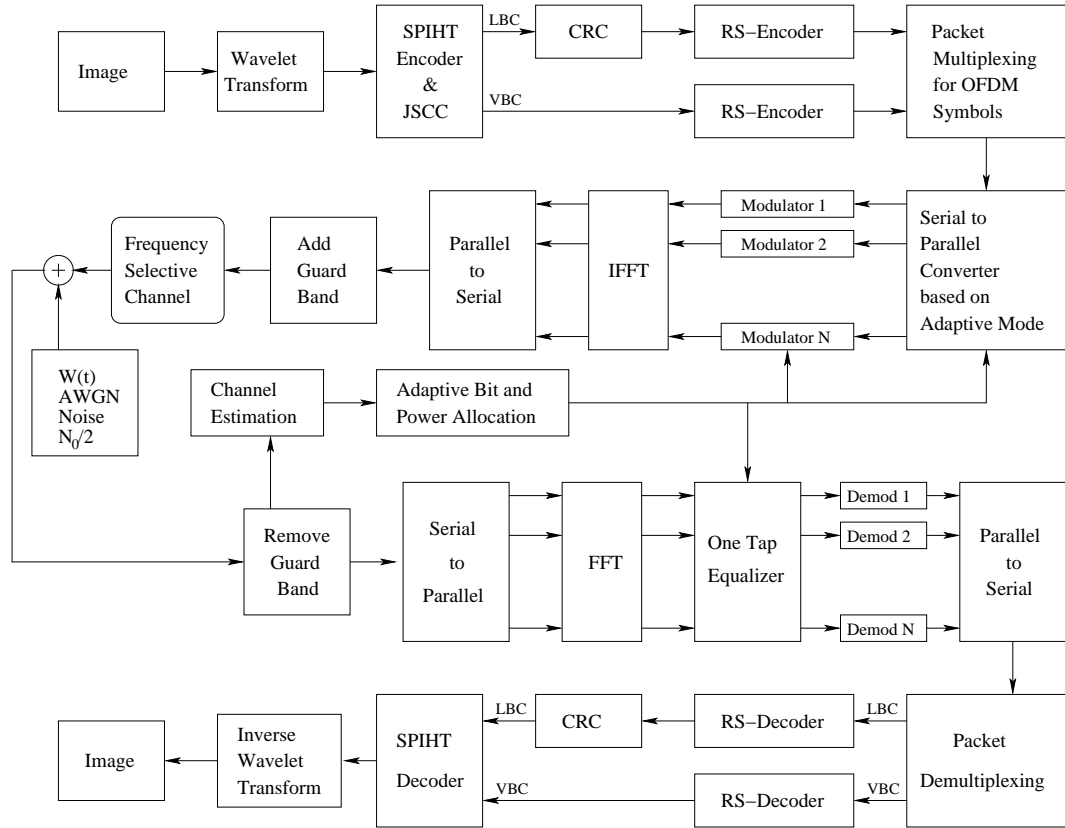


Figure 9.1: Diagram of the transmission and receiver systems

of the OFDM modulator. As described in Section 4, the assignment of bits to the sub-channels is done in a way to minimize the total energy per one OFDM symbol. Each sub-channel is modulated using a QAM (Quadrature Amplitude Modulation) modulator. Some sub-channels will send LBC bits and others will send VBC bits. In order to do the optimal bit-assignment for each sub-channel and the optimal sub-channel assignment for the two different classes of bits, we have assumed perfect CSI (Channel State Information) is available at the transmitter and receiver. So each OFDM symbol contains bits from both streams. The OFDM symbols are sent through a Rayleigh fading channel. At the output of the receiver, we use a zero-forcing equalizer to compensate for the fading gain that each sub-channel experiences. Then the bits on each detected OFDM symbol are separated into their respective classes. After error correction, we send the bits into the SPIHT decoder where the reconstruction of the transmitted image is outputted.

9.3 SPIHT Demultiplexing and D-R estimator

The output bitstream of the SPIHT algorithm is demultiplexed into two bit streams called the value bit class (VBC) and location bit class (LBC). The VBC contains sign bits and refinement bits. As mentioned previously, the LBC contains decision information about the significance of non-single coefficient sets relative to a threshold level. The decoding of SPIHT is identical to the encoding process of SPIHT. The combined bit streams of LBC and VBC show the path and order of the way the lists are manipulated, we can reconstruct the exact state of the encoder if both streams are present. So the decoder retraces the step of the encoder and the values that have been found significant are reconstructed. We have derived previously a distortion estimator of the distortion when R bits have been decoded. We repeat here this estimator from Equation 7.4

$$\begin{aligned}
\hat{D}(R) = & \frac{1}{K} \left[\sum_{i=k+1}^n N_{SBS}(i) \frac{2^{2i}}{12} \left(\frac{1}{4}\right)^{i-(k+1)} + \right. \\
& \frac{2^{2(n-k)}}{12} N d_{SBS}(n-k) + \\
& [N_{SBS}(n-k) - N d_{SBS}(n-k)] \frac{7}{3} 2^{2(n-k)} + \\
& \left. \sum_{m=0}^{n-k-1} N_{SBS}(m) \frac{7}{3} 2^{2m} \right]
\end{aligned} \tag{9.1}$$

The initial threshold level is $\tau = 2^n$, $N_{SBS}(i)$ the number of sign bits in pass i , $N d_{SBS}(i)$ the number of sign bits decoded in pass i , and K is the number of pixels. Depending on the channel, there is certain probability that a decoding failure

found by a CRC check will cause stoppage of decoding. Therefore, this formula for distortion will be averaged over the decoding failure probability for the given channel.

9.4 OFDM and Frequency Selective Channels

One of the main reasons to use OFDM is its inherent robustness against frequency selective fading and narrowband interference. Relative to a single carrier system, OFDM degrades gracefully against frequency selective channels because only a portion of the subchannels will be affected. Using error correction techniques, the small portion of subchannels that are affected by the fade can be corrected. The input data stream is split into N parallel lower rate sub-streams. Rather than transmit serially over one wideband channel, OFDM transmits data in parallel over several overlapping narrowband subchannels. Since OFDM transmits data in parallel, an *OFDM Symbol* consists of N QAM(Quadrature Amplitude) symbols. The QAM symbols are then modulated over N orthogonal sub-carriers.

The baseband channel model for a fading multipath channel with $L+1$ multipaths at each OFDM interval is of the form

$$h(t) = \sum_{i=0}^L h_i \delta(t - iT_s) \quad (9.2)$$

The h_i are zero-mean complex Gaussian independent random variables of attenuation and are normalized so that $\sum_{i=0}^L E[h_i h_i^*] = \sigma_h^2 = 1$. T_s is the basic delay constant. We further assume uncorrelated scattering, and a corresponding uniform power delay profile. For further analysis and simulation in order for the average receiver power to be the same as the transmitter power, we impose the condition that:

Under the assumptions we have made, the system can be described as a set of parallel Additive White Gaussian Noise(AWGN) with the double sided power spectral density of $N_o/2$ per dimension. Each sub-channels experience different fading gains where the fading gain on sub-channel i at time k is denoted by $|g_i(k)|^2$ where the vector $[g_0(k) g_1(k) \dots g_{N-1}(k)]$ is the N point DFT of the vector $[h_0, h_1, \dots, h_L, 0 \dots 0]$ multiplied by $N^{1/2}$. If $x_i(k)$ is the input complex QAM symbol at time k of sub-channel i , then using zero-forcing equalization criterion for each sub-channel, the output SNR of sub-channel i at time k is given by:

$$\frac{|x_i(k)|^2 |g_i(k)|^2}{N_o} \quad (9.3)$$

9.4.1 Dual Loading Algorithms

For image and image sequence simulations, the error correction code we have used are Reed Solomon (RS) [150] blocks of size $N_c = 2^n - 1$ symbols, where each symbol is n bits. For images, n is equal to 8 and for image sequences n is set to 10. Each

block is denoted by $(2^n - 1, k_c)$, where the number of information symbols k_c varies depending on the block. We assume a fixed block budget constraint B for the total number of blocks to be transmitted, where $B = B_{LBC} + B_{VBC}$. We have used a total of 128 sub-carriers and the total number of bits per OFDM symbol is 256 bits. We want to maintain progressiveness and transmit both coded LBC and VBC bits on one OFDM symbol. So on each OFDM symbol, the transmission rate for the LBC is $T_{LBC} = (B_{LBC}/B) * 256$ bits per OFDM symbol and for the VBC is $T_{VBC} = (B_{VBC}/B) * 256$ bits per OFDM symbol. We want to assign a variable energy per OFDM symbol such that the two different streams experience approximate bit errors rates of $P_{b,VBC}$ and $P_{b,LBC}$, which are respectively the raw bit error probability for the two channel coded VBC and LBC streams.

If there is Channel State Information (CSI) available, we can use it to minimize transmission energy per OFDM symbol while achieving the fixed values of T_{VBC} , T_{LBC} , $P_{b,VBC}$ and $P_{b,LBC}$. Hoo *et. al* [172] have shown that a near optimal way to do this is the Disjoint Bandwidth (DBW) algorithm. Let us assume that the subchannel gains at time k denoted by $|g_i(k)|^2$ are sorted in descending order so that $|g_0(k)|^2 > |g_1(k)|^2 > \dots |g_{N-1}(k)|^2$. This can be done without any loss of generality to the problem. The DBW method chooses a subcarrier point $M \in \{0, 1, 2, 3, \dots, N-1\}$ such that the LBC is assigned to the subcarriers from 0 to M and VBC is assigned to subcarriers $M+1$ to $N-1$. On each sub-carrier, the DBW algorithm assigns a variable size QAM where the number of bits per carrier belongs to the set $\{0, 2, 4, 6, 8, 10\}$. The optimum value of M , denoted by M^* is the one that minimizes total energy per OFDM symbol. The complexity for the DBW method is $O(N \log N)$ [172].

9.5 Dual Stream Joint Source Channel Coding

We are interested in minimizing the expected distortion while keeping the probability of decoding failure arbitrarily small. Let us denote by $D(R)$, the MSE distortion remaining after R bits have been correctly decoded and by $D_b(i)$ the distortion due to losing block i . We denote by $P_{VBC}(i, t_i)$ the probability of losing a VBC block i which has a total of $2t_i$ parity symbols. Each RS codeword will be used as a transmission block. Assuming we feed the coder a size k_c symbol information sequence, each RS code word will have a redundancy of $N_c - k_c$ for a total RS code word size of N_c . The minimum distance of the code d_{\min} is no less than $N_c - k_c + 1$. The parity bits are used by the receiver to detect and correct errors. A coder/decoder pair can correct up to $t \leq \lfloor (d_{\min} - 1)/2 \rfloor$ bytes that have been corrupted. We are interested in the error correction capability of each RS block and the probability of block failure. We denote the probability of code symbol error by P_{cs} . We also assume that the probability of code symbol error for each code symbol is independent of other code symbols in each RS block. If the channel has memory then we may use time and/or frequency interleaving to make sure that the code symbol errors are independent. Then $P_{VBC}(i, t_i)$, the probability of more than t_i symbol errors in block i , is given by

$$P_{VBC}(i, t_i) = \sum_{j=t_i+1}^{N_c} \binom{N_c}{j} P_{cs}^j (1 - P_{cs})^{N_c-j} \quad (9.4)$$

We assume our system operates at the typical raw probability of bit error 0.01 or less. So even if we do not correctly decode all blocks up to and not including block m , the remaining distortion will be close to $D_b(m)$, because of the few VBC errors in a block. We make two further assumptions based on numerical magnitude in order to simplify the objective function of our optimization problem. First, we assume that $P_{VBC}(i, t_i) \prod_{j=1}^{i-1} (1 - P_{VBC}(j, t_j))$ is approximately equal to $P_{VBC}(i, t_i)$. Secondly, we assume that the probability of having two or more block failures is small relative to $P_{VBC}(i, t_i)$ for all blocks. So if we have received B_{VBC} blocks, then there are $2^{B_{VBC}}$ possible events corresponding to combinations of block failures and successes but only B_{VBC} of these events are significant. The expected distortion $E(D)$ assuming and total source rate of R bits when there is no LBC error is approximately given by:

$$E(D) = \sum_{i=1}^{B_{VBC}} D_b(i) P_{VBC}(i, t_i) + D(R) \prod_{i=1}^{B_{VBC}} (1 - P_{VBC}(i, t_i)) \quad (9.5)$$

We will stop decoding after the first LBC block error has been detected because if we continue decoding, we will incur an increase in distortion. We insert two bytes of extra CRC bits in each LBC block so that any uncorrectable block can be detected. We would like to have a small probability of decoding failure. We have kept the number of information bits per LBC block constant, so that P_{LBC} , the probability of LBC block failure is constant. For reliable transmission, we specify that the probability of no LBC errors in B_{LBC} blocks must be greater than $1 - \varepsilon_{fail}$. In order to minimize distortion, we must find the optimal block parity vector $\vec{t} = [t_1, t_2, \dots, t_{B_{VBC}}]$ that minimizes Eqn. (6) under the block budget constraint B . So the final optimization problem is

$$\min_{\vec{t}} E(D) \quad (9.6)$$

given the constraints

$$B_{LBC} + B_{VBC} \leq B \quad (9.7)$$

$$1 - (1 - P_{LBC})^{B_{LBC}} < \varepsilon_{fail} \quad (9.8)$$

We also keep the information symbol constant in the LBC blocks. A decoding failure occurs when one of the B_{LBC} LBC blocks is not decoded correctly. The algorithm for the optimization is given by:

1. Assume $B_{VBC} = \lceil \eta B \rceil$
2. Find the optimal set of \vec{t} and evaluate $E^*[D]$
3. If Eqn. (8) is not satisfied decrement B_{VBC} go to Step 2 else use optimal set of \vec{t}

In Step 1 we have not specified the number of transmission blocks allocated to B_{VBC} . For our simulations, we have set the initial value of η to 1/3 and so the initial value of B_{VBC} is a third of B , the total block budget. In Step 2, using a gradient based method, we solve Eqn. (4) using an exponential approximation for $P_{VBC}(i, t_i)$ and $\hat{D}(R)$ given by Eqn. (1). In Step 3, we look-up the corresponding number of LBC source bits which depends on the corresponding number of VBC source bits used in finding the optimal $E^*[D]$. Until Eqn. (8) is satisfied, we need to increase B_{LBC} . And we do so by decreasing B_{VBC} . This can be done in a small amount of steps by reducing the size of the initial \vec{t} until Eqn. (8) is satisfied and then re-evaluating step 2 for the final value \vec{t} .

Let us now analyze a major benefit of demultiplexing the bitstream. If we did not use multiplexing, then we would have to stop decoding before the first block error. Denoting by $D_{tot}(R)$ the total MSE distortion after R source bits, $D_{btot}(m)$ the distortion up to and not including block m and by $P_{bl}(i)$ the probability of losing block i which has a total of $2t_i$ parity bytes, the expected distortion is exactly defined as:

$$\begin{aligned}
E(D) &= D_{tot}(0)P_{bl}(1, t_1) + \sum_{i=2}^B D_{btot}(i)P_{bl}(i, t_i) \times \\
&\quad \prod_{j=1}^{i-1} (1 - P_{bl}(j, t_j)) + \\
&\quad D_{tot}(R) \prod_{i=1}^B (1 - P_{bl}(i, t_i))
\end{aligned} \tag{9.9}$$

Now we have no control over how small $1 - \prod_{i=1}^B (1 - P_{bl}(i, t_i))$ is. And if we were to optimize Eqn. (8) under the constraint $1 - (1 - P_{LBC})^B \leq \varepsilon_{fail}$ then we would not be operating as efficiently as the demultiplexing scheme because extra and unnecessary parity bytes must also be allocated for the VBC portion. But if we used a demultiplexing scheme, since $B_{LBC} < B$, then $1 - (1 - P_{LBC})^{B_{LBC}} \leq \varepsilon_{fail}$ would be satisfied with less parity bytes. The optimization of Eqn. (9) has another drawback because the terms $P_{bl}(i, t_i) \prod_{j=1}^{i-1} (1 - P_{bl}(j, t_j))$ can give us multiple extreme points. Numerical simulation points that illustrate the significance of demultiplexing is given in the next section.

9.6 Simulation Results

For images, we have run simulations for five different values of $P_{b,VBC}$ and $P_{b,LBC}$. For each of these values, we have simulated two transmission rates of 0.49 (64 blocks) bps and 0.83 bps (107 blocks). The simulations were run for two different values of

ε_{fail} of .01 and .00001. All image simulation points were run at least 100 times for the Lenna image using binary, uncoded SPIHT for Matlab created by the author. The SPIHT for Matlab is less optimized and has about 0.2 dB PSNR loss relative to the binary uncoded C++ program of SPIHT available for download and used in [139]. Table 9.1 lists the parameters used in the OFDM simulations. We did not use arithmetic coding. Table 9.2 lists the simulation results for the 2-D SPIHT OFDM simulation. Important parameters in Table 9.2 are $P_{b,LBC}$ and $P_{b,VBC}$ which correspond respectively to the average probability of bit error that the LBC stream experienced and the probability of bit error experienced by the VBC stream. In the E_b/N_o and PSNR entries there are two values each for ε_{fail} of .01 and .00001 respectively. When the probability of LBC error is made small, the average PSNR is reduced. An interesting case occurs in the 4th and 5th row where the PSNR values for both values of ε_{fail} are the same. This is explained through the fact that we had a block budget constraint and so the LBC for the constraint $\varepsilon_{fail} = 0.01$ used more parity than necessary. If we had allocated those extra parity bits to the VBC bit stream, then we would have violated the integral number of blocks constraint because more LBC bits needed to be transmitted. A significant average PSNR increase occurs, when we increased the transmission energy allocated to the LBC portion. This is because the criterion for ε_{fail} is met using less parity bits for the LBC and so those extra parity bits can be allocated for the transmission of the VBC.

Now we solve for the optimal parity allocation for Eqn. (9) using the accurate D-R estimate in (1) and a transmission rate of 0.498 bpp and 0.833 bpp. In Table 9.3, we compare the average and ranges of the PSNR's of single stream and dual stream SPIHT in OFDM transmission. Note that the PSNR's are not only high for this noisy, fading channel, but that for dual stream the range is very narrow around the average. Our optimization constraint that the probability of decoding failure should be less than ε_{fail} , ensures with high probability that the dual-stream method does not suffer from unstable results. This is a major advantage of separation of the source bit-stream into different classes and subsequently coding them separately before transmission. It is also worth pointing out that an extra advantage of OFDM for SPIHT transmission with these two bitstreams is that each OFDM symbol contains both LBC and VBC bits. This allows more of the progressiveness of the SPIHT coder to be maintained relative to a serial transmission system.

9.7 Discussion and Conclusion

We have presented a new joint source channel coding algorithm based on the bit error response of the coder. The algorithm is a systematic and analytical method that takes into consideration the different error sensitivities of the VBC and LBC bits. Although the source coding algorithm used is SPIHT, the JSCC method is easily generalizable to any modern progressive coder that employs progressive bit-plane coding. If the

Number of subcarriers	128
Channel Model	3 tap uniform rayleigh
Length of Cyclic Prefix	3
Coherence time	10 OFDM symbol
Signal Constellations	{4,16,64,256,1024} QAM
Bit Rate	{256} bits per OFDM symbol
ε_{fail}	{1e-2,1e-5}
Adaptive Method	DBW

Table 9.1: SPIHT-Transmission OFDM Simulation Parameters

rate bpp	$P_{b,VBC}$	$P_{b,LBC}$	Eb/N_o^\dagger	$PSNR^\dagger$
0.498	0.01	0.01	{7.42,7.42}	{35.15,34.68}
0.498	0.01	0.005	{8.16,8.10}	{35.76,35.46}
0.498	0.005	0.005	{8.40,8.36}	{35.86,35.69}
0.498	0.005	0.001	{9.58,9.57}	{36.30,36.30}
0.498	0.001	0.001	{9.91,9.90}	{36.36,36.36}
0.833	0.01	0.01	{7.41,7.51}	{37.34,36.97}
0.833	0.01	0.005	{8.09,8.21}	{37.99,37.73}
0.833	0.005	0.005	{8.40,8.33}	{38.15,37.90}
0.833	0.005	0.001	{9.58,9.64}	{38.40,38.16}
0.833	0.001	0.001	{9.91,9.93}	{38.51,38.41}

$^\dagger \varepsilon_{fail} = (0.01, 0.0001)$.

Table 9.2: PSNR results for SPIHT OFDM system

rate bpp	Method	BER	Average	Worst	Best
0.498	Dual	0.01	35.15	35.10	35.17
0.893	Dual	0.01	37.34	37.31	37.35
0.498	Single	0.01	35.17	34.16	35.17
0.893	Single	0.01	37.33	30.59	37.46

Table 9.3: Single vs Dual stream OFDM transmission of SPIHT-encoded Lena image

coder decides to partition the transform of the image or image sequence for further robustness, then the optimization algorithms can be executed for each partition. The algorithm is also optimal in the sense that given a desired probability of decoding failure, it will use the minimum amount of parity checks to meet this criteria and also minimize the average MSE under a block constraint. We have also mentioned by transmitting both the VBC and LBC in parallel on one OFDM symbol, we maintain progressiveness relative to a serial transmission scheme. Using CSI, further energy reduction can be obtained by offering the higher gain subchannels to the LBC and the lower gain subchannels to the VBC. The major advantage of our JSCC method over a single stream optimal JSCC approach was that the instantaneous PSNR differs from the average PSNR only by a small margin, due to demultiplexing and subsequently requiring the probability of decoding failure to be small.

Chapter 10

Real-Time Video Transmission over MIMO OFDM Channels using Space-Time Block Codes

10.1 Introduction

In this chapter we shall consider the problem of faded wireless image and video transmission schemes over Multi-Input Multi-Output (MIMO) Orthogonal Frequency Division Multiplexing (OFDM) channels that are energy and the bandwidth constrained. Here we employ optimal equal error protection (EEP) in our joint source-channel coding scheme using OSTBC (orthogonal space time block code) for the channel with two transmitting and one or two receiving antennas, denoted (2,1) or (2,2) system. We shall show that the (2,2) system expends 12 dB less in energy per bit for the same performance as a SISO (single-input single-output) system. Our results are also significantly better than outage probability JSCC schemes used by other authors. The joint source-channel coding (JSCC) scheme demonstrates that MIMO OFDM can achieve real-time high quality video transmission in low energy regions and the system is robust against delay spread and doppler frequency shift.

We are now interested in the *spatial diversity* that the MIMO systems offer. Spatial diversity exploits the fact that the fading experienced by the multiple antennas will be independent when there is a sufficient separation between the antennas. By coding across both space and time, Orthogonal Space-Time Block Coding (OSTBC) [133] [153] [134] [165] can be used to achieve maximal diversity even when the transmitter has no knowledge of the channel. Another advantage of OSTBC codes is that they decouple the MIMO channel into parallel space-time (ST) channels which leads to a linear time maximum likelihood (ML) detection. A combination of OSTBC and OFDM (Orthogonal Frequency Division Multiplexing) leads to Space-Time OFDM (ST-OFDM). This system is robust against inter-symbol interference (ISI) and deep fades due to the time-varying nature of the channel [134] [165].

A notable paper in the design of JSCC for MIMO systems is the paper of Song and Liu [159]. They used a combination of OSTBC and OFDM for progressive SPIHT transmission of the *Lena* image over Rayleigh fading channels. They proposed a UEP (Unequal Error Protection) JSCC scheme based on dynamic programming method and used solely RS (Reed-Solomon) coding because of their excellent burst error correction capabilities. Because of the great amount of simulation required at each energy transmission point, they only simulated the *Lena* image 300 runs at only one transmission rate. Their JSCC scheme was designed based on target energy. The actual transmission energy was much greater than target energy which the JSCC was optimized over. This was done in order that a certain outage probability may be achieved. Here our target will be a bit error probability.

10.2 Analytic formulation

We again utilize our source code distortion-rate estimator $\hat{D}(R)$ of Equation 7.4 and the formula for the expected end-to-end distortion $E(D)$ in Equation 8.4 repeated below.

$$\begin{aligned}
E(D) = & \sum_{i=0}^{N-1} D_b(i) P_{bl}(i, t_i, E_i) \prod_{j=0}^{i-1} (1 - P_{bl}(j, t_j)) \\
& + D(R_s) \prod_{i=0}^{N-1} (1 - P_{bl}(i, t_i))
\end{aligned} \tag{10.1}$$

where $P_{bl}(i, t_i)$ is the probability of losing block i which has a total of $2t_i$ parity bytes and expends E_i energy per bit for block i . $D_b(m)$ denotes the distortion remaining after m blocks are successfully received. Again, we employ a CRC (cyclic redundancy check) after Reed-Solomon decoding in order to stop decoding after first packet decoding failure. As before, the block budget constraint is N and the total source rate is R_s bits.

The optimization of Equation 10.1 with fixed energy forms the objective function of the joint source channel coding scheme analyzed in [159][143] amongst many other papers mentioned therein. Here, however, we use optimal equal error protection (EEP) and, like the paper [159], we employ Reed Solomon(RS)[150] codes. The RS codeword that we use are of block size of $N_{code} = 255$ code symbols. Each code symbol is a 8 bit binary sequence. Denote the probability of code symbol error by P_{cs} . We assume that the probability of code symbol error for each code symbol is independent of other code symbols in each RS block. If the channel has memory then we may use interleaving to make sure that the code symbol errors are independent. Then $B(N_{code}, P_{cs})$, the number of symbol errors in a block, is a binomial random variable with parameters N_{code} and P_{cs} . Then P , the probability of more than t

symbol errors, is given by [150]

$$P(t) = \Pr(B(N_{code}, P_{cs}) \geq t + 1) = \sum_{i=t+1}^{N_{code}} \binom{N_{code}}{i} P_{cs}^i (1 - P_{cs})^{N_{code}-i} \quad (10.2)$$

10.2.1 MIMO OFDM using OSTBC

One of the advantages of OFDM is that the signal period of a sub-carrier is extended relative to a single carrier system. With the addition of small guardband, ISI is eliminated. Since our focus is on JSCC, we assume perfect carrier synchronization, perfect channel estimation of each of the gains of the sub-carriers and perfect suppression of multipath by the guard interval. The time-varying nature of this multipath channel is another obstacle that causes random fluctuation of the signal. This time variation arises because either the transmitter or the receiver or both are moving and therefore the location of the reflectors which cause the multipath will change over time. MIMO communication is a relatively new area in communications. MIMO systems have been shown to be robust against the fading channel. In a MIMO communications system the transmit and receive antennas are used in order to extract a substantial space diversity gain relative to the SISO (single-input single-output) system [165] [134] [133]. Antenna diversity provides the receiver with multiple samples of the same transmitted signal. Increasing the number of antennas, the probability that the fading gain of each antenna is small reduces sharply. Thus the spatial diversity of the MIMO system stabilizes the wireless link relative to a SISO system.

Figure 10.1 shows our generic MIMO OFDM STBC system. The R-S coder is used to combat fading and AWGN noise. The CRC is used for this purpose so that decoding may be stopped after first uncorrectable block error. The source and channel coder work together under our JSCC scheme so that the minimum receiver MSE is obtained at the receiver. Extra interleaving spreads possible burst errors over several RS code-words. The OFDM is used to combat ISI. Although not indicated in the diagram, we assumed that the OFDM guardband is sufficiently long enough so that ISI is suppressed completely. The Alamouti encoder is used to obtain maximal antenna transmit diversity. The decoding process at the receiver is essentially the reverse of the transmission process, except for the ML decoding procedure described in [153].

Let us denote the channel impulse response between the i th receive antenna ($i = 1, 2, \dots, M_r$) where M_r is the number of receive antennas and the j th transmit antenna ($j = 1, 2$) as $g_{i,j}[l]$ ($l = 0, 1, 2, \dots, L - 1$), where L is the maximum channel length among all the individual antennas. Let us denote a matrix $G[l]$, whose ij th element is given by $g_{i,j}[l]$. Throughout this work, we assume that every $g_{i,j}[l]$ is zero mean circularly symmetric complex Gaussian distributed and the variance of $g_{i,j}[l]$

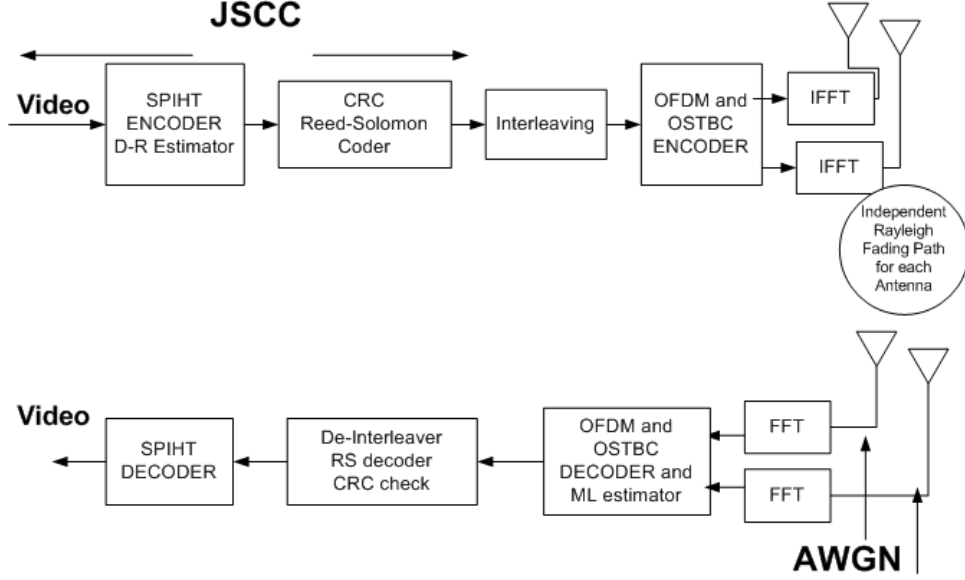


Figure 10.1: A generic model of the MIMO OFDM system

is equal to $1/L$ for $l = 0, 1, 2, \dots, L - 1$.

For the MIMO OFDM OSTBC system using the Alamouti code, the discrete base-band symbol at subcarrier index k , can be represented in the following notation[165]:

$$\mathbf{y}[k] = \mathbf{H}[k]\mathbf{s}[k] + \mathbf{n}[k] \quad (10.3)$$

where \mathbf{H} is a matrix of dimension $M_r \times 2$, $\mathbf{y}[k]$ is the $M_r \times 1$ received vector, $\mathbf{s}[k]$ is the transmit signal vector with dimension 2×1 , and $\mathbf{n}[k]$ is zero mean circularly symmetric complex Gaussian noise vector with variance N_o of dimension $M_r \times 1$. The matrix \mathbf{H} is related to the matrix G by:

$$\mathbf{H}[k] = \sum_{l=0}^{L-1} G[l] \exp(-\frac{j2\pi kl}{N_s}) \quad (10.4)$$

where N_s is the number of sub-carriers. Using the Alamouti scheme in the OFDM context, we assume that channel remains relatively constant over consecutive sub-channels. That is $\mathbf{H}[k] \approx \mathbf{H}[k + 1]$. So the data symbols s_1 and s_2 are transmitted over sub-channel k on antenna 1 and antenna 2 respectively and the data symbols $-s_2^*$ and s_1^* are transmitted over antennas 1 and 2 respectively over sub-channel $k + 1$. Alternatively one can use spatial diversity across each OFDM symbol, but this requires that the channel remains constant over two OFDM symbol period. This alternative method was used in [159].

10.3 Analytical Simulation for MIMO OFDM OSTBC

Alamouti and Tarokh *et al.* [153][133] have show that a (M_t, M_r) MIMO system using STBC achieves the same diversity gain as an equivalent $(1, M_r M_t)$ RAKE receiver using maximal ratio combining (MRC). The bit error rate (BER) performance of 4-QAM with a diversity order m using MRC with independent and identically distributed Rayleigh fading coefficients is given by[135](pg 542):

$$BER = p^m \sum_{k=0}^{m-1} \binom{m-1+k}{k} (1-p)^k \quad (10.5)$$

where p is given by:

$$p = \frac{1}{2} - \frac{1}{2} \left(1 + \frac{1}{E_b/N_o}\right)^{-\frac{1}{2}} \quad (10.6)$$

A two channel receiver scheme has a gain of 3dB over the Alamouti diversity scheme due to the array gain. So the E_b/N_o needs to be halved in Equation 10.6 for the Alamouti scheme[135] (pg 553). We can use Equations 10.5 and 10.2 in Equation 10.1 to obtain the optimal EEP and the MSE performance of the MIMO OFDM STBC system. In Figure 10.2 we have plotted the PSNR performance under an optimal EEP scheme for Lena at a rate of 0.5. The results were obtained for a SISO system using 4-QAM, a MIMO system of (2,1) and a MIMO system of (2,2). In comparison with the results of [159], our (2,1) Alamouti scheme using average probability of error outperforms their (2,2) and (2,4) system by over 8 dB in PSNR at the E_b/N_o of 5 dB. Similarly our (2,2) system at the E_b/N_o of 5 outperforms their system by 12 dB. It should be mention that in our (2,2) system we have used the array gain at the receiver. The large difference between our results and their result is due to the fact that we designed our JSCC based on average probability of error whereas their scheme is based on the outage probability. We have also used longer RS codewords in our JSCC scheme and also used an accurate D-R function. Similarly for the same PSNR of 35 dB, our (2,2) scheme saves about 12 dB in E_b/N_o relative to a SISO system. In Figure 10.3 we have obtained the optimum EEP PSNR for the first 16 frames of the luminance component of the Susie image sequence at the rates of 0.1. It should be noted again that our D-R estimator can be used for both image and image sequences.

10.4 Monte Carlo Simulation for MIMO OFDM

We now consider Monte Carlo simulation for the MIMO OFDM system. We consider a system that transmits 512 kilo-symbols/s on a carrier frequency of 2 GHz. The

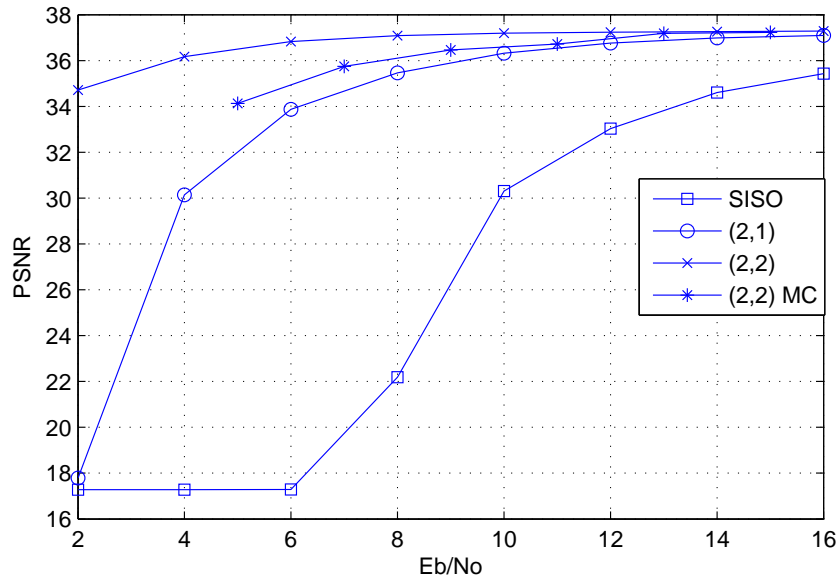


Figure 10.2: Analytic simulation results for optimum EEP for Lena at 0.5 bpp in MIMO

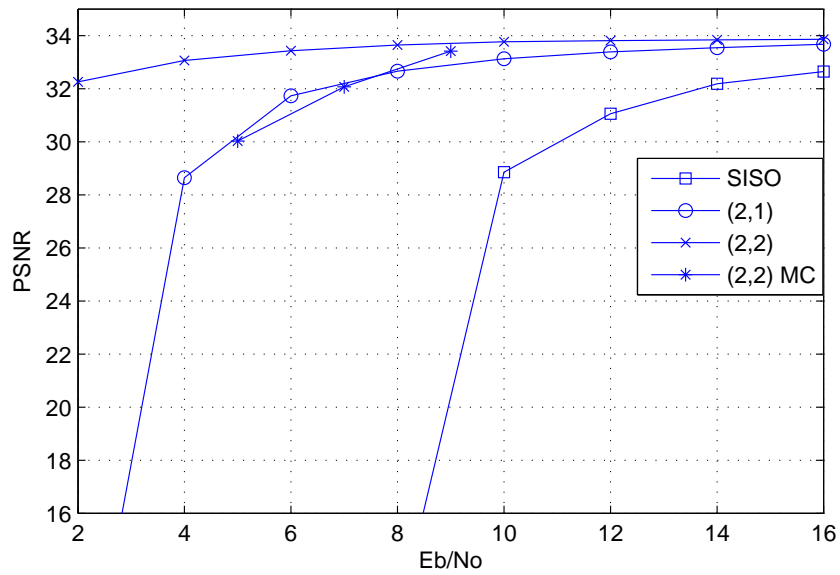


Figure 10.3: Analytic simulation results for optimum EEP for Susie at 0.1 bpp in MIMO

system uses 512 4-QAM sub-carriers. A two ray channel model with delay spread from 0 to 100 μ s is used in our simulation. To completely remove the ISI, 104 of the sub-carriers will be used as guard tones which provides a maximum tolerance of about 200 micro-second to the delay spread. The duration of each OFDM symbol is 1 milli-second. The system model is the one described in Section 2. The channel coefficients are drawn according to the model [136] which is modified from that of Jakes[157]. The modification of Jakes' approach uses orthogonal Walsh-Hadamard codewords to decorrelate the multiple fading coefficients. The steps of the JSCC are simple. First we estimate the D-R function according to Equation 7.4. Then given the assigned energy and rate constraints, we plug Equations 7.4, 10.2 and 10.5 to obtain the optimum EEP from Equation 129. Due to the large amount of simulations, and due to emphasis on MIMO systems, we have simulated all runs for the (2,2) MIMO system. We have run the simulations for the mobile speed of 120 km/sec. Each point was simulated 200 times. Both time interleaving of delay 15 millisecond and frequency interleaving over the sub-carriers are used to spread out the fading. The frequency interleaving does not cause any delays. In Figure 10.2 we have plotted the E_b/N_o vs PSNR. At an E_b/N_o of 5 dB our results are 34.12 dB in PSNR. Relative to the results of [159], this is about 10 dB improvement in PSNR for Lena at the rate of 0.5 bpp. In Figure 10.3 we ran the simulator for Susie at a rate 0.1 bpp. The Monte Carlo results are indicated by the legend MC. The results are slightly lower than the analytical simulation results predicted in Section 3. This could be due to the more realistic channel model used in the simulator [136] and the fact that the interleaving was not sufficient to make the symbol error probabilities independent as required by Equation 10.2. Since the symbol error probabilities were not completely independent, the actual probability of block error was slightly higher than that predicted by the analytical equations. Nevertheless, the results suggest that using the average probability error instead of the outage probability, a closer match to the optimal matching of the channel characteristics and the source characteristics is obtained.

10.5 Conclusion

In this chapter we presented a new real-time JSCC framework for the transmission of image and video sequences over MIMO OFDM systems. The real-time JSCC scheme was designed for fixed transmission energy and a fixed transmission rate. The OFDM was used in order to suppress ISI and the SBTC code was used to obtain spatial diversity in order to reduce the effect of fading. Further time and frequency interleaving was used to spread out deep fades. Because of the fast D-R estimator and the usage of optimal EEP, the JSCC framework presented is suitable for real-time applications. The major result here suggests that for the same energy and rate, using average probability of error to model the channel characteristics and matching it to the source produces a much higher PSNR than using the outage probability method

in [159]. The other major result is that (2,2) system obtains an almost 12 dB gain in PSNR for the same transmission energy expended.

Bibliography

- [1] S. S. Aghaian, *Hadamard Matrices and Their Applications*. Lecture Notes in Mathematics, vol. 1168, Springer-Verlag, 1985.
- [2] J. B. Andersen, "Array gain and capacity for known random channels with multiple element arrays at both ends," *IEEE J. Select. Areas Comm.*, vol. 18, pp. 2172-2178, November 2000.
- [3] A. G. Armada, "A simple bit loading algorithm for multiuser WLAN," in *Proc. IEEE Int. Conf. Communications (ICC'01)*, vol. 4, pp.1168-1171, June 2001.
- [4] A. G. Armada and J. M. Cioffi, "Multi-user constant-energy bit loading for M-PSK modulated Orthogonal Frequency Division Multiplexing," in *Proc. of IEEE Wireless Communications and Networking Conf. (WCNC'02)*, vol. 2, pp. 526-530, March 2002.
- [5] J. Armstrong, "Analysis of new and existing methods of reducing intercarrier interference due to carrier frequency offset in OFDM," *IEEE Trans. Comm.*, vol. 47, pp. 365-369, March 1999.
- [6] A. R. S. Bahai and B. R. Saltzberg, *Multi-Carrier Digital Communications: Theory and Applications of OFDM*, Kluwer Academic Publishers, 1999.
- [7] A. N. Barreto and S. Furrer, "Adaptive bit loading for wireless OFDM systems," in *Proc. of IEEE Int. Symp. on Personal, Indoor, and Mobile Radio Communications (PIMRC'01)*, vol. 2, pp. G88-G92, September/October 2001.
- [8] N. C. Beaulieu, "An infinite series for the computation of the complementary probability distribution function of a sum of independent random variables and its application to sum of Rayleigh random variables," *IEEE Trans. Comm.*, vol. 38, pp. 1463-1474, September 1990.
- [9] N. C. Beaulieu, "The evaluation of error probabilities for intersymbol and cochannel interference," *IEEE Trans. Comm.*, vol. 39, pp. 1740-1749, December 1991.

- [10] C. Biao and W. Hao, "Maximum likelihood estimation of OFDM carrier frequency offset," in *Proc. IEEE Int. Conf. Communications (ICC'02)*, vol. 1, pp. 49-53, April/May 2002.
- [11] J. Campello, "Optimal discrete bit loading for multicarrier modulation systems," in *Proc. IEEE Int. Symp. Information Theory (ISIT'98)*, pp. 193, August 1998.
- [12] J. Campello, "Practical bit loading for DMT," in *Proc. IEEE Int. Conf. Communications, (ICC'99)*, vol. 2, pp. 801-805, June 1999.
- [13] A. Carleial, "Outer bounds on the capacity of interference channels," *IEEE Trans. Information Theory*, vol. 29, pp. 602-606, July 1983.
- [14] R. W. Chang, "Synthesis of band limited orthogonal signals for multichannel data transmission," *Bell Systems Technical Journal*, vol. 45, December 1966.
- [15] R. S. Cheng and S. Verdu, "Gaussian multiaccess channels with ISI: capacity region and multiuser water-filling," *IEEE Trans. Information Theory*, vol. 39, pp. 773-785, May 1993.
- [16] H. Cheon, B. Park, and D. Hong, "Adaptive multicarrier system with reduced feedback information in wideband radio channels," in *Proc. IEEE Vehicular Technology Conf. (VTC'99-Fall)*, vol. 5, pp. 2880-2884, September 1999.
- [17] P. S. Chow, J. M. Cioffi, and J. A. C. Bingham, "A practical discrete multi-tone transceiver loading algorithm for data transmission over spectrally shaped channels," *IEEE Trans. Comm.*, vol. 43, pp. 773-775, February 1995.
- [18] P. S. Chow, J. C. Tu, and J. M. Cioffi, "Performance evaluation of a multi-channel transceiver system for ADSL and VHDSL services," *IEEE J. on Select. Areas Comm.*, vol. 9, pp. 909-919, August 1991.
- [19] P. S. Chow, J. C. Tu, and J. M. Cioffi, "A discrete multitone transceiver system for HDSL applications," *IEEE J. Select. Areas Comm.*, vol. 9, pp. 895-908, August 1991.
- [20] T. Cover and J. Thomas, *Elements of Information Theory*, Wiley & Sons, New York, 1991.
- [21] E. F. Deprettere, *SVD and Signal Processing: Algorithms, Applications and Architectures*, North-Holland, 1988.
- [22] O. A. Dobre and Y. D. Yao, "An adaptive data transmission scheme for OFDM systems," in *Proc. IEEE Vehicular Technology Conf. (VTC'02-Fall)*, vol. 3, pp. 1398-1403, September 2002.

- [23] H. Dong-Seog, S. Jae-Hyun, and K. Jung-Jin, "Fast carrier frequency offset compensation in OFDM systems," *IEEE Trans. Consumer Electronics*, vol. 47, pp. 364-369, August 2001.
- [24] ETSI ETS 300 910, "Digital cellular telecommunication system; Radio transmission and reception (GSM 05.05, V7.1.1)," ETSI Tech. Rep., 1998.
- [25] H. Erben, S. Zeisberg, and H. Nuszowski, "BER performance of a hybrid SC/MRC 2DPSK RAKE receiver in realistic mobile channels," in *Proc. IEEE Vehicular Technology Conf. (VTC'94)*, vol. 2, pp. 738-741, June 1994.
- [26] M. J. Fernandez-Getino Garcia, O. Edfors, and J. M. Paez-Borralló, "Frequency offset correction for coherent OFDM in wireless systems," *IEEE Trans. Consumer Electronics*, vol. 47, pp. 187-193, February 2001.
- [27] R. F. H. Fischer and J. B. Huber, "A new loading algorithm for discrete multi-tone transmission," in *Proc. IEEE Global Telecomm. Conf. (GLOBECOM'96)*, vol. 1, pp. 724-728, November 1996.
- [28] G. J. Foschini and M. J. Gans, "On limits of wireless communications in a fading environments when using multiple antennas," *Wireless Personal Communications*, vol. 6, pp. 311-335, March 1998.
- [29] J. Gao and M. Faulkner, "On implementation of bit-loading algorithms for ofdm systems with multiple-input multiple-output," in *Proc. IEEE Vehicular Technology Conf. (VTC'02-Fall)*, vol. 1, pp. 199-203, September 2002.
- [30] D. Gesbert, M. Shafi, D. Shiu, and P. Smith, "From theory to practice: An overview of space-time coded MIMO wireless systems," *IEEE J. Select. Areas Comm.*, vol. 21, pp. 281-302, April 2003.
- [31] B. N. Getu, J. R. Farserotu, and J. B. Andersen, "MIMO systems: optimizing the use of eigenmodes," in *Proc. IEEE Personal, Indoor, and Mobile Radio Communications, (PIMRC'03)*, vol. 2, pp. 1129-1133, September 2003.
- [32] L. Goldfeld, V. Lyandres, and D. Wulich, "Minimum BER power loading for OFDM in fading channel," *IEEE Trans. Comm.*, vol. 50, pp. 1729-1733, November 2002.
- [33] A. J. Goldsmith and M. Effros, "The capacity region of broadcast channels with intersymbol interference and colored Gaussian noise," *IEEE Trans. Information Theory*, vol. 47, pp. 219-240, January 2001.
- [34] R. Grunheid, E. Bolin, and H. Rohling, "A blockwise loading algorithm for the adaptive modulation technique in OFDM systems," in *Proc. IEEE Vehicular Technology Conf. (VTC'01-Fall)*, vol. 2, pp. 948-951, October 2001.

- [35] M. Gudmundson and P. O. Anderson, "Adjacent channel interference in an OFDM system," in *Proc. IEEE Vehicular Technology conf. (VTC 96)*, vol. 2, pp. 918-922, April/May 1996.
- [36] S. Hara and R. Prasad, "Overview of Multicarrier CDMA," *IEEE Communications Magazine*, vol. 35, pp. 126-133, December 1993.
- [37] F. J. Harris, "On the Use of Windows for Harmonic Analysis with Discrete Fourier Transform," *Proceedings of the IEEE*, vol. 66, pp. 51-83, January 1978.
- [38] B. Hirosaki, "An orthogonally multiplexed QAM system using the discrete Fourier transform," *IEEE Trans. Comm.*, vol. 29, pp. 982-989, July 1981.
- [39] B. Hirosaki, "A 19.2 kbits voice band data modem based on orthogonally multiplexed QAM techniques," in *Proc. IEEE Int. Conf. Communications (ICC'85)*, pp. 21.1.1-5, June 1985.
- [40] P. Hoeher, S. Kaiser, and P. Robertson, "Two-dimensional pilot-symbol-aided channel estimation by Wiener filtering," in *Proc. IEEE Int. Conf. Acoustics, Speech, and Signal Processing (ICASSP'97)*, vol. 3, pp. 1845-1848, April 1997.
- [41] J. L. Holzinger, "Digital communication over fixed time continuous channels with memory, with special application to telephone channels," Technical Report, M.I.T, 1964.
- [42] A. Huang and Y. Zhao, "Estimating channel response from pilot subcarrier pairs for OFDM systems," in *Proc. of the 40th Midwest Symposium on Circuits and Systems*, vol. 2, pp. 774-777, 1997.
- [43] D. Hughes-Hartogs, "Ensemble modem structure for imperfect transmission media," U.S. Patents Nos. 4,679,227 (Jul. 1987), 4,731,816 (Mar. 1988) and 4,833,706 (May 1989).
- [44] W. C. Jr. Jake, *Microwave Mobile Communications*, Wiley-Interscience, 1974.
- [45] L. Jian, L. Guoqing, and G. B. Giannakis, "Carrier frequency offset estimation for OFDM-based WLANs," *IEEE Signal Processing Letters*, vol. 8, pp. 80-82, March 2001.
- [46] N. Jindal, S. Vishwanath, and A. J. Goldsmith, "On the Duality of Multiple-Access and Broadcast Channels," in *Proc. Allerton Conf. on Communication, Control, and Computing*, October 2001.
- [47] S. Kaiser, "OFDM code-division multiplexing in fading channels," *IEEE Trans. Comm.*, vol. 50, pp. 1266-1273, August 2002.

- [48] S. Kapoor, D. J. Marchok, and Y. F. Huang, "Adaptive interference suppression in multiuser wireless OFDM systems using antenna arrays," *IEEE Trans. Signal Processing*, vol. 47, pp. 3381-3391, December 1999.
- [49] T. Keller and L. Hanzo, "Sub-band adaptive pre-equalised OFDM transmission," in *Proc. IEEE Vehicular Technology Conf. (VTC'99-Fall)*, vol. 1, pp. 334-338, September 1999.
- [50] T. Keller and L. Hanzo, "Adaptive modulation techniques for duplex OFDM transmission," *IEEE Trans. Vehicular Technology*, vol. 49, pp. 1893-1906, September 2000.
- [51] M. A. Khalighi, J. M. Brossier, G. V. Jourdain, and K. Raoof, "Water filling capacity of Rayleigh MIMO channels," in *Proc. IEEE Int. Symp. on Personal, Indoor and Mobile Radio Communications (PIMRC'01)*, vol. 1, pp. A155-A158, September 2001.
- [52] J. Kim, J. T. Chen, and J. M. Cioffi, "Low complexity bit mapping algorithm for multi-carrier communication systems with fading channels," in *Proc. IEEE Int. Conf. on Universal Personal Communications (ICUPC'98)*, vol. 2, pp. 927-931, October 1998.
- [53] Y. H. Kim, I. Song, S. Yoon, and S. R. Park, "An efficient frequency offset estimator for OFDM systems and its performance characteristics," *IEEE Trans. Vehicular Technology*, vol. 50, pp. 1307-1312, September 2001.
- [54] G. Kramer, "Genie-aided outer bounds on the capacity of interference channels," in *Proc. IEEE Int. Symp. on Information Theory (ISIT'01)*, pp. 103, June 2001.
- [55] B. S. Krongold, K. Ramchandran, and D. L. Jones, "Computationally efficient optimal power allocation algorithm for multicarrier communication systems," in *Proc. IEEE Int. Conf. Communications (ICC'98)*, vol. 2, pp. 1018-1022, June 1998.
- [56] B. S. Krongold, K. Ramchandran, and D. L. Jones, "An efficient algorithm for optimal margin maximization in multicarrier communication systems," in *Proc. IEEE Global Telecomm. Conf. (GLOBECOM'99)*, vol. 1B, pp. 899-903, December 1999.
- [57] G. Lebrun, T. Ying, and M. Faulkner, "MIMO transmission over a time-varying channel using SVD," in *Proc. IEEE Global Telecomm. conf. (GLOBECOM'02)*, vol. 1, pp. 414-418, November 2002.

- [58] J. Lee, R. V. Sonalkar, and J. M. Cioffi, "Multi-user discrete bit-loading for DMT-based DSL systems," in *Proc. IEEE Global Telecomm. Conf. (GLOBECOM'02)*, vol. 2, pp. 1259-1263, November 2002.
- [59] A. Leke and J. M. Cioffi, "Impact of imperfect channel knowledge on the performance of multicarrier systems," in *Proc. IEEE Global Telecomm. Conf. (GLOBECOM'98)*, vol. 2, pp. 951-955, November 1998.
- [60] E. Leung and P. Ho, "A successive interference cancellation scheme for an OFDM system," in *Proc. IEEE Int. Conf. Communications (ICC'98)*, vol. 1, pp. 375-379, June 1998.
- [61] H. E. Levin, "A complete and optimal data allocation method for practical discrete multitone systems," in *Proc. IEEE Global Telecomm. Conf. (GLOBECOM'01)*, vol. 1, pp. 369-374, November 2001.
- [62] Y. Li, "Pilot-symbol-aided channel estimation for OFDM in wireless systems," *IEEE Trans. Vehicular Technology*, vol. 49, pp. 1207-1215, July 2000.
- [63] Y. Li and L. J. Cimini, "Bounds on the interchannel interference of OFDM in time-varying impairments," *IEEE Trans. Comm.*, vol. 49, pp. 401-404, March 2001.
- [64] J. P. M. G. Linnartz and A. Gorokhov, "New equalization approach for OFDM over dispersive and rapidly time varying channel," in *Proc. IEEE Int. Symp. on Personal, Indoor, and Mobile Radio Communications (PIMRC'00)*, vol. 2, pp. 1375-1379, September 2000.
- [65] N. Maeda, S. Sampei, and N. Morinaga, "A delay profile information based sub-carrier power control combined with a partial non-power allocation technique for OFDM/FDD systems," in *Proc. IEEE Int. Symp. on Personal, Indoor, and Mobile Radio Communications (PIMRC'00)*, vol. 2, pp. 1380-1384, September 2000.
- [66] M. J. Medley, G. J. Saulnier, and P. K. Das, "Narrow-band interference excision in spread spectrum systems using lapped transforms," *IEEE Trans. Comm.*, vol. 45, pp. 1444-1455, November 1997.
- [67] P. H. Moose, "A technique for orthogonal frequency division multiplexing frequency offset correction," *IEEE Trans. Comm.*, vol. 42, pp. 2908-2914, October 1994.
- [68] Y. Mostofi, D. C. Cox, and A. Bahai, "ICI mitigation for mobile OFDM receivers," in *Proc. IEEE Int. Conf. Communications (ICC'03)*, vol. 5, pp. 3351-3355, May 2003.

- [69] G. Munz, S. Pfletschinger, and J. Speidel, "An efficient waterfilling algorithm for multiple access OFDM," in *Proc. IEEE Global Telecomm. (GLOBECOM'02)*, vol. 1, pp. 681-685, November 2002.
- [70] C. Muschallik, "Improving an OFDM reception using an adaptive Nyquist windowing," *IEEE Trans. Consumer Electronics*, vol. 42, pp. 259-269, August 1996.
- [71] M. Nakamura, T. Seki, M. Itami, K. Itoh, and A. H. Aghvami, "New estimation and equalization approach for OFDM under Doppler-spread channel," in *Proc. IEEE Int. Symp. on Personal, Indoor, and Mobile Radio Communications (PIMRC'02)*, vol. 2, pp. 555-560, September 2002.
- [72] R. Narasimhan, "Performance of diversity schemes for OFDM systems with frequency offset, phase noise and channel estimation errors," in *Proc. IEEE Int. Conf. Communications (ICC'02)*, vol. 3, pp. 1551-1557, May 2002.
- [73] R. Nilsson, O. Edfors, M. Sandell, and P. O. Borjesson, "An analysis of two-dimensional pilot-symbol assisted modulation for OFDM," in *Proc. IEEE Int. Conf. on Personal Wireless Communications*, pp. 71-74, December 1997.
- [74] T. Pollet, M. Van Bladel, and M. Moeneclaey, "BER sensitivity of OFDM systems to carrier frequency offset and Wiener phase noise," *IEEE Trans. Comm.*, vol. 43, pp. 191 -193, February/March/April 1995.
- [75] J. G. Proakis, *Digital Communications*, McGraw Hill, 1995.
- [76] G. G. Raleigh and J. M. Cioffi, "Spatio-temporal coding for wireless communication," *IEEE Trans. Comm.*, vol. 46, pp. 357-366, March 1998.
- [77] T. S. Rappaport, *Wireless Communications: Principles and Practice*, Prentice Hall, 1996.
- [78] W. Rhee and J. M. Cioffi, "Increase in capacity of multiuser OFDM system using dynamic subchannel allocation," in *Proc. IEEE Vehicular Technology Conf. (VTC 2000-Spring)*, vol. 2, pp. 1085-1089, May 2000.
- [79] P. Robertson and S. Kaiser, "The effects of Doppler spreads in OFDM(A) mobile radio systems," in *Proc. IEEE Vehicular Technology Conf. (VTC'99-Fall)*, vol. 1 , pp. 329-333, September 1999.
- [80] P. Robertson and S. Kaiser, "Analysis of the loss of orthogonality through Doppler spread in OFDM systems," in *Proc. IEEE Global Telecomm. Conf. (GLOBECOM'99)*, vol. 1B, pp. 701-706, December 1999.
- [81] V. K. Rohatgi, *An Introduction to probability theory and mathematical statistics*, John Wiley & Sons, 1976.

- [82] M. Russell and G. Stuber, "Interchannel interference analysis of OFDM in a mobile environment," in *Proc. IEEE Vehicular Technology Conf. VTC'95*, vol. 2, pp. 820-824, July 1995.
- [83] A. Salvekar and J. Cioffi, "Robust loading in the presence of channel profile selection," in *Proc. IEEE Int. Conf. on Signal Processing (ICSP'00)*, vol. 3, pp. 1786-1789, August 2000.
- [84] B. R. Salzberg, "Performance of an efficient parallel data transmission system," *IEEE Trans. Comm.*, vol. 15, December 1967.
- [85] K. Sathananthan, R. M. A. P. Rajatheva, and B. S. Slimane, "Cancellation technique to reduce intercarrier interference in OFDM," *Electronics Letters*, vol. 36, pp. 2078-2079, December 2000.
- [86] K. Sathananthan, R. M. A. P. Rajatheva, and S. B. Slimane, "Analysis of OFDM in the presence of frequency offset and a method to reduce performance degradation," in *Proc. IEEE Global Telecomm. Conf. (GLOBECOM'00)*, vol. 1, pp. 72-76, December 2000.
- [87] K. Sathananthan and C. Tellambura, "Probability of error calculation of OFDM systems with frequency offset," *IEEE Trans. Comm.*, vol. 49, pp. 1884-1888, November 2001.
- [88] K. Sathananthan and C. Tellambura, "Forward error correction codes to reduce intercarrier interference in OFDM," in *Proc. IEEE Int. Symp. on Circuits and Systems (ISCAS'01)*, vol. 4, pp. 566-569, May 2001.
- [89] A. Scaglione and S. Barbarossa, "Optimal power loading for OFDM transmissions over underspread Rayleigh time-varying channels," in *Proc. IEEE Int. Conf. Acoustics, Speech, and Signal Processing (ICASSP'00)*, vol. 5, pp. 2969-2972, June 2000.
- [90] C. Schurgers and M. B. Srivastava, "Single parameter model for loaded multicarrier systems," in *Proc. IEEE Global Telecomm. Conf. (GLOBECOM'01)*, vol. 6, pp. 3358-3364, November 2001.
- [91] K. A. Seaton and J. Armstrong, "Polynomial cancellation coding and finite differences," *IEEE Trans. Information Theory*, vol. 46, January 2000.
- [92] C. Sgraja and J. Lindner, "Estimation of rapid time-variant channels for OFDM using Wiener filtering," in *Proc. IEEE Int. Conf. Communications (ICC'03)*, vol. 4, pp. 2390-2395, May 2003.
- [93] R. V. Sonalkar and R. R. Shively, "An efficient bit-loading algorithm for DMT applications," *IEEE Communications Letters*, vol. 4, pp. 80-82, March 2000.

- [94] Z. Song, K. Zhang, and Y. L. Guan, "Joint bit-loading and power-allocation for ofdm systems based on statistical frequency-domain fading model," in *Proc. IEEE Vehicular Technology Conf. (VTC'02-Fall)*, vol. 2, pp. 724-728, September 2002.
- [95] Z. Song, K. Zhang and Y. L. Guan, "Statistical adaptive modulation for QAM-OFDM systems," in *Proc. IEEE Global Telecomm. Conf. (GLOBECOM'02)*, vol. 1, pp. 706-710, November 2002.
- [96] M. R. Souryal and R. L. Pickholtz, "Adaptive modulation with imperfect channel information in OFDM," in *Proc. IEEE Int. conf. Communications (ICC'01)*, vol. 6, pp. 1861-1865, June 2001.
- [97] A. Stamoulis, S. N. Diggavi, and N. Al-Dhahir, "Estimation of fast fading channels in OFDM," in *Proc. IEEE Wireless Communications and Networking Conf. (WCNC'02)*, vol. 1, pp. 465-470, March 2002.
- [98] Q. Su, L. J. Cimini, and R. S. Blum, "On the problem of channel mismatch in constant-bit-rate adaptive modulation for OFDM," in *Proc. IEEE Vehicular Technology Conf. (VTC'02-Spring)*, vol. 2, pp. 585-589, May 2002.
- [99] P. Tan and N. C. Beaulieu, "Reduced ICI in OFDM Systems Using the Better Than Raised-Cosine Pulse," *IEEE Communications Letters*, vol. 8, pp. 135-137, March 2004.
- [100] X. Tang, M. S. Alouini, and A. J. Goldsmith, "Effect of channel estimation error on M-QAM BER performance in Rayleigh fading," *IEEE Trans. Comm.*, vol. 47, pp. 1856-1864, December 1999.
- [101] U. Tureli, D. Kivanc, and L. Hui, "Experimental and analytical studies on a high-resolution OFDM carrier frequency offset estimator," *IEEE Trans. Vehicular Technology*, vol. 50, pp. 629-643, March 2001.
- [102] A. Vahlin and N. Holte, "Optimal finite duration pulses for OFDM," *IEEE Trans. Comm.*, vol. 44, pp. 10-14, January 1996.
- [103] J. J. Van De Beek, M. Sandell, and P. O. Borjesson, "ML estimation of time and frequency offset in OFDM systems," *IEEE Trans. Signal Processing*, vol. 45, pp. 1800-1805, July 1997.
- [104] R. Van Nee and R. Prasad, *OFDM for wireless multimedia communications*, Artech House Publishers, 2000.
- [105] S. Verdu, "Multiple-access channels with memory with and without frame synchronism," *IEEE Trans. Information Theory*, vol. 35, pp.605-619, May 1989.

- [106] S. Verdu, *Multiuser Detection*, Cambridge University Press, 1998.
- [107] P. Viswanath, D. N. C. Tse, and V. Anantharam, "Asymptotically optimal water-filling in vector multiple-access channels," *IEEE Trans. Information Theory*, vol. 47, pp. 241-267, January 2001.
- [108] S. B. Weinstein and P. M. Ebert, "Data transmission by frequency division multiplexing using discrete Fourier transform," *IEEE Trans. Comm.*, vol. 19, October 1971.
- [109] M. Z. Win and J. H. Winters, "Exact error probability expressions for H-S/MRC in Rayleigh fading: a virtual branch technique," in *Proc. IEEE Global Telecomm. Conf. (GLOBECOM'99)*, vol. 1A, pp. 537-542, December 1999.
- [110] M. Z. Win and J. H. Winters, "Analysis of Hybrid Selection/Maximal Ratio combining in Rayleigh fading," *IEEE Trans. Comm.*, vol. 47, pp. 1773-1776, December 1999.
- [111] C. Y. Wong, R. S. Cheng, K. B. Letaief, and R. D. Murch, "Multiuser OFDM with adaptive subcarrier, bit, and power allocation," *IEEE J. Select. Areas Comm.*, vol. 17, pp. 1747-1758, October 1999.
- [112] K. K. Wong, S. K. Lai, R. S. K. Cheng, K. B. Letaief, and R. D. Murch, "Adaptive spatial-subcarrier trellis coded MQAM and power optimization for OFDM transmissions," in *Proc. IEEE Vehicular Technology Conf. (VTC'00-Spring)*, vol. 3, pp. 2049-2053, May 2000.
- [113] C. Xiaodong and G. B. Giannakis, "Low-complexity ICI suppression for OFDM over time- and frequency-selective Rayleigh fading channels," in *Proc. Asilomar Conf. on Signals, Systems and Computers*, vol. 2, pp. 1822- 1826, November 2002.
- [114] C. Yang-Seok, P. J. Voltz, and F. A. Cassara, "ML estimation of carrier frequency offset for multicarrier signals in Rayleigh fading channels," *IEEE Trans. Vehicular Technology*, vol. 50, pp. 644-655, March 2001.
- [115] S. Ye, R. S. Blum, and L. J. Cimini, "Adaptive modulation for variable-rate OFDM systems with imperfect channel information," in *Proc. IEEE Vehicular Technology Conf. (VTC'02-Spring)*, vol. 2, pp. 767-771, May 2002.
- [116] N. Yee, J. P. Linnartz, and G. Fettweis, "Multi-carrier CDMA in indoor wireless radio networks," in *Proc. IEEE Int. Symp. Personal, Indoor, and Mobile Radio Communications (PIMRC'93)*, pp. 109-113, September 1993.
- [117] H. Yin and H. Liu, "An efficient multiuser loading algorithm for OFDM-based broadband wireless systems," in *Proc. IEEE Global Telecomm. Conf. (GLOBECOM'00)*, vol. 1, pp. 103-107, December 2000.

- [118] W. Yu and J. M. Cioffi, "On constant power water-filling," in *Proc. IEEE Int. Conf. Communications (ICC'01)*, vol. 6, pp. 1665-1669, June 2001.
- [119] W. Yu and J. M. Cioffi, "Competitive equilibrium in the Gaussian interference channel," in *Proc. IEEE Int. Symp. Information Theory (ISIT'00)*, pp. 431, June 2000.
- [120] W. Yu and J. M. Cioffi, "FDMA capacity of Gaussian multiple-access channels with ISI," *IEEE Trans. Comm.*, vol. 50, pp. 102-111, January 2002.
- [121] W. Yu, G. Ginis, and J. M. Cioffi, "Distributed multiuser power control for digital subscriber lines," *IEEE J. Select. Areas Comm.*, vol. 20, pp. 1105-1115, June 2002.
- [122] W. Yu, W. Rhee, S. Boyd, and J. M. Cioffi, "Iterative water-filling for Gaussian vector multiple access channels," in *Proc. IEEE Int. Symp. Information Theory (ISIT'01)*, pp. 322, June/July 2001.
- [123] C. Zeng, L. M. C. Hoo, and J. M. Cioffi, "Optimal water-filling algorithms for a Gaussian multiaccess channel with intersymbol interference," in *Proc. IEEE Int. Conf. Communications (ICC'01)*, vol. 8, pp. 2421-2427, June 2001.
- [124] Y. Zhang and K. B. Letaief, "Multiuser subcarrier and bit allocation along with adaptive cell selection for OFDM transmission Communications," in *Proc. IEEE Int. Conf. Communications (ICC'02)*, vol. 2, pp. 861-865, May 2002.
- [125] Y. Zhao, "In-band and out-band spectrum analysis of OFDM communication systems using ICI cancellation methods," in *Proc. Int. Conf. on Communications Technology (ICCT'00)*, vol. 1, pp. 773-776, August 2000.
- [126] Y. Zhao and S. G. Haggman, "Sensitivity to Doppler shift and carrier frequency errors in OFDM systems-the consequences and solutions," in *Proc. IEEE Vehicular Technology Conf. (VTC 96)*, vol. 3, pp. 1564-1568, April/May 1996.
- [127] Y. Zhao and S. G. Haggman, "Intercarrier interference compression in OFDM communication systems by using correlative coding," *IEEE Communications Letters*, vol. 2, pp. 214 -216, August 1998.
- [128] Y. Zhao and S. G. Haggman, "BER analysis of OFDM communication systems with intercarrier interference," in *Proc. Int. Conf. on Communication Technology (ICCT'98)*, vol. 2, October 1998.
- [129] Y. Zhao and S. G. Haggman, "Intercarrier interference self-cancellation scheme for OFDM mobile communication systems," *IEEE Trans. Comm.*, vol. 49, pp. 1185 -1191, July 2001.

- [130] L. Zheng and D. Tse, "Diversity and Multiplexing: A Fundamental Trade-off in Multiple Antenna Channels," *IEEE Trans. Information Theory*, vol. 49, pp. 1073-1096, May 2003.
- [131] S. Zhou, G. B. Giannakis, and A. Swami, "Digital multi-carrier spread spectrum versus direct sequence spread spectrum for resistance to jamming and multipath," *IEEE Trans. Comm.*, vol. 50, pp. 643-655, April 2002.
- [132] Masoud Farshchian, Sungdae Cho & William A. Pearlman, "Robust Image and Video Transmission Using Unequal Error Protection Algorithm and OFDM ", *IEEE Transactions on Signal Processing Letters*, vol. 11, no. 10, pp. 780-783, 2004
- [133] V. Tarokh, H. Jafarkhani, and A. R. Calderbank, "Space-time block codes from orthogonal designs," *IEEE Transactions on Information Theory*, vol. 45, pp. 1456-1467, Jul. 1999.
- [134] Erik G. Larsson and Petre Stoica, *Space-Time Block Coding for Wireless Communications*, Cambridge University Press, 2004
- [135] Barry, J.R, Lee, E.A, and Messerschmitt, D.G, *Digital Communications*, Kluwer Academic Publishers, 2004
- [136] P. Dent, G. Bottomley and T. Croft, "Jakes fading model revisited," *IEE Electronics Letters*, vol 29, no 13, pp. 1162-1163, June, 1993
- [137] T. S. Rappaport, *Wireless Communications: Principles and Practices*, Prentice Hall 1996, 2001.
- [138] B-J. Kim and W.A. Pearlman, "An Embedded Wavelet Video Coder Using Three-Dimensional Set Partitioning in Hierarchical Trees," *IEEE Data Compression Conference*, pp. 251-260, March 1997
- [139] A. Said and W. A. Pearlman. "A new, fast, and efficient image coded based on set partitioning in hierarchical trees." *IEEE Transactions on Circuits and Systems for Video Technology*, 6(3):243-250, June 1996.
- [140] P. G. Sherwood and K. Zeger, "Progressive image coding for noisy channels," *IEEE Signal Processing Letters*, vol. 4, pp 189-191, July 1997
- [141] S. Appadwedula, D. L. Jones, K. Ramchandran, and I. Konzentsev, "Joint source-channel matching for wireless communications link," in *Proceedings of ICIP98, 1998*
- [142] J. Lu, A. Nosratinia, and B. Aazhang, "Progressive source-channel coding of images over bursty error channels," in *Proceedings of ICIP98, 1998*

- [143] A. Nosratinia, J. Lu, and B. Aazhang, "Source-channel rate allocation for progressive transmission of images," *IEEE Transactions on Communications*, vol. 51, no. 2, pp 186-196, Feb. 2003.
- [144] Frederick W. Wheeler, "Trellis Source Coding and Memory Constrained Image Coding", Ph.D. Thesis, Rensselaer Polytechnic Institute, September, 2000.
- [145] Masoud Farshchian, "Robst Demultiplexed SPIHT transmission for OFDM", M.S. Thesis, Rensselaer Polytechnic Institute, December, 2003
- [146] Alireza Seyedi, "Robust Multi-Carrier Communication Systems for Fading Channels", Rensselaer Polytechnic Institute, May, 2004
- [147] S. Cho and W. A. Pearlman, "Error Resilient Video Coding with Improved 3-D SPIHT and Error Concealment," *SPIE/IS&T Electronic Imaging 2003*, Proceedings SPIE Vol. 5022, Jan. 2003
- [148] C. D. Creusere, "A new method of robust image compression based on the embedded zerotree wavelet algorithm," *IEEE Trans. Image Processing*, vol. 6, pp. 1436–1442, Oct. 1997.
- [149] J. M. Cioffi, *EE379C Advanced Digital Communications Course Notes*, available online at <http://www-leland.stanford.edu/class/e379c/>
- [150] S. B. Wicker, *Error Control Systems*. New Jersey: Prentice Hall, 1995.
- [151] S. Ross, *A First Course in Probability*. Prentice Hall, 2002.
- [152] van Nee, R., Awater, G., Morikura, M., Takanashi, H., Webster, M., and Halford, K. (1999). New high-rate wireless LAN standards. *IEEE Communications Magazine*, 37(12):82-88.
- [153] Alamouti, S.M. (1998). A simple transmit diversity technique for wireless communications. *IEEE Journal on Selected Areas in Communications*, 16:(8):1451-1458
- [154] Masoud Farchchian, Sungdae Cho & William A. Pearlman, "Robust Image and Video Transmission Using Unequal Error Protection Algorithm and OFDM ", *IEEE Transactions on Signal Processing Letters*, vol. 11, no. 10, pp. 780-783, 2004
- [155] Masoud Farchchian, Sungdae Cho & William A. Pearlman, "Optimal Error Protection for Real Time Progressive Image and Video Transmission ", *ICASSP*, no. 4, pp. 625-628, 2004

- [156] Masoud Farchchian, Sungdae Cho & William A. Pearlman, "Robust Image and Video Transmission Using a New JSCC Algorithm and Dual Adaptive OFDM," SPIE/IS&T Electronic Imaging, pp. 636-646, 2004
- [157] W. C. Jakes, *Microwave Mobile Communications*, Wiley, 1974.
- [158] A. R. S. Bahai, and B. R. Saltzberg, *Multi-Carrier Digital Communications: Theory and Applications of OFDM*, Kluwer Academic Publishers, 1999
- [159] J. Song and K. J. R. Liu, "Robust progressive image transmission over OFDM systems using space-time block code", *IEEE Transactions on Multimedia.*, vol. 4, pp. 394-406, september 2002.
- [160] V. Chande and N. Farvardin, "Progressive transmission of images over memoryless noisy channels," *IEEE Journal of Selected Areas in Communications.*, Vol. 18, pp. 850-860, July 2000.
- [161] Y. Charfi, R. Hamzaoui, and D. Saupe, "Model-based real-time progressive transmission of images over noisy channels," in *IEEE Conference on Wireless Communications and Networking*, vol. 2, Mar. 2003, pp. 784-789.
- [162] L. Qian, D. L. Jones, K. Ramchandran, and S. Appadwedula, "A general joint source-channel matching method for wireless video transmission," in *Proc. Data Compression Conference*, Snowbird, UT, 1999, pp. 414-423.
- [163] Mallat, S., Falzon, F., "Analysis of low bit rate image transform coding," *IEEE Transaction on Signal Processing.*, April 1998.
- [164] M. Hata, "Empirical formula for propagation loss in land mobile radio services," *IEEE Transaction on Vehicular Technology.*, Vol. 29, No. 3, pp. 317-325
- [165] [55] Paulraj, A., Nabar, R., and Gore, D. (2003). *Introduction to space-time communications*. Cambridge University Press, Cambridge, UK.
- [166] R. Gray, *Toeplitz and Circulant Matrices: A review*. available online at <http://www.isl.stanford.edu/~gray/toeplitz.pdf>, 2001.
- [167] J. A. C. Bingham, *Multicarrier modulation for data transmission: An idea whose time has come*, *IEEE Communication Magazine*, pp. 5-14, May, 1990.
- [168] B.-J Kim, Z. Xiong, and W. A. Pearlman *Low bit-rate scalable video coding with 3-D Set partitioning in Hierarchical Trees (3-D SPIHT)*, *IEEE Trans. Circuits and Systems for Video Technology*, vol. 10, pp. 1374-1387, December 2000.
- [169] A.A. Alatan, M.Zhao and A. N. Akansu, *Unequal error protection of SPIHT encoded image bit*, *IEEE Journal on Selected Areas in Communications*, vol. 18, no. 6, pp. 814-818, June 2000.

- [170] J. Hagenauer, *Rate-compatible punctured convolutional codes (RCPC codes) and their applications*, IEEE Transactions on Communications, vol. 36, pp. 389-400, April, 1988
- [171] P. G. Sherwood and K. Zeger, *Progressive Image Coding for Noisy Channels*, IEEE Signal Processing Letters, vol. 4, pp. 189-191, July, 1997
- [172] L.M.C. Hoo, J. Tellado, J.M. Cioffi, *Discrete dual QoS loading algorithms for multicarrier systems*, International Conference on Communications(ICC), vol. 2, pp. 796-800, 1999.

Appendix A

Fischer's Bit-Loading Algorithm

Here we briefly describe Fischer's bit-loading algorithm. Further details can be found in [27]. In the Fischer's algorithm the Symbol Error Rate (SER) of QAM modulation is approximated with

$$\begin{aligned} P_e &\approx KQ \left(\sqrt{\text{SNR}} \right) \\ &\approx 4Q \left(\sqrt{\frac{d^2}{2P_N}} \right), \end{aligned} \tag{A.1}$$

where K is the number of nearest neighbors (assumed to be equal to 4), d is the minimum distance between the constellation points, P_N is the noise power after equalization. Using this unique formula for all QAM constellations, Fischer shows that the overall SER is minimized if the SNR values for all sub-channels are designed to be equal.

In the Fischer's Algorithm, first the number of bits for each sub-channel is found from

$$B_i = \frac{B_T}{N'} + \frac{1}{N'} \sum_{l \in \mathcal{I}} \log_2 P_{N,l} - \log_2 P_{N,i}, \tag{A.2}$$

where, B_i denotes the number of bits assigned to sub-channel i , $P_{N,i}$ is the noise power on sub-channel i after equalization, B_T is the total number of bits per OFDM symbol, \mathcal{I} is the set of all sub-channels carrying data (initially containing all sub-channels), and N' is the size of \mathcal{I} (initially equal to N , the total number of sub-channels). Then, all sub-channels with negative B_i are omitted from \mathcal{I} . The values of B_i for these sub-channels is set to zero and B_i for the remaining sub-channels are recalculated. This process is repeated until all B_i are non-negative. The B_i values are then quantized to the available modulation levels to form $B_{Q,i}$. If the quantization process causes the total number of bits to be different from B_T , the $B_{Q,i}$ values with largest/smallest quantization errors are incremented/decremented until a total of B_T bits are loaded.

The energy of each symbol is then determined from

$$P_{S,i} = \frac{P_S P_{N,i} 2^{B_{Q,i}}}{\sum_{l \in \mathcal{I}} P_{N,l} 2^{B_{Q,l}}}, \quad (\text{A.3})$$

where P_S is the total energy available for the OFDM symbol.

Appendix B

Matrix Forms for ZF and MRC Receivers

Assume that the vector $\mathbf{s} = [s_0, \dots, s_{N-1}]^T$ is transmitter through a vector channel \mathbf{H} and at the receiver the vector $\mathbf{r} = [r_0, \dots, r_{N-1}]^T$ is received, or

$$\mathbf{r} = \mathbf{H}\mathbf{s} + \mathbf{n}, \quad (\text{B.1})$$

where \mathbf{n} is a complex Gaussian noise vector with mean zero and covariance matrix $\mathbf{K} = \sigma^2 \mathbf{I}_N$. If the channel matrix \mathbf{H} is not diagonal, self-interference exists. In other words, in this case r_n is a function of all the input symbols. At the receiver the transmitted symbols are estimated by

$$\begin{aligned} \hat{\mathbf{s}} &= \mathbf{G}\mathbf{r} \\ &= \mathbf{G}\mathbf{H}\mathbf{s} + \mathbf{G}\mathbf{n} \end{aligned} \quad (\text{B.2})$$

where \mathbf{G} is the equalization and combining matrix.

B.1 ZF Receiver

A Zero-Forcing equalizer and combiner removes the self-interference without any regard to the noise performance. In other words we have

$$\mathbf{G}_{ZF} = \mathbf{H}^{-1}. \quad (\text{B.3})$$

Hence,

$$\begin{aligned} \hat{\mathbf{s}}_{ZF} &= \mathbf{H}^{-1}\mathbf{r} \\ &= \mathbf{s} + \mathbf{H}^{-1}\mathbf{n} \\ &= \mathbf{s} + \mathbf{n}_{ZF}, \end{aligned} \quad (\text{B.4})$$

where \mathbf{n}_{ZF} has zero mean and covariance function

$$\begin{aligned}\mathbf{K}_{ZF} &= \sigma^2 \mathbf{G}_{ZF} \mathbf{G}_{ZF}^\dagger \\ &= \sigma^2 \mathbf{H}^{-1} (\mathbf{H}^{-1})^\dagger\end{aligned}\tag{B.5}$$

where $(.)^\dagger$ represents the Hermitian transpose.

B.2 MRC Receiver

A Maximal Ratio Combiner, on the other hand, minimizes the amount of noise on each estimated symbol without considering the self-interference. To estimate s_i The MRC combines r_j according to the amount of coefficient of s_i in r_j . In other words, from (B.1) we can write

$$r_j = \sum_{i=1}^N h_{ji} s_i + n_j.\tag{B.6}$$

Thus, neglecting all the symbols except for s_i , the MRC forms the estimate of s_i as

$$\hat{s}_i = \frac{\sum_{j=1}^N h_{ji}^* r_j}{\sum_{j=1}^N |h_{ji}|^2}.\tag{B.7}$$

Note that the denominator normalizes the estimate such that \hat{s}_i has the same magnitude as s_i . In matrix form (B.7) can be expressed as

$$\begin{aligned}\hat{\mathbf{s}}_{MRC} &= \mathbf{G}_{MRC} \mathbf{r} \\ &= \mathbf{G}_{MRC} \mathbf{H} \mathbf{s} + \mathbf{n}_{MRC}\end{aligned}\tag{B.8}$$

where

$$\mathbf{G}_{MRC} = \text{diag}(\mathbf{H}^\dagger \mathbf{H})^{-1} \mathbf{H}^\dagger,\tag{B.9}$$

where $\text{diag}(\mathbf{A})$ is a diagonal matrix with elements equal to the diagonal elements of \mathbf{A} , and \mathbf{n}_{MRC} has zero mean and covariance matrix

$$\begin{aligned}\mathbf{K}_{MRC} &= \sigma^2 \mathbf{G}_{MRC} \mathbf{G}_{MRC}^\dagger \\ &= \sigma^2 \text{diag}(\mathbf{H}^\dagger \mathbf{H})^{-1} \mathbf{H}^\dagger \mathbf{H} \text{diag}(\mathbf{H}^\dagger \mathbf{H})^{-1}\end{aligned}\tag{B.10}$$

Although the MRC has the optimal noise performance, it does not remove the self-interference. Thus an interference cancellation technique must be employed together with MRC, to obtain the symbol estimates without interference.